Evaluating the desorption of oxygen from wine

by

Steven Sutton

Thesis presented in partial fulfilment of the requirements for the degree of

Master of Agricultural Sciences

at

Stellenbosch University

Department of Viticulture and Oenology, Faculty of AgriSciences

Supervisor: Prof. Wessel Du Toit

Co-supervisor: Prof. Robert Pott

April 2022

ii

Declaration

By submitting this thesis electronically, I declare that the entirety of the work contained therein is my own, original work, that I am the sole author thereof (save to the extent explicitly otherwise stated), that reproduction and publication thereof by Stellenbosch University will not infringe any third-party rights and that I have not previously in its entirety or in part submitted it for obtaining any qualification.

Date: April 2022

Summary

The removal of dissolved oxygen through desorption is commonly done in winemaking. Winemakers have indicated that under the same conditions, this process takes place at different rates, for different wines. The mass transfer of oxygen in six wines and various model wine solutions, was examined by evaluating the oxygen desorption volumetric mass transfer coefficient ($k_L a$), the Sauter mean bubble diameter (D_{32}), gas holdup (ε), the interfacial area (a), and the oxygen mass transfer coefficient (k_L). One of the wines used was split into two batches, with one half treated with bentonite, and the other not. A bubble column with a stone sparger was used for the experiments. The gassing out procedure and a 2nd order model was used to determine $k_L a$. Bubble imaging was done to determine the interfacial area, and subsequently the k_L.

During oxygen desorption within wine, the $k_L a$ values varied between 0.0125 s^{-1} and 0.0275 s^{-1} depending on the wine. The $k_L a$ value during oxygen desorption within a 10 % ethanol solution was found to be 0.0275 s^1. The addition of a small amount glycerol to this system reduced the $k_L a$ to 0.0225 s^{-1}. Further additions of organic acids did not affect the $k_L a$, while the addition of protein in the form of BSA and yeast extract reduced the $k_L a$ to approximately 0.0175 s^{-1}. The $k_L a$ for during oxygen desorption within a wine that was protein unstable improved from 0.009 s^1 to 0.015 s^1 after being treated with bentonite.

During desorption, there were no significant variations in the D_{32} and the interfacial area between systems containing wines or model wine solutions. Consequently, the variations between the $k_L a$ values could all be ascribed to differences in the k_L. During oxygen desorption, the k_L values were found to be between 0.015 and 0.045 mm/s within the different wines. The k_L values were found to be between 0.03 and 0.04 mm/s within a 10% ethanol solution, and within the model wine solutions containing glycerol and organic acids. The k_L values dropped between 0.02 and 0.03 mm/s with the addition of protein to the model wine solution. Treating a protein unstable wine with bentonite increased the k_L value from 0.017 mm/s to 0.0225 mm/s.

The combination of the reduction in the k_L when protein was added to a model wine solution, and the improvement of the k_L when wine was treated with bentonite, suggested that proteins in wine significantly affect oxygen desorption rates. It is suggested that winemakers can improve the oxygen k_L within their system by operating at higher gas flowrates to increase the turbulence during desorption. However, the most effective way of improving the desorption rate is by using a sparger that produces smaller bubbles, so as to increase the interfacial area. It is suggested that desorption is performed after fining, as the k_L will be greater.

Opsomming

Die verwydering van opgeloste suurstof deur middel van desorpsie kom algemeen in wynbereiding voor. Wynmakers het aangedui dat, onder dieselfde toestande, hierdie proses teen verskillende tempo's vir verskillende wyne plaasvind. Die massa-oordrag van suurstof in ses wyne en verskillende model-wynoplossings is ondersoek deur die volumetriese massa-oordragkoëffisiënt ($k_L a$) van suurstof desorpsie, die Sauter gemiddelde borreldeursnee (D_{32}), gasvertraging (*gas holdup*) (ε), die oppervlakte van die koppelvlak (a) en die suurstof massa-oordragkoëffisiënt (k_L) te evalueer. Een van die wyne wat gebruik is, is in twee verdeel, die een helfte waarvan met bentoniet behandel is en die ander nie. 'n Borrelkolom met 'n klip sprinkeltoestel (*stone sparger*) is vir die eksperimente gebruik. Die ontgassingsprosedure (*gassing out*) en 'n tweede-orde model is gebruik om $k_L a$ te bepaal. Borrel beelding (*imaging*) is gedoen om die oppervlakte van die koppelvlak, en gevolglik die k_L, te bepaal.

Tydens suurstofdesorpsie in die wyn het die $k_L a$-waardes tussen 0.0125 s^{-1} en 0.0275 s^{-1} gewissel, afhangend van die wyn. Die $k_L a$-waarde tydens suurstofdesorpsie met 'n 10% etanoloplossing was 0.0275 s^1. Die toevoeging van 'n klein hoeveelheid gliserol aan hierdie stelsel het die $k_L a$ tot 0.0225 s^{-1} verminder. Verdere toevoegings van organiese sure het nie die $k_L a$ geaffekteer nie, terwyl die toevoeging van proteïen in die vorm van BSA en gis-ekstrak die $k_L a$ tot ongeveer 0.0175 s^{-1} verminder het. Die $k_L a$ tydens suurstofdesorpsie in 'n wyn wat proteïen-onstabiel was, het verbeter van 0.009 s^1 tot 0.015 s^1 ná behandeling met bentoniet.

Tydens desorpsie was daar geen betekenisvolle verandering in die D_{32} en in die oppervlakte van die koppelvlak tussen stelsels wat wyn of model-wynoplossings bevat het nie. Gevolglik kon die verskille in die $k_L a$-waardes almal aan verskille in die k_L toegeskryf word. Tydens suurstofdesorpsie was die k_L-waardes in die verskillende wyne tussen 0.015 en 0.045 mm/s. Die k_L-waardes was tussen 0.03 en 0.04 mm/s in 'n 10% etanoloplossing, asook in die model-wynoplossings wat gliserol en organiese sure bevat het. Die k_L-waardes het met tussen 0.02 en 0.03 mm/s gedaal met die toevoeging van proteïen aan die model-wynoplossing. Die behandeling van 'n wyn wat proteïen-onstabiel was met bentoniet het die k_L-waarde van 0.017 mm/s tot 0.0225 mm/s verhoog.

Die kombinasie van die afname van die k_L toe proteïen by 'n model-wynoplossing gevoeg is en die verbetering van die k_L toe die wyn met bentoniet behandel is, suggereer dat proteïene in wyn die suurstofdesorpsie-tempo's aansienlik beïnvloed. Daar word voorgestel dat wynmakers die suurstof-k_L in hulle stelsel kan verbeter deur teen hoër gasvloeitempo's te werk om die turbulensie tydens desorpsie te verhoog. Die doeltreffendste manier om die desorpsietempo te verbeter, is egter om 'n sprinkeltoestel te gebruik wat kleiner borrels produseer om sodoende die oppervlakte

van die koppelvlak te vergroot. Daar word ook voorgestel dat desorpsie ná brei uitgevoer word, aangesien die k_L groter sal wees.

Biographical sketch

Steven Sutton was born on the 11th of July 1996 in East London. He grew up in Polokwane and matriculated in 2013. In 2018 he graduated with a BSc. in Chemical Engineering at the University of Cape Town. He enrolled in an MScAgric (Wine Biotechnology) in 2020, at the Department of Viticulture and Oenology at Stellenbosch University.

Acknowledgements

I wish to express my sincere gratitude and appreciation to the following persons and institutions:

My supervisors Prof. Wessel Du Toit and Prof. Robert Pott for setting this project up and for all their support and guidance throughout.

Ayman Abufalgha, for all his assistance with the experimental setup and guiding me through the experimental process.

Marisa Nell, Edmund Lakey and Andy van Wyk, for all their assistance in the experimental cellar.

My parents, Anne and Chris Sutton, for all their support.

Preface

This thesis is presented as a compilation of 5 chapters.

Chapter 1   **Introduction and Aims**

Chapter 2   **Literature Review**

Chapter 3   **Materials and Methods**

Chapter 4   **Results and Discussion**

Chapter 5   **Conclusion**

Table of Contents

1.1.   Introduction 1

1.2.   Aims and objectives.. 4

Chapter 2: Literature Review……………………………………………………………………….6

2.1.   Introduction... 6

2.2.   Methods for the removal of dissolved oxygen 7

2.3.   Desorption 10

2.4.   Two-film theory and the mass transfer equation 12

2.5.   Factors that affect desorption 15

    2.5.1.   Physico-chemical factors... 16

    2.5.2.   Hydrodynamic conditions 17

    2.5.3.   Design factors.. 20

    2.5.4.   Operating factors... 21

2.6.   Studies on the physico-chemical factors that affect oxygen mass transfer 21

    2.6.1.   Mass transfer studies of oxygen in wine 24

    2.6.2.   Studies on the changing viscosity in wine... 27

    2.6.3.   Mass transfer studies of oxygen in aqueous solutions 28

    2.6.4.   Summary of oxygen mass transfer... 30

2.7.   Methods for measuring the volumetric mass transfer coefficient and the interfacial area
    30

    2.7.1.   Methods for measuring the volumetric mass transfer coefficient...................... 30

    2.7.2.   Measuring the interfacial area.. 33

2.8.   Summary of the literature review... 33

Chapter 3: Materials and Methods…………………………………………………………….....35

3.1.   Materials 35

    3.1.1.   Model aqueous and wine solutions 35

    3.1.2.   Wines 35

3.2.   Methods 36

    3.2.1.   Experimental setup 36

    3.2.2.   Experimental procedure 39

    3.2.3.   Measuring the kLa.. 40

    3.2.4.   Measuring the gas holdup 41

    3.2.5.   Measuring the Sauter mean diameter 42

    3.2.6.   Measuring the interfacial area and the mass transfer coefficient 46

Nomenclature

$k_L a$	The volumetric mass transfer coefficient (s^{-1})
k_L	Mass transfer coefficient (mm/s)
a	Specific interfacial area (mm^2/mm^3)
J	Flux (kg/m^{2}s^1)
K_G	Total gas side mass transfer coefficient (s^{-1})
K_L	Total liquid side mass transfer coefficient (s^{-1})
p_G	Partial pressure of the species in the bulk gas (Pa)
C_L	Concentration of the species in the liquid (mg/L)
p_i	Partial pressure of the species at the gas-liquid interface (Pa)
C_i	Concentration of the species at the gas-liquid interface (mg/L)
H	Henry's Law Constant (Pa.L/g)
p^*	Partial pressure of the species when each phase is in equilibrium (Pa)
C^*	Equilibrium concentration of the species (mg/L)
N	Total mass flowrate per unit volume per sec (kg/m^{3}s^1)
$C_{L,t}$	The concentration of the species in the liquid at time t (mg/L)
$C_{L,0}$	The initial concentration of the species in the liquid (mg/L)
θ	Constant for correcting the $k_L a$ value for temperature
τ_P	Oxygen probe response lag (s)
Q_G	Volumetric flowrate of a gas (m^3/s)
Q_{air}	Volumetric flowrate of air (m^3/s)
ρ_G	Density of a gas (kg/m^3)
P	Pressure (atm)
T	Temperature (°C)
$C_{O2,t}$	The concentration of oxygen in the liquid at time t (mg/L)
$C_{O2,i}$	The initial concentration of oxygen in the liquid (mg/L)
k_p	Probe constant (s^{-1})
C_p	The concentration of the species as measured by the oxygen probe (mg/L)
$\dfrac{C_p}{C}$	Ratio of the measured probe concentration and the initial concentration
ε_G	Gas holdup
$H_{sparging}$	The height of the liquid in the bubble column during sparging, as measured from the base of the column
H_0	The height of the liquid in the bubble column when at rest, as measured from the base of the column
D_{32}	Sauter mean bubble diameter (mm)
D_F	Feredt diameter of bubble (mm)
A_P	The projected area of the bubble (mm^2)
τ	Shear stress (Pa)
$\dfrac{d\gamma}{dt}$	Rate of shear strain (s^{-1})
μ	Dynamic viscosity (Pa.s)

Chapter 1: Introduction and Aims

1.1. Introduction

The removal of excess dissolved oxygen from wine prior to bottling is commonly done in winemaking. Too much oxidation can lead to browning reactions and the loss of fresh and fruity aromas (Coetzee & Du Toit, 2015). However, too little dissolved oxygen may result in reductive sulphur derived off-odours, while some dissolved oxygen is desired to help develop red wine, enhancing the colour and reducing astringency (Lopes, Silva, Pons, *et al.*, 2009; Singleton, Trousdale & Zaya, 1979). The level of dissolved oxygen in wine prior to packaging is an important parameter to control.

Wine picks up oxygen throughout the winemaking process, wherever it comes into contact with air. Often, the total oxygen pickup by the end of the process is higher than desired. The desired concentration is typically below 1.25 mg/L, but this is dependent on the winemaker and the style of wine (Steiner, 2013). It is usually just before the point of packaging that the wine will be contacted with an inert gas, in a process known as desorption or sparging. The inert gas is often nitrogen, argon, carbon dioxide, or a mixture of nitrogen and carbon dioxide. Nitrogen is preferred over argon as it is cheaper. A mix of nitrogen and carbon dioxide is often used to maintain dissolved carbon dioxide levels within the wine, but it is less efficient than pure nitrogen (Vidal & Moutounet, 2008). Sparging often takes place in a vessel, in which a sparger is placed at the bottom, and the inert gas rises through the wine, removing dissolved oxygen. An in-line sparger is also used, and the same principles apply to it (Nordestgaard, 2018).

Winemakers have indicated that under similar conditions, the desorption of oxygen from different wines sometimes seems to occur at different rates. An indicator of the rate of oxygen desorption is the oxygen desorption volumetric mass transfer coefficient ($k_L a$), which can be determined experimentally within a bubble column. $k_L a$ is a composite parameter made up of individual parameters: the mass transfer coefficient (k_L), and the interfacial area (a) (Besagni, Inzoli & Ziegenhein, 2018).

Two film theory is used to model gas-liquid mass transfer. It describes the interface between the gas bubble and the liquid, as containing two layers: the liquid side layer and the gas side layer (Garcia-Ochoa & Gomez, 2009). When sparging takes place, a concentration gradient of the compound is created across the interface, and the equilibrium between the component

in the liquid and gas is disrupted. Mass transfer will occur until the equilibrium is reached, at which point the gradient is flattened.

For the desorption of oxygen from wine, the gas and the liquid side layer on either side of the interface, make up the resistance to mass transfer. However, in the case of low soluble gases such as oxygen in wine, the gas side layer provides very little resistance and is considered negligible, and the total resistance can be described by the liquid side layer resistance to mass transfer: k_L. The interfacial area is the total area through which mass transfer can take place, and it is the surface area of the gas bubbles exposed to the liquid, divided by the total volume of gas in the liquid, at any moment in time (Pittoors, Guo & Van Hulle, 2014). Together these form the $k_L a$. By evaluating these individual parameters, a greater understanding of gas-liquid mass transfer is gained.

The determination of $k_L a$ is performed using a gassing out procedure (GOP), in which the system is saturated with oxygen from air, and subsequently sparged with nitrogen. A probe measures the change in concentration of dissolved oxygen, and from this the $k_L a$ is determined. The probe often has an associated probe lag – a delay in which what is measured by the probe is not the actual dissolved oxygen concentration within the system at that instantaneous time (Clarke & Manyuchi, 2012). A second order mass transfer measurement model, with $k_L a$ as a parameter, can be used to account for this lag and more accurately obtain $k_L a$.

The interfacial area can be determined through image analysis. Obtaining images of bubbles within the system allows for the measurement of the Sauter mean bubble diameter (D_{32}), which is a measure of the mean bubble size within the column during sparging. From this, and the gas holdup (the volume fraction of gas present within the active system at any moment in time), the interfacial area can be obtained. The k_L can subsequently be obtained from the measured $k_L a$ and a.

Four categories of factors influence the volumetric mass transfer coefficient (Besagni *et al.*, 2018). These are design, operating, physico-chemical, and hydrodynamics factors.

The hydrodynamics of the system describe the way in which the bubbles interact within the system. Hydrodynamic conditions can be grouped into different flow regimes. The homogeneous regime is indicative of bubbles steadily moving upwards in a uniform pattern. The heterogeneous regime is indicative of a turbulent system in which bubbles can coalesce

easily and move radially and downwards throughout the system (Kantarci, Borak & Ulgen, 2005; Ruzicka, Drahoš, Mena, *et al.*, 2003). The homogeneous regime allows for more efficient mass transfer. It can easily be obtained by operating at lower gas flowrates and with a bubble column that has a height to diameter ratio of at least 5 (Besagni, Gallazzini & Inzoli, 2019). In this study, all experiments will be performed in a bubble column, operating within the homogenous regime.

The design factors that affect desorption are vessel dimensions and sparger design. Operating factors that can affect desorption are temperature, pressure, and gas flowrate. The physico-chemical factors that can affect $k_L a$ include viscosity, surface tension, liquid diffusivity, and liquid and gas density (Akita & Yoshida, 1973). These properties are dependent on the composition of the liquid and gas within the system. Additionally, the manner in which compounds interact at the gas-liquid boundary will also affect desorption (Zahradník, Fialová & Linek, 1999). Of importance to this project is understanding the physico-chemical properties that can affect the oxygen desorption $k_L a$ in wine. The significant variation of certain compounds in wine may indicate why desorption occurs more readily in some wines versus others.

There have been limited studies evaluating the changes in $k_L a$ within the context of wine. These studies have been done to evaluate micro-oxygenation during fermentation. This is an absorption process (gas to liquid mass transfer). Results from absorption studies can be useful as they are often representative of how desorption systems may react to similar changes in certain factors (Hamborg, Kersten & Versteeg, 2010). It should be noted though, that despite desorption being driven by the same physical mechanisms as absorption, opposite effects have sometimes been observed (Devatine, Chiciuc, Poupot, *et al.*, 2007; Elhajj, Al-Hindi & Azizi, 2014). This may be explained by Maxwell-Stefan diffusion, in which the diffusion of a species may occur at different rates depending on whether molecules of different species are diffusing in the same or opposite directions, as the direction affects the frictional forces imposed between each species (Krishna & Wesselingh, 1997).

The only study looking to evaluate the oxygen desorption $k_L a$ for wine within a bubble column, investigated how dissolved carbon dioxide affects desorption. Its presence was shown to increase the desorption rate (Devatine *et al.*, 2007). Absorption studies in wine have been limited to determining the effect of ethanol, phenolic compounds, sulphur dioxide, sugar, and carbon dioxide concentrations, on the oxygen absorption $k_L a$ in model wine solutions (Chiciuc, Farines, Mietton-Peuchot, *et al.*, 2010). Ethanol has been shown to affect $k_L a$, although it is

uncertain whether this effect is observed within the ranges of ethanol concentrations found in wine. Sugar was shown to affect $k_L a$ but only at concentrations greater than 250 g/L.

There are numerous studies examining the effect of other compounds within organic and aqueous solutions, on the oxygen $k_L a$. It has been found that the presence of alcohols, acids, surfactants, the ionic strength, and changes in pH, can all affect $k_L a$ (Besagni *et al.*, 2018; Ferreira, Cardoso, Teixeira, *et al.*, 2013; Gurol & Nekouinaini, 1985; Jamnongwong, Loubiere, Dietrich, *et al.*, 2010)

Wine typically contain ethanol concentrations between 7 and 16 % v/v; sugar contents up to 150 g/L; glycerol concentrations up to 25 g/L; a variety of sulphates and ions; organic acids; polyphenols; esters; and proteins (Kunkee & Eschnauer, 2016). Changes in these compounds can affect the physico-chemical properties of wine, such as viscosity, surface tension, and density, which can consequently affect the $k_L a$.

The high concentrations of ethanol, glycerol, and sugar in wine, and their significant range in concentration between wines, means they stand out as potential factors that could affect the desorption $k_L a$. It has been also been shown that even the presence of compounds at very small concentrations may influence $k_L a$, such as organic acids or surfactants. (Jamnongwong *et al.*, 2010).

There are gaps in knowledge about the mechanics that control oxygen desorption in wine. There is a greater understanding of the absorption of oxygen during wine processing, and in general there is a greater focus on assessing absorption processes as opposed to desorption processes. This study provides new insight as to the extent that oxygen desorption varies in different wines. It contributes towards determining how certain compounds in wine affect desorption. By analyzing both the interfacial area and the oxygen mass transfer coefficient, a more detailed understanding can be gained as to how changes in the concentration of these compounds exactly affect oxygen desorption. This build-up of knowledge on the oxygen desorption process in wine will allow for improvements in the design of desorption units and operation of the desorption process.

1.2. Aims and objectives

The main research aims for this study were:
- To determine the extent of the variation of oxygen desorption rates within different wines.

- To determine which mechanisms are responsible for the variation of oxygen desorption rates within different wines.
- To identify compounds in wine that are significant in affecting the oxygen desorption rate.

The objectives required to achieve these aims were:

- Develop an experimental setup that will allow for the following parameters to be accurately measured: The oxygen desorption $k_L a$, the gas holdup, the Sauter mean bubble diameter, the interfacial area, and the k_L.
- Evaluate the oxygen desorption $k_L a$, the interfacial area, and the k_L, for a set of wines.
- Observe how changes in operating conditions affect the $k_L a$ within the experimental setup.
- Conduct a review of literature to establish what compounds are likely to have a significant effect on the oxygen desorption rate within wine.
- Design a set of experiments such that the effect of a particular compound's presence on oxygen desorption can be elucidated.
- Evaluate the oxygen desorption $k_L a$, the interfacial area, and the k_L, for a set of model wine solutions.
- Establish whether wine fining can affect the oxygen desorption rate, by evaluating the oxygen desorption $k_L a$, the interfacial area, and the k_L, for a wine that has undergone two different types of treatment.

Chapter 2: Literature Review

2.1. Introduction

Exposure of oxygen to must and wine occurs throughout the winemaking process. At the point of packaging, the dissolved oxygen in the wine is the sum of the dissolved oxygen that remains at the end of fermentation and the oxygen absorbed from air in subsequent process steps, minus the oxygen consumed through oxidation reactions and by yeast (Ugliano, 2013).

The process steps within which oxygen can be picked up by the wine include racking, pumping, cold stabilisation, filtration and packaging (Castellari, Simonato, Tornielli, *et al.*, 2004; Steiner, 2013). Cold stabilisation and refrigeration are often listed as the two process steps that result in the highest oxygen pickup. This is probably due to the rise in dissolved oxygen saturation concentration due to the decrease in temperature (Coetzee & Du Toit, 2015). The saturation concentration is the maximum concentration of dissolved oxygen that wine can contain at a specific set of conditions. When temperature is reduced, the oxygen saturation concentration in wine increases, allowing for a greater pickup of oxygen (Bewtra, Nicholas & Polkowski, 1970).

The rate at which oxygen is transferred from either the surrounding gas into the wine, or from the wine to the surrounding gas, is the oxygen transfer rate (OTR). It is estimated that at the end of wine processing, at the point of packaging, the concentration of dissolved oxygen in wine is within the range of 1 and 8.5 mg/L (Coetzee & Du Toit, 2015; Ugliano, 2013). The desired amount of dissolved oxygen in must or wine is dependent on numerous factors, but it is typically below or at the lower end of this range. Steiner (2013) recommends that prior to packaging, the dissolved oxygen concentration should be below 1.25 mg/L for red wines and below 0.6 mg/L for rosés and white wines.

During fermentation, a certain amount of oxygen is required to ensure that the fermentation can fully take place (Zoecklein, Fugelsang, Gump, *et al.*, 1999). Dissolved oxygen is not inert within wine, and oxidation reactions can occur with some of the compounds in wine (Coetzee & Du Toit, 2015). Many of these reactions are undesirable and consequently the presence of excess amounts of dissolved oxygen in wine can be detrimental to the quality of the wine. Dissolved oxygen can induce browning reactions and produce off-aromas (Saa, Pérez-Correa, Celentano, *et al.*, 2013). In white wine, too much oxidation can lead to the loss of fresh and fruity aromas (Coetzee & Du Toit, 2015; Singleton *et al.*, 1979). It has also been suggested that too little oxygen exposure within the wine can result in reductive off-odours (Lopes *et al.*, 2009). Some amount of oxygen contact is considered beneficial for red wine maturation,

particularly as it is believed to result in phenolic reactions that produce enhanced colours, polymerized phenolics and reduced astringency (Lopes *et al.*, 2009; Singleton *et al.*, 1979). Hence there is a desire to control the dissolved oxygen concentration present in the wine just before packaging.

The concentration of dissolved oxygen in wine is an important process parameter to be controlled or monitored during winemaking. There is often a dedicated step within wineries for the reduction of dissolved oxygen. The typical point at which dissolved oxygen is removed from wine is right at the end of the winemaking process. This is done to minimise further oxygen pickup, allowing for better control of the dissolved oxygen concentration present just before packaging.

2.2.   Methods for the removal of dissolved oxygen

The typical step for removing dissolved oxygen from wine is through sparging an inert gas through a vessel such as a bubble column or through an in-line sparger (Cant, 1960; Vidal & Moutounet, 2008). While there are other methods for removing dissolved oxygen from solution, they are often not suitable for wine. These included boiling at atmospheric pressure or boiling under reduced pressure (Butler, Schoonen & Rickard, 1994). However, boiling of wine at atmospheric or reduced pressure is an energy intensive step compared to sparging. It would also be detrimental to the quality of the wine, with the destruction of favourable aromatic components as well as the loss of ethanol.

Recently, membrane contactors have been introduced into some wine industries (Nordestgaard, 2018). They are considered less invasive, as the process does not remove aromatic compounds from the wine. However, they require a larger capital cost, regular cleaning of the membrane, and the wine needs to be well filtered before being contacted with the membrane (Nordestgaard, 2018). It also does not remove aromatic compounds, which has been an industry concern. Recent research, however, has also shown that sparging with nitrogen does not remove any significant amount of aromatic compounds in some wines (Walls, 2019). The study by Walls (2019) was performed on a Chenin Blanc and a Sauvignon Blanc wine, in which sparging was performed for an hour from a stone sparger. It should be considered that the results might not be replicable for wines containing different sets of aromatic compounds.

A wide range of gases can be used for the removal of dissolved oxygen in wine. The criteria for gas would be one that it is inert and does not react with the compounds it comes into

contact with. It is also important that the gas is widely available and cheap. Gases that best fit this criteria are nitrogen, carbon dioxide and argon (Zoecklein *et al.*, 1999).

Using carbon dioxide may cause the undesirable effect of saturating the wine with carbon dioxide, resulting in the sensory alteration of the wine, which may cause the wine to taste 'spritzy' or 'fizzy' (Ough, 2018). Nitrogen and argon are significantly less soluble in wine than carbon dioxide, and so this effect does not occur. However, sparging with just nitrogen or argon may reduce the dissolved carbon dioxide levels to undesirable amounts. Carbon dioxide plays a role in the taste and astringency of wine (Gawel, Schulkin, Smith, *et al.*, 2020). Too little carbon dioxide can negatively affect the quality of the wine by contributing to undesired perceived tastes of the wine or 'flat' characteristics (Zoecklein *et al.*, 1999). The optimal range of carbon dioxide present in still wine is between 500 and 1800 mg/L for white wine, and between 500 and 1000 mg/L for red wine (Gawel *et al.*, 2020). After fermentation, carbon dioxide levels are typically within this region. To deal with the possibility of carbon dioxide removal, many wineries sparge with a blend of nitrogen and carbon dioxide (Zoecklein *et al.*, 1999), or re-sparge with carbon dioxide once the nitrogen sparging is done. Sparging with a blend of carbon dioxide and nitrogen is not as effective at oxygen removal as using pure nitrogen (Cant, 1960). It has been reported that as the proportion of carbon dioxide in a gas mixture increases, the dissolved oxygen removal rate decreases (Vidal & Moutounet, 2008).

The most widely used methods for oxygen removal in wine are in-line sparging or sparging through a vessel. A bubble/stripping column is typically the most effective vessel for the removal of dissolved oxygen. Bubble columns have a larger height to diameter ratio, allowing for a greater contact time as the gas passes through the wine. The gas bubbles enter the column through a hose or sparger/sinter at the base of the column. Under standard operating conditions for gases with low solubilities such as oxygen, the removal of the dissolved gas occurs throughout the whole column. Even for tall columns, bubbles will continue to remove oxygen as they rise to the top of the column. Typically, the rate of oxygen transfer is too slow relative to the bubble residence time and consequently no equilibrium is reached between the oxygen in the gas bubble and the liquid. Hence, a bubble will continue to remove oxygen until it breaches the top of the liquid (Besagni *et al.*, 2018).

Advantages of the bubble column are that they typically have very good mass transfer characteristics (Kantarci *et al.*, 2005). An in-line sparger introduces small gas bubbles directly into a stream of wine flowing through a pipe. The efficiency of a bubble column versus an in-line sparger is dependent on numerous factors.

Cant (1960) compared the efficiency of using an in-line nitrogen sparger and a bubble column for the removal of dissolved oxygen. It was found that, for oxygen saturated wine, a single pass through a bubble column reduced the dissolved oxygen concentration to a greater extent than through an in-line sparger. For wine with lower levels of dissolved oxygen, the two methods were found to be similarly effective. However, the results of the study are not necessarily indicative of one unit being more effective than the other, as there are numerous unaccounted-for factors that will affect the efficiency of each process. The process behind each unit is the same – facilitating liquid-gas mass transfer through the contacting of an inert gas to wine.

Bubble columns are widely used in lab scale and pilot scale plants, as they give a good estimate of what occurs during industrial scale operations. As the process for in-line sparging is the same as sparging through a bubble column, data obtained from bubble column experiments is also useful for understanding and improving in-line sparging operations.

A basic diagram of a bubble column and an in-line sparger is shown in Figure 2.1 below.
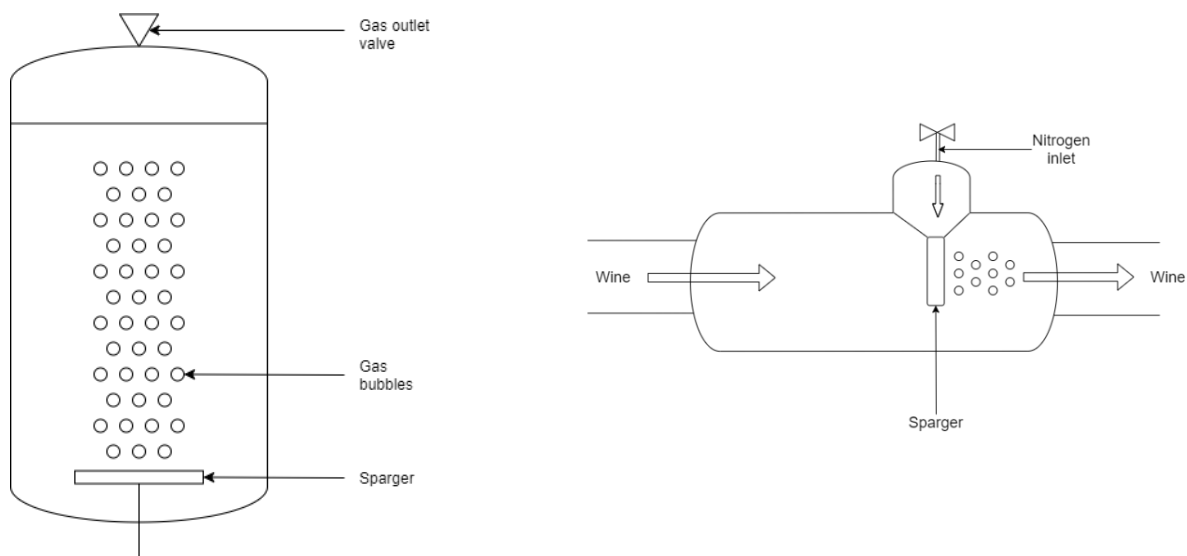

Figure 2.1: Basic diagram of a bubble column on the left, and an in-line sparger on the right

Currently, either of these two units are applied in winemaking. Less attention has been applied to evaluating the processes that occur within these units compared to other winemaking steps. As the dissolved oxygen level is an important parameter that requires controlling, it is useful to understand the mechanics behind sparging with an inert gas.

Wineries will have various ways in which they estimate how much nitrogen they may need for a sparging operation. Figure 2.2 below, adapted from Zoecklein et al. (1999), provides a guide that gives a basic estimate of how much nitrogen can be used to remove a certain amount of dissolved oxygen from wine. However, the actual amount of nitrogen required will depend on several factors not accounted for in the graph, such as the equipment used for nitrogen sparging, operating temperature, operating pressure, the gas flowrate, as well as the characteristics of the wine.
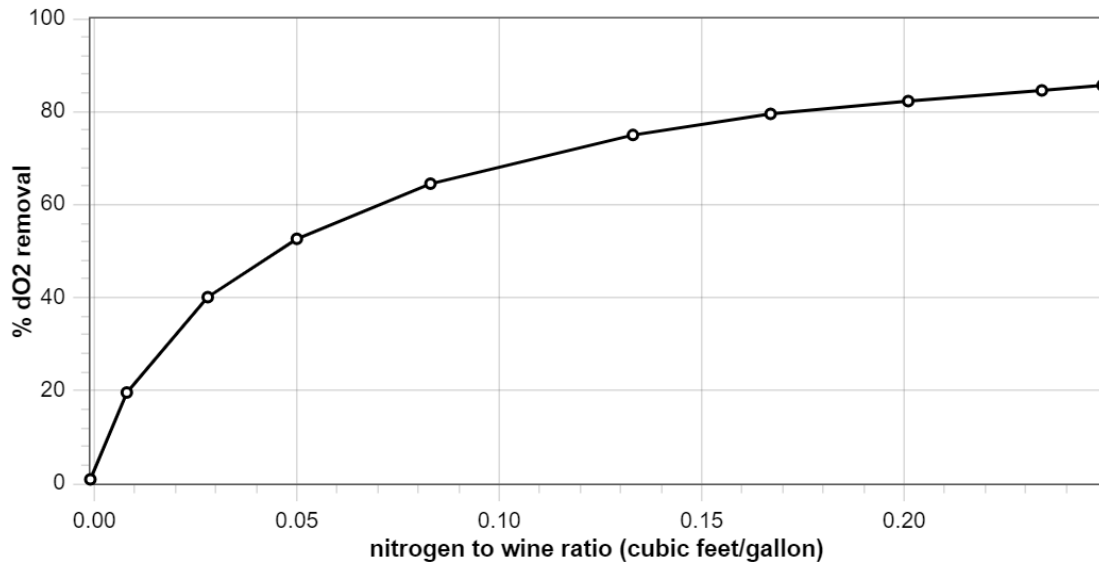

Figure 2.2: Graph shown the estimated amount of nitrogen needed to remove varying portions of dissolved oxygen in wine in a bubble column, redrawn from a graph presented by Zoecklein et al. (1999).

Ultimately, having a greater knowledge of the process will allow for greater control of the exact desired oxygen level in the wine prior to packaging, as well as allowing for more cost effective and efficient ways for sparging to take place.

2.3. Desorption

The mechanism through which nitrogen removes dissolved oxygen from wine is liquid-gas mass transfer. Absorption and desorption are two types of liquid-gas mass transfer. Absorption is a process in which compounds are removed from a gas stream into a liquid stream. Desorption is the opposite process in which liquid soluble compounds are transferred from a liquid into a gas stream.

The driving force for the mass transfer in both cases is the difference in the concentration of the compounds in the gas and the liquid phase (Elhajj *et al.*, 2014). A gas-liquid equilibrium is reached when the rate of transfer of the gas into the liquid is equal to the rate of transfer from the liquid into the gas. The equilibrium concentration of dissolved oxygen in a liquid, when

exposed to air, will also be the oxygen saturation concentration in air. In absorption cases, the dissolved oxygen concentration increases until the saturation concentration is reached. In desorption cases, contacting a liquid to a gas containing no oxygen or a gas containing oxygen less than the equilibrium concentration, creates a partial pressure difference. This drives the dissolved oxygen from the liquid into the gas (Pittoors *et al.*, 2014). If a continuous supply of an inert gas containing no oxygen, such as nitrogen, is contacted with a liquid containing dissolved oxygen (as in the case of bubbling inert gas through a bubble column), the amount of dissolved oxygen in the liquid will eventually reduce to zero (Garcia-Ochoa & Gomez, 2009).

Figure 2.3 is a basic diagram showing the desorption of oxygen from a bulk liquid into a nitrogen bubble. This is the basic mass transfer process that will be examined for the nitrogen sparging of wine.
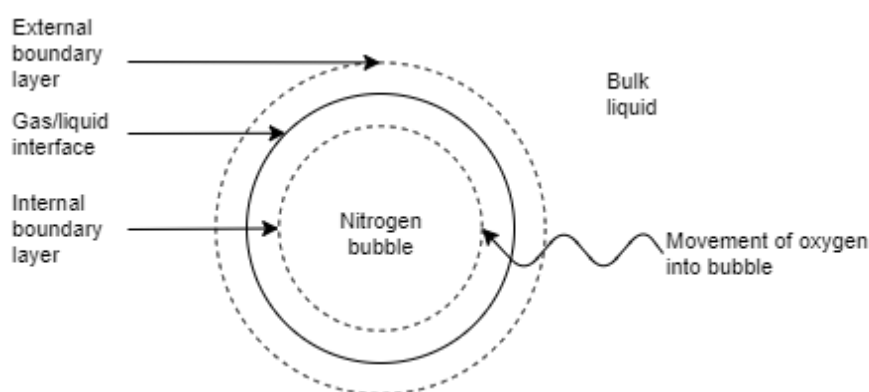

Figure 2.3: Diagram demonstrating the desorption of oxygen into a nitrogen bubble

Aside from the difference in the partial pressures of oxygen in the liquid and gas, there is another parameter that is key to the understanding of the liquid-gas mass transfer of oxygen. This is a composite parameter known as the volumetric mass transfer coefficient ($k_L a$), which describes the resistance experienced by a compound as it moves through the boundary layers between the liquid and the gas (Garcia-Ochoa & Gomez, 2009). The understanding of this coefficient is key to the understanding of liquid-gas mass transfer.

The only papers found specifically examining the mechanics of gas-liquid mass transfer within wine, including evaluating the volumetric mass transfer coefficient, have focused on enhancing micro-oxygenation in wine during fermentation (Chiciuc *et al.*, 2010; Devatine, Chiciuc & Mietton-Peuchot, 2011; Devatine *et al.*, 2007; Moenne, Saa, Laurie, *et al.*, 2014; Saa *et al.*, 2013). There have been several studies examining and quantifying the addition of oxygen, and to a lesser extent the removal of oxygen, from a variety of aqueous mixtures. These studies are useful within the context of this project, as they provide insight into how changes in liquid and gas properties affect mass transfer. They also demonstrate how mass

transfer in bubble columns can be assessed and quantified. Extensive reviews of these studies have been performed by Kantarci et al. (2005), Besagni et al. (2018) and Manjrekar (2016).

2.4. Two-film theory and the mass transfer equation

Two-film theory is the theory most widely used to describe liquid-gas mass transfer phenomena (Hamborg *et al.*, 2010; Pittoors *et al.*, 2014). While absorption is the most studied liquid-gas mass transfer process, desorption can be modelled based on the two-film theory in the same manner that absorption can (Hamborg *et al.*, 2010).

The two films in question in two-film theory are the gas film and the liquid film, which are on either side of the interface of the gas and liquid as shown in Figure 2.3. Beyond the gas film, is the bulk gas phase and beyond the liquid film is the bulk liquid phase. The edge of each film is known as the boundary layer. The liquid and gas films control the transport of molecules across the interface (Pittoors *et al.*, 2014).

If, during mass transfer, the compound transferring from one phase to another was instantly mixed into the bulk of one phase, then no film would be present. However, this is not the case due to slow mixing, and instead, there is a concentration gradient between the interface and the edge of the film. The edge of the film is the point at which the concentration of the compound is the same as the concentration of that compound within the bulk phase. The slower the movement of the compound from the interface to the bulk phase is, the greater the concentration difference between the two will be, and the greater the resistance to mass transfer (Wiesmann, Choi & Dombrowski, 2006). Figure 2.4 below shows how the concentration of oxygen would vary across the films in a typical desorption process. The end of the film occurs when the concentration flattens.
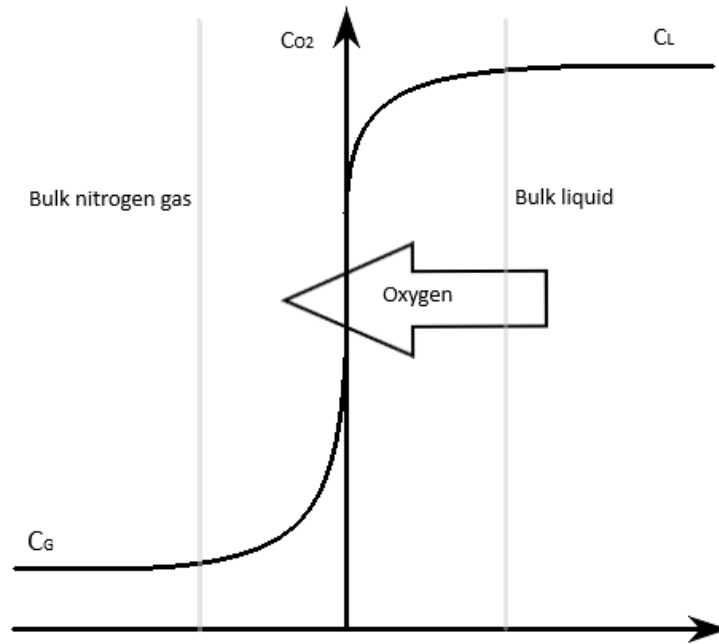
Figure 2.4: Two film theory adapted from Wiesmann et al. (2006)

Sometimes, the resistance of one film is significantly less than that of the other film. This is the case when a molecule enters the gas film from the interface and subsequently disperses much more quickly into the bulk gas phase than the relative molecule in the bulk liquid phase moving into the liquid film. One example of this is for gases that are not very soluble within the bulk liquid, which is typically the case for nitrogen or oxygen. In these cases, the transfer resistance within the gas film is several orders of magnitude lower than the resistance in the liquid film, and only the liquid film resistance is then taken into account (Garcia-Ochoa & Gomez, 2009).

Two-film theory can be described mathematically. Firstly, the flux (J) through each film can be described as shown in equation 1. The flux is the flow of the compound per unit area per unit time.

$$J = k_G(p_G - p_i) = k_L(C_i - C_L) \tag{1}$$

Both k_G and k_L are the local mass transfer coefficients for the gas and liquid side respectively, representative of the resistance to mass transfer of each film. Both p_i and C_i represent the partial pressure of the species and the concentration of the species at the gas -liquid interface, respectively. Both p_G and C_L represent the partial pressure and concentration of the species in the bulk gas and bulk liquid, respectively (Garcia-Ochoa & Gomez, 2009). As the concentration of species at the interface is very difficult to measure accurately (Garcia-Ochoa & Gomez, 2009), this equation is typically rewritten as shown in equation 2.

$$J = K_G(p_G - p^*) = K_L(C^* - C_L) \tag{2}$$

In this case, p^* is the compound pressure when each phase is in equilibrium. K_L and K_G are the total mass transfer coefficients for the liquid and gas side respectively. For a simple gas that follows Henry's law, p^* can be equated to the equilibrium concentration (C^*) of the species using a Henry's law constant (H) for that species, as shown in equation 3.

$$p^* = HC^* \tag{3}$$

C^* is the compound equilibrium concentration in the liquid phase. The total mass transfer resistance is the sum of the resistance in the gas film ($\frac{1}{Hk_G}$), and the resistance in the liquid film ($\frac{1}{k_L}$), as shown in equation 4 (Wiesmann *et al.*, 2006)

$$\frac{1}{K_L} = \frac{1}{Hk_G} + \frac{1}{k_L} \tag{4}$$

In the case of compounds that are not very soluble in liquids such as simple gases like nitrogen and oxygen, the H value is very high, making that term negligible relative to the liquid side resistance, and so the equation reduces to equation 5, in which the total mass transfer coefficient is equated to the local mass transfer coefficient.

$$\frac{1}{K_L} = \frac{1}{k_L}; K_L = k_L \tag{5}$$

In this case, the flux can then be described through equation 6.

$$J = k_L(C^* - C_L) \tag{6}$$

For absorption situations, when the liquid is exposed to air, the saturation concentration of oxygen in air will be its equilibrium concentration. In lab scale bubble columns, in the cases of desorption of low saturation gases such as oxygen, it is often assumed that the partial pressure of the desorbed oxygen in the bubble will have a negligible effect on the total pressure in the gas bubble as it continues to rise through the bubble column (Garcia-Ochoa & Gomez, 2009). This is due to the relatively slow mass transfer of oxygen, and that the volume fraction of dissolved oxygen removed versus the volume of nitrogen bubbled through the column is very small. Under this assumption, the equilibrium concentration of dissolved oxygen in a liquid, when exposed to a continuously flowing gas with a negligible concentration of oxygen, will tend to zero.

The total mass transfer of a compound from liquid to a gas per unit area of volume can then be obtained through multiplying the total flux through the specific interfacial area (a) of the gas and the liquid phases as shown in equation 7.

$$N_{oxygen} = a.J = k_L a(C^* - C_L) \tag{7}$$

The value $k_L a$ is referred to as the volumetric mass transfer coefficient. The final oxygen transfer rate can be described as shown in equation 8.

$$OTR = \frac{dC_{oxygen}}{dt} = k_L a(C^* - C_L) \tag{8}$$

In cases of desorption where the equilibrium concentration is assumed to be zero, this equation will simplify to equation 9.

$$OTR = \frac{dC_{oxygen}}{dt} = k_L a(-C_L) \tag{9}$$

The integration of the two above equations result in the following two equations for absorption (equation 10) and desorption (equation 11) of oxygen in a bubble column respectively (Garcia-Ochoa & Gomez, 2009).

Absorption:

$$ln\left(1 - \frac{C_{L,t}}{C^*}\right) = -k_L a.t \tag{10}$$

Desorption:

$$ln\left(\frac{C_{L,t}}{C_{L,0}}\right) = -k_L a.t \tag{11}$$

Where $C_{L,t}$ is the concentration of oxygen in the liquid at time t, and $C_{L,0}$ is the initial concentration of dissolved oxygen in the liquid.

Two-film theory provides an effective way for determining the volumetric mass transfer coefficient, by measuring the change in dissolved oxygen concentration over time. Measuring the $k_L a$ accurately for different systems and system conditions allows for an evaluation of factors that may affect the $k_L a$.

2.5. Factors that affect desorption

In this section, factors that affect the volumetric mass transfer coefficient and its constituents will be discussed. It is important to note that the volumetric mass transfer coefficient is a composite parameter, the components of which are the mass transfer coefficient (k_L) and the interfacial area (a).

The interfacial area is a measure of the total area of gas exposed to the liquid over the total volume of gas in the liquid, at any moment in time. As a gas bubble rises through the column, it may coalesce with other bubbles, or may break up into smaller bubbles (particularly the case if encountering an obstacle such as an impeller). The bubble may rise uniformly and straight to the surface, or it may move radially through the column, or be drawn downwards back towards the bottom of the column. These changes will all affect the total interfacial area.

The mass transfer coefficient is a measure of rate at which a compound diffuses across the liquid-gas interface. For the case of a dissolved oxygen molecule that encounters a nitrogen gas bubble, the concentration gradient between the gas-liquid interface and the edge of the outer bubble film allows the molecule to diffuse across into the gas phase. This outer bubble film provides an 'obstacle' that the molecule must pass through, controlling the rate of desorption, and the k_L is a good measure for evaluating this resistance.

Many studies that examine gas-liquid mass transfer focus solely on the measurement of the $k_L a$. Understanding the factors that affect the components of the $k_L a$ allows for a better understanding of the mechanics of the mass transfer taking place (Kantarci *et al.*, 2005).

Factors that affect the volumetric mass transfer coefficient and its constituents can be split into four broader categories (Besagni *et al.*, 2018). These are physico-chemical, operating, design, and hydrodynamic factors. The hydrodynamic factors are significantly affected by the other three factors (Garcia-Ochoa & Gomez, 2009). In this section, the physico-chemical, operating, and design factors, and their effect on the volumetric mass transfer coefficient will be examined, along with the hydrodynamic conditions that occur within a bubble column.

2.5.1.   *Physico-chemical factors*

This section will discuss what liquid and gas properties affect $k_L a$, and the manner in which they affect $k_L a$. In section 2.6, the specific compounds within wine that may have an impact on the physico-chemical factors that may affect liquid-gas mass transfer in wine will be considered.

The physico-chemical properties of a system that have been shown to affect the volumetric mass transfer coefficient include liquid viscosity, liquid phase diffusivity, liquid and gas density, and surface tension (Akita & Yoshida, 1973). Changes to these properties can affect both or either of k_L and a.

It has been widely demonstrated that in most cases increasing viscosity results in a decrease in $k_L a$ due to lower gas-liquid interfacial areas (Besagni *et al.*, 2018; Kantarci *et al.*, 2005). At higher viscosities, bubbles tend to detach from the base of the sparger later, when the bubble size has increased, thus resulting in a reduced interfacial area (Besagni *et al.*, 2018). There is also a dual effect of viscosity on bubble size. When the viscosity is increased significantly, there is an increased turbulence within the system, leading to increased bubble coalescence. However this is not observed if the viscosity remains below a certain threshold point, where

the increase in viscosity actually stabilises the rising bubble, reducing coalescence, and increasing the boundary layer thickness (Fukuma, Muroyama & Yasunishi, 1987). Ruzicka *et al.* (2003) estimated that viscosities between 1 and 3 mPa.s stabilised the flow of bubbles (reduced bubble coalescence), while viscosities between 3 and 22 mPa.s enhanced the turbulence of the system, increasing bubble coalescence.

Changing viscosity can also affect the k_L indirectly via affecting the liquid diffusivity (Song, Seibert & Rochelle, 2014). Increased viscosity reduces the rate at which a molecule travels across the gas-liquid boundary layer thickness, consequently reducing both of k_L and $k_L a$.(Song *et al.*, 2014).

The gas density in a system is affected by the type of gas used, or the pressure of the system, which is a function of the height of the liquid in the vessel. It was found that $k_L a$ values typically increase with an increasing gas density (Jordan & Schumpe, 2001; Kantarci *et al.*, 2005). It is estimated that at lower surface tensions, the bubbles rising from a sparger will be smaller. Hence, at lower surface tensions, an increase in the interfacial area of a system is expected (Matsunaga, Kano, Maki, *et al.*, 2009).

It can also be observed which physico-chemical factors affect $k_L a$, from numerous correlations for estimating the $k_L a$. These correlations are often very system specific, but can give an idea as to the extent that changing physico-chemical properties have on $k_L a$. Liquid diffusivity, viscosity, surface tension and liquid density were all taken into account in a broader correlation by Akita & Yoshida (1973). Gas density was considered an important factor in correlations by Jordan & Schumpe (2001), and Matsunaga et al. (2009). Kantarci et al. (2005) provides an extensive overview of several correlations that have been developed for bubble columns.

It is likely then, that if the different compositions of wines significantly affect the physico-chemical properties of the wine, the oxygen desorption $k_L a$ will vary.

2.5.2.   *Hydrodynamic conditions*

Another consideration for determining the mass transfer characteristics within a vessel are the various range of hydrodynamic conditions that occur within a vessel (Besagni *et al.*, 2018). The hydrodynamic conditions define the way in which the gas and liquid interact within the system. The manner in which gas bubbles interact with each other is important to understand when considering liquid-gas mass transfer. A common way of evaluating the hydrodynamic conditions within a vessel, is to classify the type of conditions into flow regimes (Kantarci *et al.*, 2005).

Different hydrodynamic conditions are typically classified into two or three flow regimes. Manjrekar (2016) indicate three flow regimes: homogenous and heterogeneous regimes, with a transition regime between. Kantarci et al. (2005) describe three regimes: bubbly flow (homogeneous), turbulent flow (heterogeneous), and slug flow. Factors that will affect the flow regime within a vessel are superficial gas velocity, sparger configuration, liquid phase properties, gas phase density, operating pressure and column dimensions (Besagni *et al.*, 2018). It is important to understand which flow regime occurs within a system, as results for one system may only be valid for another system if the flow regime occurring within both is the same.

The superficial gas velocity is a function of the gas flowrate and the cross-sectional area of the vessel. The superficial gas velocity significantly affects the type of regime present. A bubbly flow regime or a homogeneous flow regime is encountered at superficial gas velocities less than 5 cm/s. This is a general rule of thumb, as it can vary depending on physico-chemical properties of the gas and the liquid (Besagni *et al.*, 2019). It is defined as homogeneous as there will be relatively little bubble size variation, and relatively uniform bubble rise velocity. There will also be less bubble break-up or coalescence (Kantarci *et al.*, 2005).

A system transfers from the homogeneous to the heterogeneous regime as the superficial gas velocity is increased (Ruzicka *et al.*, 2003). Within a heterogeneous regime, there are greater variations in bubble size throughout the column, and radial dispersion of the bubbles is significantly increased (Kantarci *et al.*, 2005).

Slug flow will typically only occur at even higher gas flow velocities, in vessels with diameters less than 0.3 m, and with highly viscous fluids (Deckwer & Schumpe, 1993). Slug flow can be characterised by the presence of very large misshapen bubbles, that often flow along the wall of the column, or across the entire diameter of the column (Kantarci *et al.*, 2005).

In order to understand the implications of operating within different regimes, it is important to understand gas holdup. Gas holdup is an important parameter when assessing flow regimes. Gas holdup is the ratio of the volume of gas in the liquid, to the total volume of gas and liquid in the bubble column. $k_L a$ is often correlated with gas holdup. A regularly used correlation is that $k_L a$ is proportional to gas holdup to the power of 1.1 (Deckwer & Schumpe, 1993).

This correlation is a very general approximation. It is expected then that conditions that affect the rate at which gas holdup changes will likely affect how $k_L a$ changes.

The implication of operating in the homogeneous regime is that, due to less variation in bubble sizes relative to the other regimes, it is easier to predict how gas holdup and consequently $k_L a$, may increase with increasing superficial gas velocity.

Within the heterogeneous and slug-flow regime, the coalescence of bubbles is greater and much less predictable, creating a much wider range of bubble sizes. How gas holdup increases with increasing superficial gas velocity within this regime will be more dependent on vessel dimensions (Besagni *et al.*, 2018).

Gas holdup typically increases linearly with superficial gas velocity under homogeneous conditions. However, this effect is often no longer observed within the transition regime, where the gas holdup can often remain stable, or even drop with increases in superficial gas velocity (Besagni *et al.*, 2018). Once the heterogeneous regime is reached with further increases in superficial gas velocity, the gas holdup begins to increase again, but at a slower rate relative to its increase within the homogenous regime (Deckwer & Schumpe, 1993). This effect is shown in Figure 2.5.

It is suggested that the reason for the observed effect on gas holdup in the transition regime, is that a sudden increase in bubble coalescence occurs, which increases the rate at which bubbles rise to the surface (Besagni *et al.*, 2019; Ruzicka *et al.*, 2003).
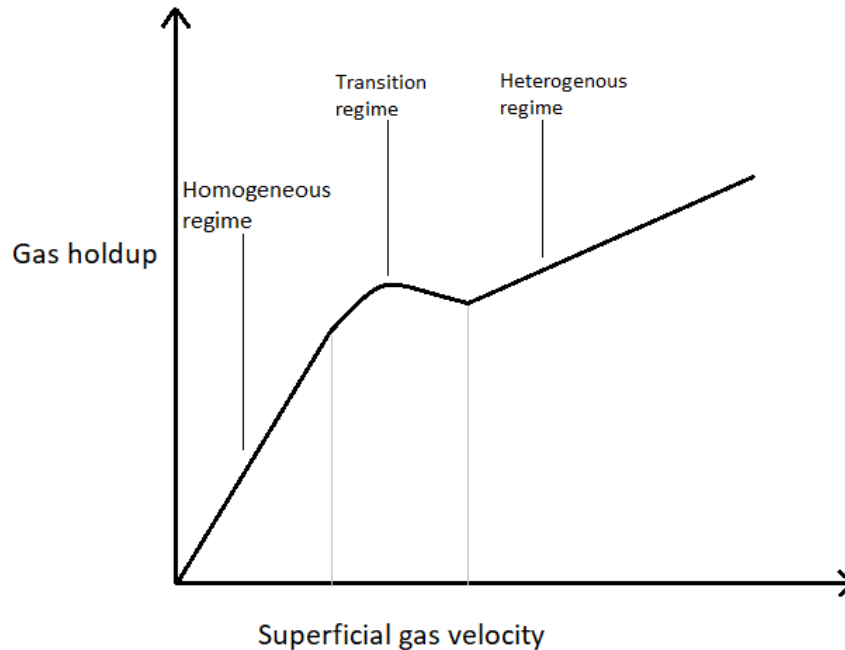
Figure 2.5: This figure demonstrates how increases in superficial gas velocity affect gas holdup in the homogeneous, transition and heterogenous regime. Adapted from (Ruzicka *et al.*, 2003).

The homogenous regime is often the preferred operating regime, as it is more controlled and allows for more efficient mass transfer to take place. The preferred regime within an industrial unit will depend on numerous factors, such as required speed of operation, required efficiency of operation in terms of raw materials and energy input, and the design of the unit

2.5.3.   *Design factors*

The design factors that typically affect the volumetric mass transfer coefficient are the vessel dimensions, and the dimensions, material and pore size of the sparger (Besagni *et al.*, 2018).

Bubble columns are designed to maximize the gas-liquid contact, and therefore typically operate with a height to diameter ratio of at least 5 (Kantarci *et al.*, 2005). This is to increase the length of time that a bubble must travel through the liquid. Operating in standard vessels that are relatively shorter and wider, will result in lower residence times for bubbles.

The column diameter does affect the $k_L a$, but typically only up to a certain point. Deckwer & Schumpe (1993) state that this effect occurs if the column diameter is less than 0.6 m, while Akita & Yoshida (1973) state it only occurs in diameters less than 0.15 m. It is likely that this is due to the wall effects on the gas flow within the column.

When it comes to column design, it is generally typically better to have a column which allows for homogenous flow to take place (Besagni *et al.*, 2018). For this to happen, the column

needs to be sufficiently wide, typically greater than 0.15 m (Besagni *et al.*, 2019). Tanks already in the cellar can be used for sparging operations, in which case, tanks that have a greater height will be preferred, although mass transfer efficiency may be less effective than in a bubble column.

2.5.4. Operating factors

Operating factors that could affect $k_L a$ include temperature, gas flowrate, and system pressure. Changing the temperature of a liquid will result in changes to the liquid properties. Increasing temperature was found to decrease the liquid viscosity and the surface tension, which are also linked to the formation of smaller bubbles on top of the sparger. The decrease in liquid viscosity and surface tension is linked to an increase in the volumetric mass transfer coefficient (Sehabiague & Morsi, 2013).

In addition to changing the bubble diameter out of the sparger, it was found that increasing temperature also increases gas diffusivity through the liquid (Sehabiague & Morsi, 2013). These changes will result in an increased mass transfer rate with an increase in temperature.

Bewtra, Nicholas and Polkowski (1970) developed a basic correlation to describe oxygen mass transfer (OTR) as a function of temperature, specifically in water, as shown in equation 12.

$$OTR \propto k_L a = k_L a_{20°C}(\theta^{(T-20)}) \qquad (12)$$

Where $k_L a_{20°C}$ is the $k_L a$ at 20 °C, and θ is a constant. For water, a constant value of 1.024 is regularly used, but values anywhere between 1.008 and 1.048 have been reported in literature (Lee, 2017). A recent study by Walls (2019) has found that increasing the temperature of wine increases the oxygen removal rate.

It has been observed that higher operating pressures in a column increase the $k_L a$, as bubble sizes are decreased at higher pressures. In addition, the OTR can also be increased as higher pressures also increase the driving force for mass transfer (Besagni *et al.*, 2018). Increasing the gas flowrate will also increase the mass transfer rate, as it increases the amount of gas in contact with the liquid at any moment in time. However, as has been mentioned, the rate at which this occurs depends on the flow regime within the vessel (Besagni *et al.*, 2018).

2.6. Studies on the physico-chemical factors that affect oxygen mass transfer

In the previous section the various factors that can affect liquid-gas mass transfer were presented. Of particular importance is how physico-chemical properties affect liquid-gas mass transfer. As mentioned, it has been noted by winemakers that under similar conditions, oxygen

desorption occurs at different rates within different wines. This indicates that differing physico-chemical properties of different wines can have a significant effect on oxygen desorption.

In this section, literature pertaining to how different properties and compounds of wine affect $k_L a$, or its physical chemical properties will be presented. In addition, literature evaluating $k_L a$ for systems which contain compounds similar to, or the same as those found in wine, will also be presented. It is important to note that most studies have examined the absorption $k_L a$, and not the desorption $k_L a$.

When comparing desorption and absorption it is important to consider the diffusion rate occurring in each instance. The diffusion rate directly affects k_L. Typically, Fick's laws of diffusion are used to describe the movement of molecules within a system. These laws describe the direction of diffusion, and consequently mass transfer, as taking place along a concentration gradient, from a place of high concentration to low concentration (Boudin, Grec, Salvarani, *et al.*, 2012).

According to this law, the same physical mechanisms that apply to absorption also apply to desorption. Fick's law of diffusion is often valid, and it is often the case that absorption and desorption values are similar, particularly for binary systems (Hamborg *et al.*, 2010).

However, there are external forces that are not considered in Fick's law. For multicomponent mixtures, Fick's law does not account for potential external forces on the system such as electrostatic or centrifugal force fields, or the concentration gradients of other compounds within the system (Krishna & Wesselingh, 1997). In instances where the rate of diffusion is not proportional to the to the concentration gradient as described by Fick's law, Maxwell-Stefan diffusion can be considered.

According to Maxwell-Stefan laws of diffusion, diffusion happens in a much more complex way. Maxwell-Stefan equations take into account how the frictional forces between different molecules of compounds influence the behaviour of the mixture (Boudin *et al.*, 2012).

In this case, rates of mass transfer in a system may differ depending on the direction in which molecules are diffusing through the gas-liquid boundary layer, particularly if there are two compounds diffusing simultaneously, even if all other conditions within the system remain the same (Cussler, 2009; Krishna & Wesselingh, 1997). Consequently, it is not unexpected if absorption and desorption values differ. This is important to consider when examining the mechanics behind absorption in a specific case.

For both desorption and absorption, increases in temperature, gas flowrate, liquid flowrate, and energy input all have a positive impact on $k_L a$ (Al-hindi & Azizi, 2018). Hamborg, Kersten and Versteeg (2010) found no differences in desorption and absorption mass transfer coefficient values for a variety of gases in a variety of solutions with varying viscosities.

However, there are instances in which the absorption and desorption $k_L a$ are not the same (Al-hindi & Azizi, 2018; Devatine *et al.*, 2007; Elhajj *et al.*, 2014; Hamborg *et al.*, 2010). This has notably been seen in the absorption/desorption of of CO_2. It has been found that desorption values in this case can be greater when carbon dioxide is supersaturated. This causes the nucleation of carbon dioxide bubbles, which introduces a new mechanism for carbon dioxide removal, in addition to desorbing into the inert gas (Al-hindi & Azizi, 2018).

There has also been observed a great discrepancy in the oxygen desorption and absorption rates for a specific system, in the presence of dissolved carbon dioxide (Devatine *et al.*, 2011). In this case, the Maxwell-Stefan diffusion may explain the discrepancy, as during desorption, both carbon dioxide and oxygen diffuse in the same direction across the gas-liquid boundary (from the liquid into the gas bubble). During absorption, oxygen and carbon dioxide diffuse in opposite direction, with oxygen diffusing into the liquid, while carbon dioxide diffuses into the gas. Maxwell-Stefan diffusion uses kinetics theory, to determine diffusion rates based on momentum transfer between molecules (Cussler, 2009).

In the absorption case, the carbon dioxide entering the gas bubble exerts a frictional force (transferring momentum) upon the oxygen molecules traveling in the opposite direction. If this frictional force is great enough, the carbon dioxide may 'drag' the oxygen molecules away from the gas-liquid boundary back into the bulk gas, reducing the concentration gradient of oxygen at the gas-liquid interface, and consequently the driving force for oxygen mass transfer.

For the case of desorption, there would be no opposing frictional force, and the carbon dioxide 'dragging' the oxygen from the boundary layer, into the bulk gas would not impede the gas transfer (It potentially may even improve the oxygen desorption rate). This would explain the phenomenon observed by Devatine *et al.* (2007), in which increasing the concentration of dissolved carbon dioxide within a system, increased the discrepancy between the desorption and absorption rate of oxygen.

Al-Hindi and Azizi (2020) also found that the carbon dioxide absorption and desorption $k_L a$ values differed within waters of various alkalinity and salinity. It was found that both the absorption and desorption $k_L a$ decreased with increasing salinity up to a threshold, although not at the same rate. There was no similar trend found for alkalinity. Absorption values decreased with increasing alkalinity, while there was no discernable effect of alkalinity on desorption values.

When carbon dioxide contacts water, it undergoes three specific chemical reactions involving carbonic acid, the bicarbonate ion, and the carbonate ion. These reaction kinetics are sensitive to the water chemistry. Adjustment in pH or salinity can significantly affect the way in which the dissolution of carbon dioxide into these various components occurs, which may subsequently affect the rate of gas to liquid mass transfer (Al-Hindi & Azizi, 2020).

It is expected that most factors that will affect absorption, will also likely have an impact on desorption, but not necessarily in the same way. Since there is a limited amount of research into desorption relative to absorption, it still remains important to review studies on absorption.

2.6.1.   Mass transfer studies of oxygen in wine

There have been few studies looking at quantifying liquid-gas mass transfer of oxygen within the context of wine. Of these studies, the primary focus has been on understanding oxygen absorption during micro-oxygenation, so as to improve micro-oxygenation during the fermentation process (Chiciuc *et al.*, 2010; Devatine *et al.*, 2007; Moenne *et al.*, 2014).

In a study done by Devatine et al. (2007), the effect that dissolved carbon dioxide had on oxygen absorption during micro-oxygenation was investigated. They evaluated both the oxygen absorption and desorption $k_L a$ for model wine solutions (12 % v/v ethanol, 5 g/L tartaric acid, pH = 3.5), and wines, all containing different levels of dissolved carbon dioxide. They found that for model wine solutions, the desorption $k_L a$ was similar to the absorption $k_L a$ when there was no dissolved carbon dioxide in solution.

However, a significant deviation was found between the oxygen absorption and desorption $k_L a$ when dissolved carbon dioxide was present in the system. They found that increasing carbon dioxide levels in the model wine solution decreased the absorption $k_L a$, while the desorption $k_L a$ was increased. The desorption $k_L a$ increased by about 60 % when dissolved carbon dioxide was raised from 0 to 0.4 g/L. Further increases in carbon dioxide did not increase the desorption $k_L a$. The increase was attributed to dissolved carbon dioxide desorbing into the gas bubbles, which increases the bubble size as it rises through the column, creating a greater interfacial area through which dissolved oxygen can desorb (Devatine *et*

al., 2007). However, as mentioned in the previous pages, the discrepancy could also be ascribed to the difference in frictional forces between the carbon dioxide and oxygen molecules depending on whether absorption or desorption is taking place.

The absorption $k_L a$ in wine and model wine solutions decreased by nearly an order of magnitude when the dissolved carbon dioxide concentration was raised from 0 to 1.4 g/L. The suggested reason for this effect is that during absorption, carbon dioxide desorbs into the oxygen bubble, and as a result decreases the oxygen partial pressure within the bubble, slowing the oxygen absorption transfer rate. As wine often contains dissolved carbon dioxide levels above 800 mg/L, observing the rate of absorption as an indication for the rate of desorption may not provide accurate information. Due to the significant effect of dissolved carbon dioxide on absorption and desorption of oxygen in wine, elucidating the effect of other compounds on absorption and desorption rates can be difficult, unless the carbon dioxide level is controlled, which is most easily done by completely removing it.

Chiciuc et al. (2010) looked at the effect that ethanol, sugar, sulphur dioxide and polyphenols concentrations had on oxygen absorption during micro-oxygenation. Hydro-alcoholic solutions containing tartaric acid and with a pH of 3.5 were used for the tests. They looked at the effect of ethanol concentration on the oxygen $k_L a$ for ethanol concentrations between 0.005 % and 40 % v/v. They compared the $k_L a$ values to that of oxygen in distilled water. They found that at values up to 0.01 % there was a mild increase in the $k_L a$ value of about 50 %, but that there was a sudden increase by 2.5-fold at an ethanol concentration of 0.05 % v/v. Beyond this, the $k_L a$ remained relatively constant before a small drop from 2 % to 12 % v/v, from which the $k_L a$ remained constant again. The first significant increase in $k_L a$ at 0.05 % v/v was linked to a qualitatively observed drop in bubble size. Manjrekar (2016) suggests that the reason for reduction in bubble size when alcohol is added to an aqueous solution, is that the surface tension of the mixture is reduced.

Figure 2.6 shows the mole fraction of three alcohols and their related surface tension. The surface tension does drop significantly as the ethanol concentration is increased to 10 % v/v. The decrease is less significant between 10 to 40 % v/v (Gliński, Chavepeyer, Platten, *et al.*, 1998). However, the reduction in surface tension when ethanol is added to water to create a 0.05 % v/v solution is minor relative to the significant increase in $k_L a$ that is observed. This indicates that another mechanism significantly affects the increase in $k_L a$. Evaluating $k_L a$ in terms of its individual components may provide better information as to the reasons behind this effect.
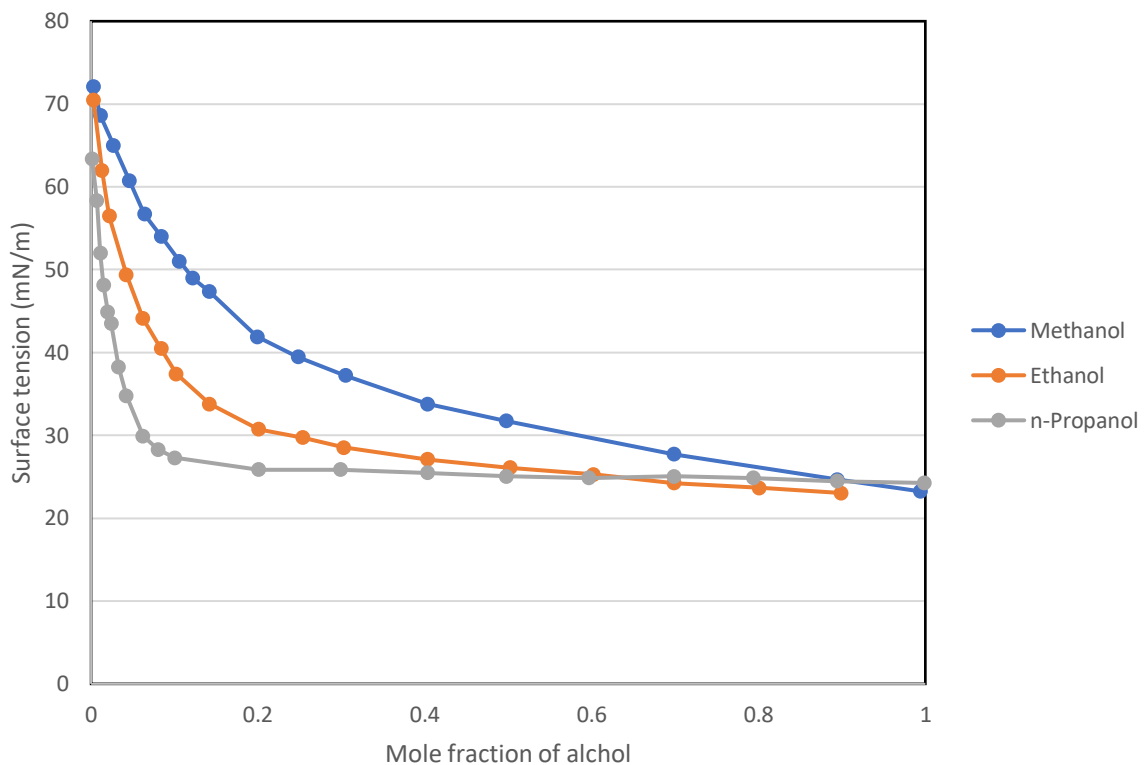
Figure 2.6: Surface tension as a function of mole fraction of alcohol for solutions of methanol, ethanol, and n-propanol. The figure was created from data obtained by Gliński *et al.* (1998)*.*

No effect was found on the absorption $k_L a$ in model wine solutions when sulphur dioxide or phenolic compounds were added. Three wines containing different phenolic contents were also evaluated (pink, white and red). The absorption $k_L a$ was found to be not significantly different between the different wines and the model wine solution, for all gas flowrates tested.

Moenne (2013) found that the oxygen absorption $k_L a$ was higher for a sterile synthetic fermentation media solution, compared to one in which biomass was present. This was attributed to increases in viscosity due to the compositional changes from the additional biomass, resulting in an increase in the liquid film resistance to mass transfer.

This concludes the literature for work in which $k_L a$ was directly examined within the context of understanding gas-liquid mass transfer in wine. However, there is further work in which correlations between concentrations of certain compounds in wine and the viscosity of wine (which $k_L a$ is a function of) have been examined, and these studies are reviewed in the next section.

2.6.2.   Studies on the changing viscosity in wine

Shehadeh et al. (2019) examined the effect that ethanol, glycerol, glucose, and tartaric acid had on the viscosity of model wine solutions and wine samples. It was found that increases in ethanol, glycerol, glucose, and tartaric acid all increased viscosity.

Neto et al. (2014) examined the effect that ethanol, dry extract and reducing sugars had on the viscosity of red wines. The dry extract is the remaining non-sugar solids in the wine after evaporation. This typically consists of organic acids, some minerals, proteins, and tannins. A positive correlation was found between dry extract concentration on viscosity, while there was a minor correlation between ethanol and viscosity. Reducing sugar content was shown to have no correlation to viscosity. The study was conducted on 9 dry Brazilian red wines, containing sugar concentrations between 2.6 and 3.8 g/L. It is possible that the reason this study showed no correlation between sugar and viscosity is that the ranges tested were significantly smaller than in the study by Shehadeh et al. (2019).

Yanniotis et al. (2007) also examined the effect that varying ethanol, sugar, and glycerol concentrations had on the viscosity of wine. They found that alcohol and sugar concentration were the predominant factors affecting the viscosity of wine, while glycerol had no effect. Model wine solutions containing 0-15 % v/v ethanol, and 0-20 g/L glycerol, showed that for every 1 % v/v increase in ethanol, the rise in viscosity was in the region of an order of magnitude greater than the viscosity increase for each additional 1 g/L of glycerol. The typical variation of glycerol in wines is between 5 and 25 g/L, while for ethanol it is 7 to 15 % v/v (Kunkee & Eschnauer, 2016). Based on this data, the change in viscosity of a wine due to the addition of 20 g/L of glycerol would be similar to the change in viscosity of wine due to the addition of 2% v/v ethanol. Dry white wines had lower viscosities than dry red wines, while sweet wines had the highest viscosity, which was attributed to their significantly higher sugar concentration.

These studies indicate that it is possible that varying concentrations of ethanol, glycerol, sugar, dry extract, and tartaric acid may affect the rate of oxygen desorption in a solution by affecting the viscosity of the solution. The results of some of the studies contradict each other, which may be because of small sample sizes used, and the range of concentrations tested. It is important to note that changes in viscosity may not correlate to changes in $k_L a$, as changes in the concentrations of similar compounds may simultaneously affect other parameters that impact $k_L a$. In addition, changes in the properties of model wine solutions may not always be representative of changes that may occur in the properties of wine, as model wine solutions

only contain a small fraction of the compounds present in wine, and possible interactions between the multitude of compounds present in wine would not be accounted for.

It is worthwhile to take a step back and look at additional studies that evaluate how absorption and desorption of oxygen in aqueous solutions are affected by changes in compounds that are found in wine or are similar to those in wine. A review of these studies is presented in the following section.

2.6.3.   Mass transfer studies of oxygen in aqueous solutions

There have been many studies evaluating the absorption and desorption of oxygen in mixtures and solutions containing compounds found in wine. These studies may provide clues as to which compounds in wine affect the oxygen desorption rate.

Gurol & Nekouinaini (1985) investigated how the presence of various organic compounds affected the absorption of oxygen into water. In addition, they examined the effect that pH and ionic strength had on absorption. They evaluated the effect on mass transfer through determining $k_L a$, interfacial area and gas holdup. The organic compounds tested were various phenols, tertiary butyl alcohol (TBA) and acetic acid. It was found that the addition of phenols increased the $k_L a$ relative to water, although this increase was dependent on how hydrophilic or hydrophobic the phenol was. For the most hydrophobic phenol – xylenol – the $k_L a$ was increased by as much as 300 %. The polyphenols in wines can be most simply classified as flavonoid and non-flavonoid polyphenols. These phenols are significantly more complex than the ones used in the study by Gurol & Nekouinaini (1985). Flavonoids contain hydroxyl groups, which are hydrophilic, and aromatic rings which are hydrophobic. The different structures of polyphenols in wine will result in differing hydrophobic properties (Federico Cassasa, 2017; Gutiérrez-Escobar, Aliaño-González & Cantos-Villar, 2021).

Gurol & Nekouinaini (1985) also found that concentrations of acetic acid and TBA at 0.4 mM increased $k_L a$ by 300 and 200 % respectively relative to water. It was found that for all the organic compounds tested, there was a reduction in bubble size once they were added to water from a mean bubble size of approximately 3 mm to 1mm. The reason presented for the formation of smaller bubbles due to organics addition, was the prevention of bubble coalescence. The increase in $k_L a$ as a result of the addition of organics was attributed almost entirely to the increase in a, as it was found that the k_L was not affected by the addition of organic compounds.

It was also found that increasing the ionic strength of water increased $k_L a$, which was attributed to the ions also inhibiting bubble coalescence. The $k_L a$ was between 50 and 100 % greater for a 0.1 ionic strength solution compared to a 0.01 ionic strength solution, depending on the gas flowrate.

Further, the effect that the presence of a surfactant, sodium dioctyl sulfosuccinate (SDS) had on oxygen absorption was evaluated. It was found that the addition of SDS at 4 mg/L reduced the k_L by approximately 50 % relative to that found in water. The surfactant reduced k_L by adsorbing to the gas liquid interface, increasing resistance to mass transfer. However, the surfactant also reduced bubble size, from an equivalent diameter of 2 mm observed in water, to an equivalent diameter of 0.5 mm, which consequently increasing the interfacial area. The overall effect of the surfactant on the oxygen absorption $k_L a$, was that it was initially reduced relative to water, before increasing with increases in concentration as the resulting increase in interfacial area overcame the reduction in k_L, resulting in an overall increase in $k_L a$ (Gurol & Nekouinaini, 1985).

Besagni, Inzoli and Ziegenhein (2018) provide a comprehensive review on two-phase bubble columns. They presented results that showed that gas holdup increased with an increase in electrolyte concentration, up to a critical concentration, beyond which the increase in gas holdup was negligible, with the gas holdup being up to 1.5 times greater than that of distilled water at the critical salt concentration. This critical concentration was between 0.03 and 0.4 mol/L, depending on the salt (Zahradník, Fialová, Růžička, *et al.*, 1997).

A comprehensive paper by Jamnongwong et al. (2010) examined how the addition of salt, sugar and surfactant affected the oxygen diffusion coefficient, bubble diameter and k_L. The diffusion coefficient for NaCl dropped by 50 % when its concentration was increased from 1.6 g/L to 100 g/L salt, while for glucose there was approximately a 30 % decrease in the diffusion coefficient as its concentration was increased from 0 g/L to 100 g/L. The mean bubble diameter and k_L dropped with increasing sugar concentration, from 4 mm to 3 mm; and 0.46 mm/s to 0.22 mm/s respectively.

Ferreira et al. (2013) examined the effect that pH had on the oxygen k_L in a bubble column. They showed that aqueous systems containing HCl or KOH had reduced $k_L a$ values relative to neutral water, although the extent of this variation was dependant on the superficial gas velocity within the column. At the highest velocities tested, the $k_L a$ dropped by approximately 30 % when the pH was reduced from 6.7 to 3.5 through the addition of HCl.

For all flowrates tested, the $k_L a$ dropped by approximately 20 to 40 % when the pH was raised from 6.7 to 8 through the addition of KOH. Further increases to the pH did not affect more change on the $k_L a$. The change in the $k_L a$ was predominantly due to different values of k_L between the systems. This was ascribed to contamination at the gas bubble interface, resulting in a reduced k_L value.

These studies demonstrate how sensitive oxygen transfer can be to small additions or changes in the concentration of compounds in a solution. Based on these studies, it is quite possible that varying concentrations of organic compounds found in wine could affect $k_L a$. The pH levels and ionic content in wine could also have an effect. Any compound within wine, including dry matter, even at very low concentrations, that acts as a surfactant, could also significantly affect $k_L a$.

2.6.4. Summary of oxygen mass transfer

Ethanol, glycerol, and sugars are the major compounds within wine due to their relatively high concentration and the fact that they can vary significantly from one wine to the next. Wine contains a range of ethanol, typically between 7 and 16 % v/v; sugar contents up to 150 g/L, and glycerol concentrations up to 25 g/L (Kunkee & Eschnauer, 2016). The high concentrations of ethanol, glycerol, and sugar in wine, and their significant range between wines, present themselves as potential factors that could affect the desorption $k_L a$.

Wine also contains a variety of sulphates, ions, acids, esters, and proteins, which could also affect $k_L a$ (Kunkee & Eschnauer, 2016). It has been shown that even the presence of compounds at a very small concentration, that may act as surfactants, could influence the desorption $k_L a$. Compounds in wine that could act as surfactants include proteins, polysaccharides and polyelectrolytes (Moeller, Zehnsdorf, Pokorná, *et al.*, 2018).

The complexity of wine makes it incredibly difficult to assess how changes in each compound affects $k_L a$. In addition, it is possible that compounds interact with each other such that there may not be one identifiable compound that controls the rate of oxygen desorption.

2.7. Methods for measuring the volumetric mass transfer coefficient and the interfacial area

2.7.1. Methods for measuring the volumetric mass transfer coefficient

The mass transfer rate can be measured through either chemical or physical techniques (Tribe, Briens & Margaritis, 1995). A widely used chemical method is the sodium sulphite

oxidation method. It is based on the reaction of sodium sulphite to dissolved oxygen in the system. The $k_L a$ can be calculated from the change in sodium sulphite concentration over time. This technique is relatively easy to perform and can be performed within a bubble column. However, the addition of sodium sulphite and the produced sulphates, as well as the addition of the catalyst needed for the process, can affect the physical properties of the solution, and as a result change the $k_L a$ value obtained, which may consequently be inaccurate relative to the actual $k_L a$ (Garcia-Ochoa & Gomez, 2009). This technique requires higher ionic concentrations from the compounds added, which can affect $k_L a$ in some systems, rendering the technique potentially inaccurate under some circumstances, and potentially only representative of $k_L a$ in strongly ionic solutions (Van't Riet, 1979).

The typical physical methods used involve a step change of the concentration of the gas in the solution. The most common physical method for measuring $k_L a$ is through the gassing out procedure (GOP). The system is based on measuring the response of a system's dissolved oxygen concentration to a change in oxygen partial pressure in the gas that is sparged into the system, usually via an oxygen probe (Clarke & Manyuchi, 2012).

An alternative method is the pressure step procedure (PSP), which involves evaluating the response of the concentration of dissolved oxygen in the system when a pressure change is imposed on the system. The PSP method has been shown to be an accurate method, however, it is more mathematically and experimentally challenging than other physical methods, and the GOP method is usually preferred (Clarke & Manyuchi, 2012; Zedníková, Orvalho, Fialová, *et al.*, 2018)

For measuring oxygen desorption $k_L a$, the GOP procedure begins (in the case of the presence of other dissolved gases such as carbon dioxide) with the sparging of nitrogen through the system solution until all other dissolved gases have been removed. Subsequently, air or pure oxygen is sparged into solution until it is oxygen saturated. Following this, a second step of nitrogen sparging begins (Garcia-Ochoa & Gomez, 2009). The probe response to dissolved oxygen is measured until the dissolved oxygen level is at zero, or close to zero. Equation 13 can be used to determine the desorption $k_L a$ for each point in time measured. C_{L0} is the initial dissolved oxygen concentration in the system after oxygen or air sparging. $C_{L,t}$ is the concentration of dissolved oxygen at time t.

$$\ln\left(\frac{C_{L0}}{C_{L,t}}\right) = k_L a \cdot t \qquad (13)$$

Figure 2.7 below shows the expected change in dissolved oxygen concentration when desorption (input of nitrogen) occurs and when absorption (input of oxygen) occurs for an aqueous solution. For each experiment in which desorption and absorption is performed, a graph such as the one below is generated from which $k_L a$ for desorption and absorption can be obtained.
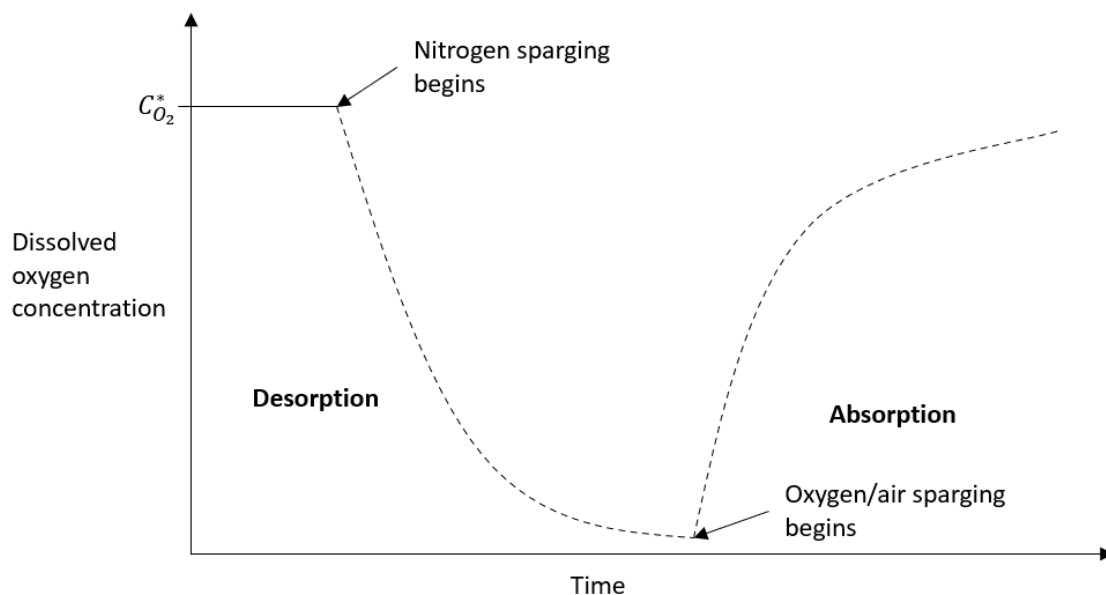

Figure 2.7: An example of how the oxygen concentration is expected to change using a typical dynamic method for determining the volumetric mass transfer coefficient, adapted from Garcia-Ochoa & Gomez (2009)

Inaccuracies with this method may occur if the probe response lag (τ_P) is not taken into account. The probe output obtained during the measurement might not be directly related to the instantaneous value of the system as a result of the lag. The lag is dependent on the type of oxygen probe used, as well as the properties of the system (Van't Riet, 1979). Depending on the probe response time relative to the oxygen transfer rate, it may be necessary to determine the probe response lag to ensure $k_L a$ accuracy. Van't Riet (1979) described the probe response time as typically the time required for a probe to register a 63 % stepwise change in gas input. The lower the τ_P is relative to the mass transfer response time ($1/k_L a$) the more accurate the probe measurement will be (Tribe *et al.*, 1995; Van't Riet, 1979). Generally, the probe response may be neglected if $1/k_L a$ is greater than $10\tau_P$ (Garcia-Ochoa & Gomez, 2009). This will be dependent on accuracy requirements, but in a review by Van't Riet (1979), it was found that the error was less than 6 % for probe responses less than $10/k_L a$. However this is seldom the case in bubble columns (Garcia-Ochoa & Gomez, 2009), and if the lag response time is within the region of $1/k_L a$, a second order model is needed in order to accurately determine k_L.

2.7.2.   *Measuring the interfacial area*

In order to determine the effect that changing factors have on k_L and the interfacial area, one of them needs to be determined separately from the measurement of the $k_L a$. The interfacial area is typically easier to calculate, and can be done through the measuring of the gas hold-up and the Sauter mean bubble diameter (Sehabiague & Morsi, 2013). The Sauter mean diameter is a measure of the mean bubble size that occurs during sparging. There are other measures of mean bubble sizes, however the Sauter mean bubble diameter is almost always used for mass transfer studies (Azzopardi, 2011). This is primarily because D_{32} provides a more accurate mean diameter when the final desired measurement is the average surface area of a particle (Rawle, 2003).

The measurement of the Sauter mean diameter is typically done through high-speed photography, from which the area of the bubble sizes can be determined as a function of the pixels it inhabits, and a ratio of units of distance to pixels. The Sauter mean bubble diameter is then inferred from this, as described in the following chapter.

The k_L can be determined once the interfacial area has been obtained along with the $k_L a$. Securing the data of each of these parameters for each system will allow for a better understanding of how the system reacts to changes applied to it.

2.8. Summary of the literature review

The concentration of dissolved oxygen in wine is an important parameter that needs to be controlled in the winemaking process to ensure that the quality of the wine is maintained once it has been packaged. Desorption is done through sparging an inert gas through wine and determining the rate of desorption through measuring the oxygen desorption $k_L a$. Understanding which factors affect $k_L a$ allows for a better understanding of the mechanics of the mass transfer taking place, allowing for better design of gas-liquid mass transfer processes in winemaking. Of particular importance to this study is assessing which compounds in wine can affect the $k_L a$.

There is literature examining gas-liquid transfer in wine, model wine solutions, and aqueous solutions containing compounds found in wine. Literature is mostly focused on oxygen absorption, however these studies are still useful as the physical mechanisms that drive absorption are the same as those that drive desorption (Hamborg *et al.*, 2010). It has been found that dissolved carbon dioxide and ethanol can have a significant effect on the oxygen absorption $k_L a$, but that phenolics and sulphur dioxide do not (Chiciuc *et al.*, 2010; Devatine

et al., 2007). It was shown that changing concentrations of ethanol, glycerol, sugar, and dry extract could all affect the viscosity of wine, which could consequently affect the oxygen desorption rate (Glampedaki, Hatzidimitriou, Paraskevopoulou, *et al.*, 2010; Shehadeh *et al.*, 2019; Yanniotis *et al.*, 2007). Other studies have found that in aqueous solutions, the presence of phenols, acids, alcohol, surfactants and ions all affected changes on the oxygen $k_L a$ (Ferreira *et al.*, 2013; Gurol & Nekouinaini, 1985; Jamnongwong *et al.*, 2010).

Wines contain numerous types of sugars and alcohols, a vast array of phenolic compounds, aldehydes, organic acids, esters, proteins, and minerals (Kunkee & Eschnauer, 2016). The complexity of wine makes it incredibly difficult to assess how changes in each compound affects $k_L a$. In addition, it is possible that compounds interact with each other such that there may not be one identifiable compound that controls the rate of oxygen desorption. However, the studies evaluating the oxygen $k_L a$ in different solutions do direct attention to certain compounds having a significant effect on oxygen desorption.

Ethanol, glycerol, and sugars are typically the biggest and most variable compounds within wine, and it is quite possible that changes in the concentration of these compounds could affect oxygen desorption $k_L a$. Compounds at relatively small concentrations that act as surfactants can also affect the oxygen desorption $k_L a$. Compounds in wine that may act as surfactants include proteins and polysaccharides (Moeller *et al.*, 2018).

Assessing how these changes affect the $k_L a$ can be done using the gassing out procedure, in which the dissolved oxygen is measured in solution, as an inert gas is sparged through (Clarke & Manyuchi, 2012). The interfacial area and k_L can be calculated through high-speed photography.

The capturing of data through these methods will allow for a greater understanding of the oxygen desorption process in wine. It is clear there is limited knowledge as to which compounds in wine result in oxygen desorption of wine taking place at different rates. Determining the extent of the variation of oxygen desorption rates within wine, and which compounds are responsible, is the focus throughout the experimental work of this study. Understanding this will allow for the development of more efficient sparging processes, and the development of practices that can overcome slow oxygen desorption rates in wines.

Chapter 3: Materials and Methods

3.1. Materials

The experiments performed in this study utilised a variety of compounds to formulate model wine solutions. A variety of different wines were also used. Compressed air from a 24 L Ross air compressor was used for saturating the solutions and the wines. 99.5 % technical nitrogen was used for the removal of dissolved oxygen.

3.1.1. Model aqueous and wine solutions

The various compounds used to create the various model wine solutions are shown in Table 3.1.

Table 3.1: Material list for compounds used in the model wine solutions

Material list	Details	Source
Ethanol	96.4 v/v %	Sigma-Aldrich
Glycerol	99.8 wt. %	Sigma-Aldrich
Tartaric acid	L-(+)-Tartaric acid; assay spec ≥99.5%	Sigma-Aldrich
Malic acid	L-(-)-Malic acid; assay spec ≥99.5%	Sigma-Aldrich
Citric acid	Citric acid; assay spec ≥99.5%	Sigma-Aldrich
Sugar	Refined white sugar	Huletts Sugar
Yeast extract	Fermoplus DAP Free autolysed yeast	AEB Group
Bovine serum albumen	Bovine serum albumin fraction V	Roche

The composition of each of the model wine solutions used in this study are shown in Table 3.2 below.

Table 3.2: Summary of the composition of the different model wine solutions used in the experiments in this study

Compound	10 % Ethanol	MWS-Glycerol	MWS-Acids	MWS-BSA	MWS-Yeast
Ethanol (% v/v)	10	10	10	10	10
Glycerol (g/L)	0	15	15	15	15
Tartaric acid (g/L)	0	0	5	5	5
Malic acid (g/L)	0	0	5	5	5
Citric acid (g/L)	0	0	2	2	2
Sugar (g/L)	0	0	5	5	5
Bovine Serum Albumen	0	0	0	0.1	0
Yeast extract (g/L)	0	0	0	0	0.2

3.1.2. *Wines*

The wines used in experimental runs are shown in Table 3.3.

Table 3.3: Wine list for wines used in the experimental runs

Wine labels	Wine type
White-A	Namaqua dry white wine (non-vintage)
White-B	2019 KWV Chenin Blanc (dry)
White-C	2020 In-house Sauvignon Blanc (dry)
Rosé	4th Street sweet rosé (non-vintage)
Red	Just Wine dry red (non-vintage)
PU-Wine	2021 Kaapzicht protein un-stable white wine (dry)
BT-Wine	2021 Kaapzicht protein stabilised white wine (Bentonite treated; dry)

3.2. Methods

3.2.1. *Experimental setup*

A diagram of the experimental setup used for all experimental runs is shown in Figure 3.1. The bubble column used was a glass column with an inner diameter of 15 cm and a total

height of 90 cm. A stone sparger with a mean pore size of approximately 40 µm was placed at the bottom of the column and was 14 cm in diameter. A Cole-Parmer 150 mm flowmeter was used to determine and control the gas flowrate. It was placed between the gas supply and the sparger. This was calibrated so that a correlation could be developed between the flowmeter reading (mm) and gas flowrate (L/min). Cole-Parmer provides a data sheet with air flowmeter readings related to gas flowrate. From this the gas flowrate for nitrogen could be corrected using equation 14.

$$Q_G = Q_{air} * \sqrt{\frac{0.001230}{\rho_G}} \tag{14}$$

Where Q_{air} is the air gas flowrate at 70 °F and 1 atm, and ρ_G is the density of the gas at 70 °F and 1 atm. Equation 15 was then used to correct for temperature.

$$Q_{G,actual} = Q_G * \sqrt{\frac{530}{T} * \frac{P}{760}} \tag{15}$$

Where T is the temperature in Rankine, and P is the pressure in mmHg.

The bubble column was positioned inside a Perspex box with a height of 60 cm. This was filled with water, acting as a heat sink so that the required experimental temperatures could be maintained within the bubble column. The temperature was controlled manually. The column temperature remained ± 1 °C for 20 minutes before needing adjustment. The water temperature was adjusted by replacing a portion of the water within the Perspex box with refrigerated or hot water.

A lighting rig was used for image capturing purposes. The lighting rig consisted of a panel of LEDs. It had dimensions of 30 cm by 70 cm. This was placed behind the bubble column to backlight it. A plastic diffusion sheet was placed between the LED panel and the bubble column so that light was scattered evenly across the back of the column. For capturing images at higher gas flowrates, a smaller diffusion sheet of approximately 5 cm by 30 cm was placed within the bubble column, affixed about 1cm from the front of the column. This was done to prevent image interference from bubbles at the back of the column, allowing a clearer image to be taken. A 10 mm in diameter steel ball was placed in the column, providing a reference point, so that the size of bubbles within the column could be determined.

The dissolved oxygen concentration of the solution within the bubble column was measured using a Mettler-Toledo InPro 6900 polarographic oxygen probe. Before the experimental runs, a new membrane was placed within the probe and filled with an O_2 electrolyte solution. The probe was inserted through the lid of the bubble column so that the tip of the probe was approximately 5 cm below the surface of the solution. A Mettler Toledo M300 transmitter was connected to the oxygen probe, and it was used to calibrate the oxygen probe. Calibration for the measurement of dissolved oxygen in this experiment was a one-point slope calibration in air with a known air saturation level. The probe was polarized 24 hours before calibration took place. A calibration slope was then generated, converting the measured voltage to dissolved oxygen concentration. A M300 Configuration tool was operated through Windows and was used to capture data from the probe.

A Canon EOS 550D DSLR camera was used for image capturing. The shutter speeds used were between 1/800 to 1/3200. The aperture values used were between F4.0 to F5.6. ISO values of 3200 or 6400 were used. The camera was held at approximately 20 cm from the front of the bubble column, to ensure the entire bubble column width could be captured. The steel ball was placed into the bubble column 30 cm above the base of the sparger. The camera was held level with the steel ball during imaging.
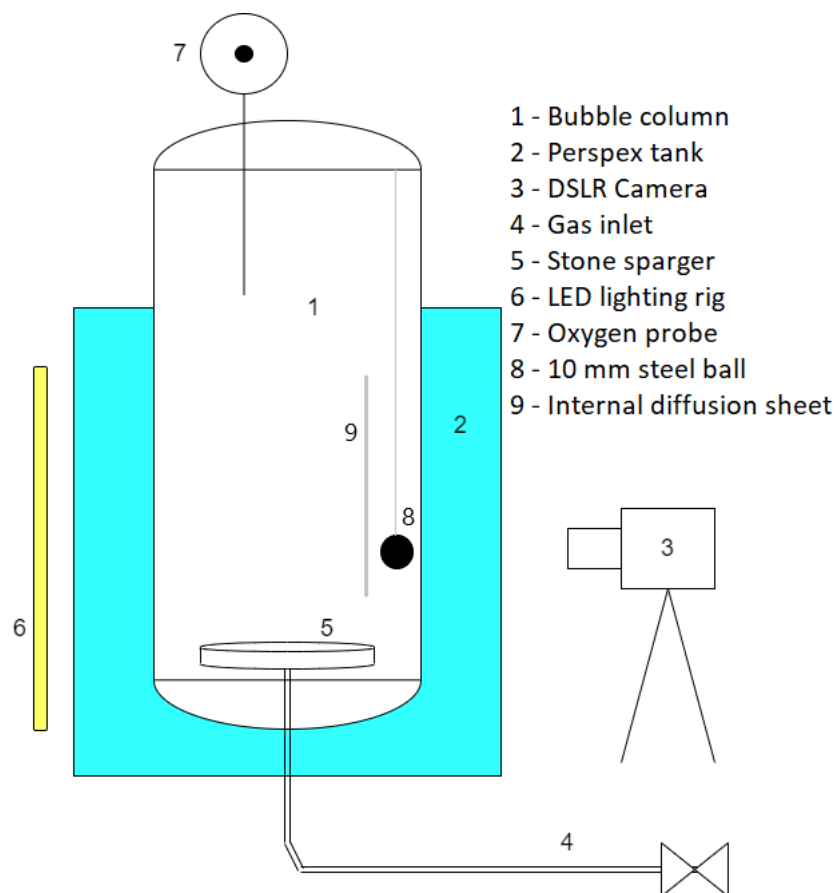

1 - Bubble column
2 - Perspex tank
3 - DSLR Camera
4 - Gas inlet
5 - Stone sparger
6 - LED lighting rig
7 - Oxygen probe
8 - 10 mm steel ball
9 - Internal diffusion sheet

Figure 3.1: Diagram of the experimental setup used for all experimental runs

3.2.2. Experimental procedure

The bubble column was rinsed with hot water and scrubbed before use. The Perspex box was filled with water up to the 40 cm mark. The temperature was controlled using refrigerated or hot water mixed with tap water to reach the desired temperature. The temperature was measured using a mercury thermometer.

Aqueous glycerol ethanol solutions and model wine solutions were prepared for use in the experimental runs. The solutions needed were well mixed before being placed into the bubble column. Solutions containing glycerol and ethanol were thoroughly mixed in a volumetric flask before being placed into the bubble column. The tartaric acid, malic acid, citric acid, and sugar were thoroughly mixed with hot water before being placed into the column once fully dissolved. The yeast extract was thoroughly mixed in 35 °C water until fully dissolved before being placed in the column. The bovine serum albumen was mixed in lukewarm water and allowed to stand for 30 minutes before being placed in the column.

The temperature of the model wine solutions was adjusted by controlling the temperature of the water component added to the solution. The bubble column was filled with 13.5 litres of the solution or wine. For the experiments performed on wine, the wine was either refrigerated or placed into large vessels within a hot water bath to warm to the required temperature. The solution in the bubble column was saturated with oxygen from an air compressor until the reading obtained from the oxygen probe remained stable (± 0.1 mg/L) for 30 seconds. The air sparging was then halted and the height of the solution within the bubble column was recorded once all bubbles had left the solution. Nitrogen was then sparged through the system at the specified gas flowrate.

The exact time that the first nitrogen bubbles exited the sparger was recorded and used as the initial time for the data obtained. During sparging, the height of the liquid was recorded at three separate intervals, with the first one taken 1 minute after sparging with nitrogen had begun. Sparging was continued until the reading by the oxygen probe was measured at 0.1 mg/L. Following the experimental run, the bubble column was drained, scrubbed, and rinsed thoroughly with hot water.

For the image capturing, the LED lights were switched on, and all other light sources were switched off. For each experimental run at least 10 images were captured. The first image was only taken after the sparging had been taking place for 1 minute.

3.2.3. Measuring the $k_L a$

Once the dissolved oxygen data for an experimental run had been obtained, a first order approximation of the $k_L a$ was performed, using equation 16.

$$\ln\left(\frac{C_{O2,t}}{C_{O2,i}}\right) = -k_L a.t \tag{16}$$

The $k_L a$ was obtained by plotting $\ln\left(\frac{C_{O2,t}}{C_{O2,i}}\right)$ vs. time. The gradient obtained was the first order approximation of the $k_L a$. Figure 3.2 demonstrates an example of this plot. In this case the first order $k_L a$ was calculated as 0.0122 s^{-1}.
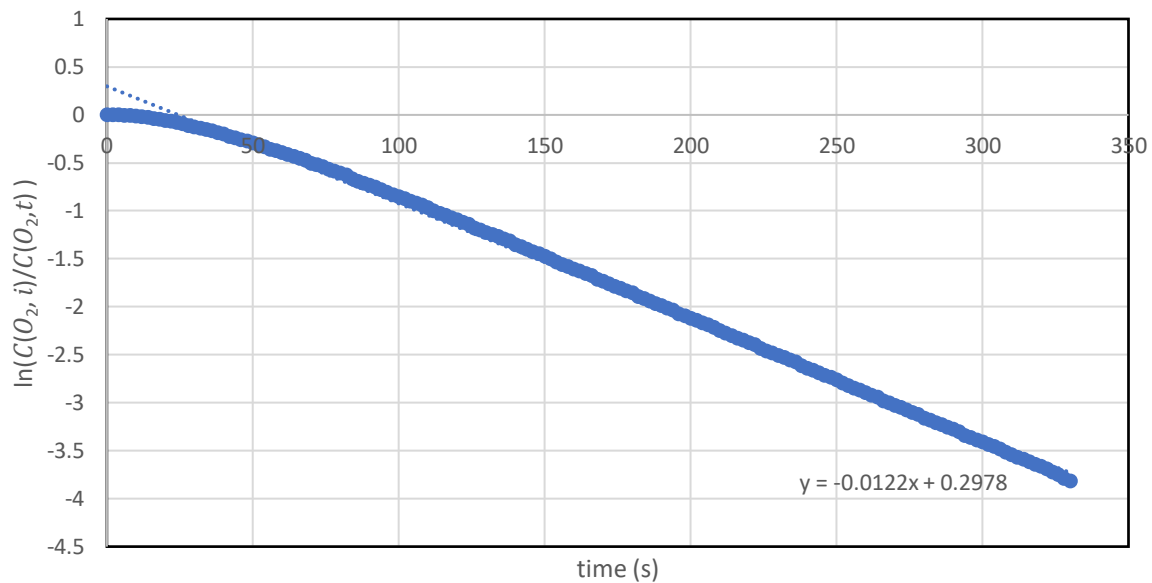

Figure 3.2: Example of a graph generated to determine a first order approximation of the $k_L a$. In this case, this is a first order approximation of the oxygen desorption $k_L a$ for water at 25 °C at a gas flowrate of 2.3 L/min.

A second order approximation of the $k_L a$ was then determined with the first order value used as an initial estimate. A probe constant (k_p) was measured for use in the second order model. The probe constant was determined in a similar way to the first order $k_L a$ model, as shown by equation 17.

$$\ln\left(\frac{C_{O2,i}}{C_{O2,p}}\right) = -k_p.t \tag{17}$$

The second order model equation could then be used to generate $\frac{C_p}{C}$ values for each point of time as shown by equation 18.

$$\frac{C_p}{C} = \frac{1}{k_p - k_L a}[k_p e^{-k_L a*t} - k_L a e^{-k_p*t}] \tag{18}$$

Where $\frac{C_p}{C}$ is the probe concentration (C_p) at t, as a fraction of the oxygen concentration (C) at $t = 0$. An iterative solution was used to obtain the 2nd order approximation of the $k_L a$ using the

Microsoft excel solver function. The solver was used to reduce the total sum of errors between $\frac{C_p}{C}$ data from the experiments, and the $\frac{C_p}{C}$ data from the second order model. This was done by adjusting the $k_L a$ value in the above equation. The first order approximation of the $k_L a$ was used as an initial guess. The sum of errors was calculated for each time interval, as shown in equation 19.

$$SSE = \sum_{i=1}^{n} \left(100 * \frac{C_p}{C}_{ex} - 100 * \frac{C_p}{C}_{2nd} \right)^2 \qquad (19)$$

The $k_L a$ value resulting in the lowest SSE value was the 2nd order approximation of the $k_L a$. Figure 3.3 shows the $\frac{C_p}{C}$ values for the experimental data and the 2nd order model values once the solver function was used.
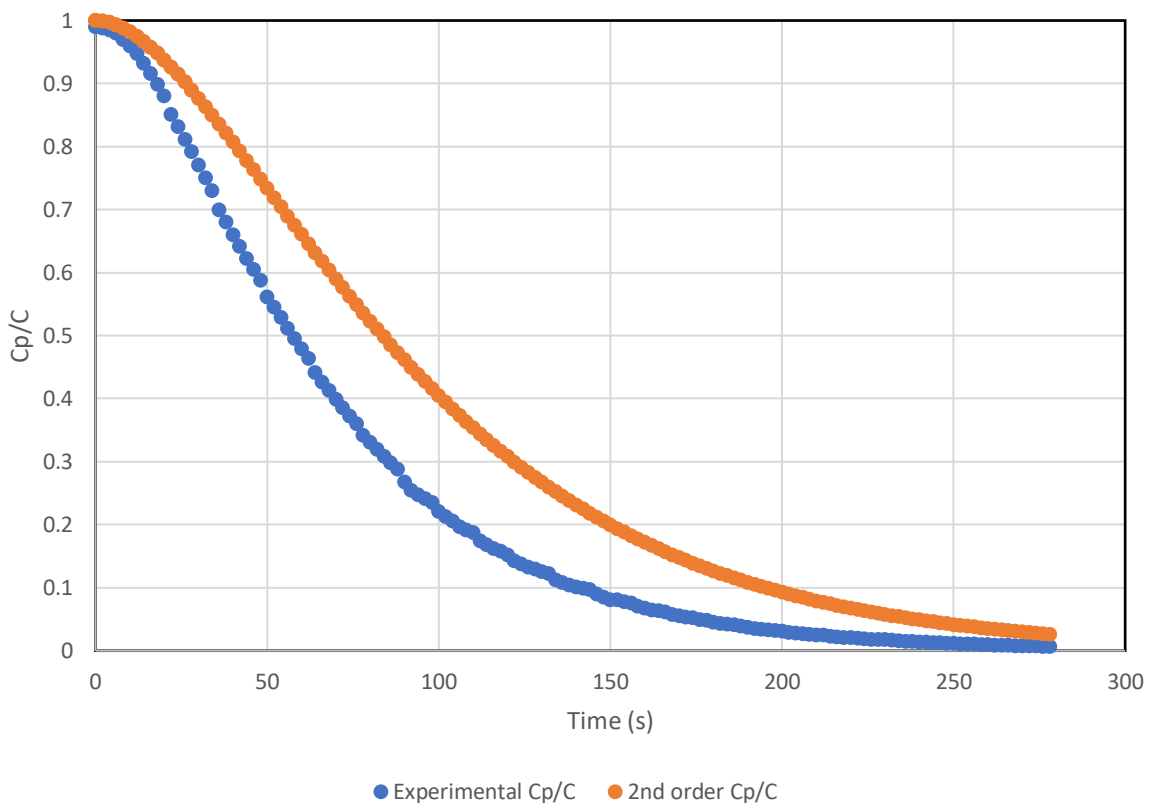

Figure 3.3: Graph showing the adjusted Cp/C values once the SSE value was minimized, with the Cp/C 2nd order data obtained using the excel solver algorithm in order to minimize the sum of errors between the experimental data and the 2nd order model.

3.2.4. Measuring the gas holdup

The measurement of the gas holdup was done by measuring the height of the solution in the bubble column when no sparging was taking place and then by measuring the height of the solution while sparging was taking place. Three measurements were taken during nitrogen sparging, with the first one taken 1 minute after the sparging had begun. A measuring tape was fixed onto the side of the bubble column, and this was used to determine the difference

in height between the solution before and during sparging. The height of the solution in the bubble column before sparging was measured from the top of the base of the bubble column. The gas holdup was calculated as shown in equation 20.

$$\varepsilon_G = \frac{H_{sparging} - H_0}{H_{sparging}} \qquad (20)$$

With $H_{sparging}$ the height of the solution from the top of the base of the column during sparging, and H_0 the height of the solution from the top of the base of the column before sparging. For cases in which foaming occurred, the height of the liquid during sparging was measured at the base of the foaming head.

3.2.5.   Measuring the Sauter mean diameter

A MATLAB program was used to determine the area, perimeter, and estimated diameter, of individual bubbles within an image. A series of MATLAB functions were used to reduce the input image to outlines of bubbles that could be filled in, from which the above data was obtained. From this generated data, the Sauter mean diameter was calculated. The MATLAB program used was obtained from Abufalgha (2018).

The first function used was *imread* to read the input image. Once the image had been read, a scale converting pixels to mm was used. For all images, a 10 mm diameter steel ball was present. Dragging a line across the diameter of the steel ball was done so that a ratio of mm/pixel could be obtained.

The image was then reduced using the function *medfilt2*, which is a median filtering function. It converts the value of each pixel in the image to the median of all its neighbouring pixels. The image was then converted from grey scale into binary, after which another *medfilt2* function was applied.

Following this the *imdilate* and *imerode* functions were applied, which joined the pixels within the image together, and removed outlier pixels. Another *imdilate* function was used to further dilate the image, which joined the binary pixels in the image together. The *bwmorph* function was then used, performing a morphological operation in which 'noise' pixels were removed from the boundaries of identified objects, without breaking the border of the object.

After this the *medfilt2* function was applied again to further remove all 'noise' around the 'object'. This presented the outer boundaries of the identified bubbles. A function was then applied to fill in the outline of the identified bubble.

From the measurement of the filled-in pixels, the projected area of the bubble was identified. A second ellipse method was also used to determine the area of the bubbles. This method involved producing two lines across each bubble forming a cross. An ellipse was then fitted over the lines, with the ellipse measured to determine the bubble area. The MATLAB code used is presented in S2: MATLAB code for bubble image analysis.

The figures below show the evolution of the bubble image as it underwent the various sets of functions just described.
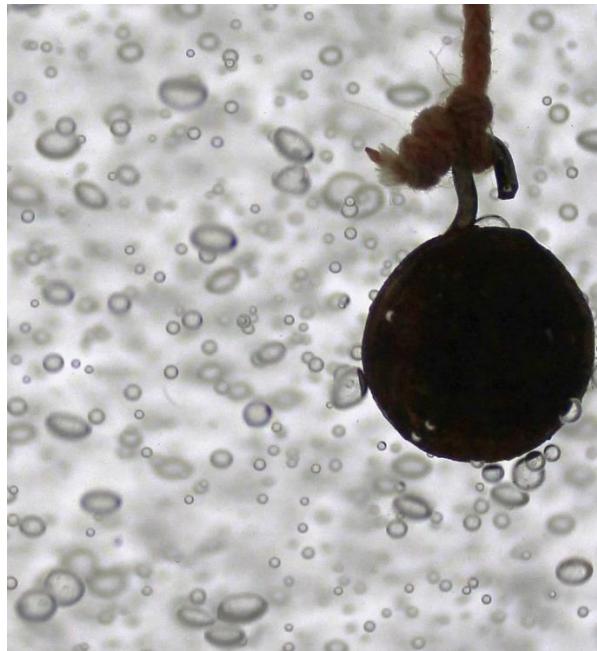

Figure 3.4: Initial bubble fed into the MATLAB program

44

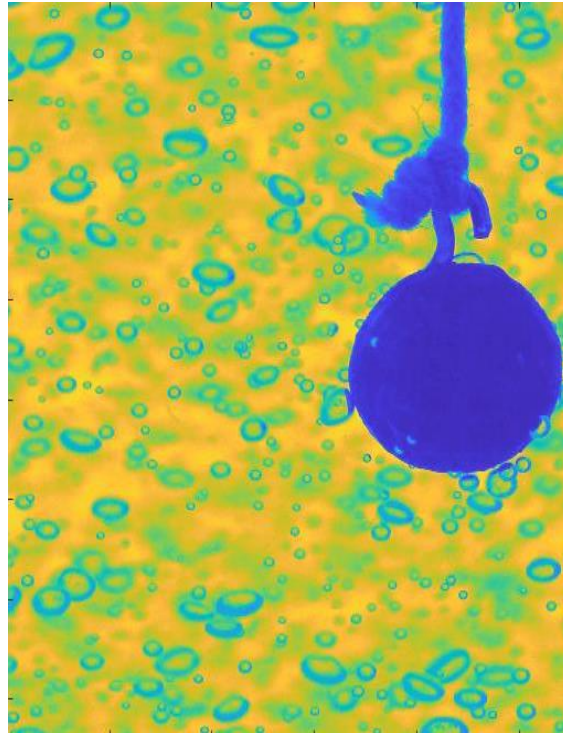*Figure 3.5: The bubble image produced by the MATLAB program before undergoing the set of functions described above*
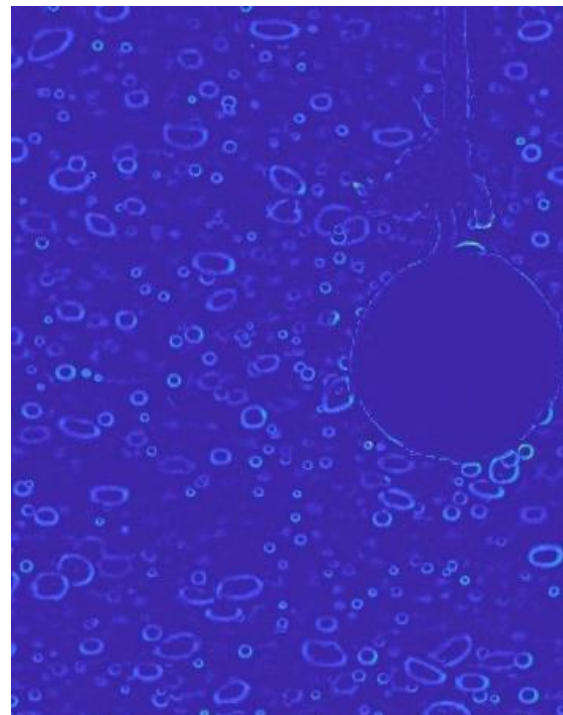

Figure 3.6: The bubble image after applying the medfilt2 function and converting the image to binary

45
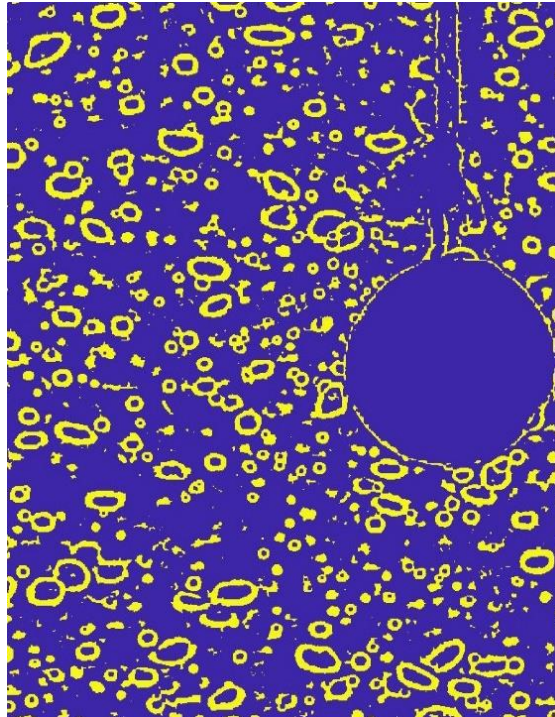
Figure 3.7: Bubble image after applying the imdilate and imerode functions
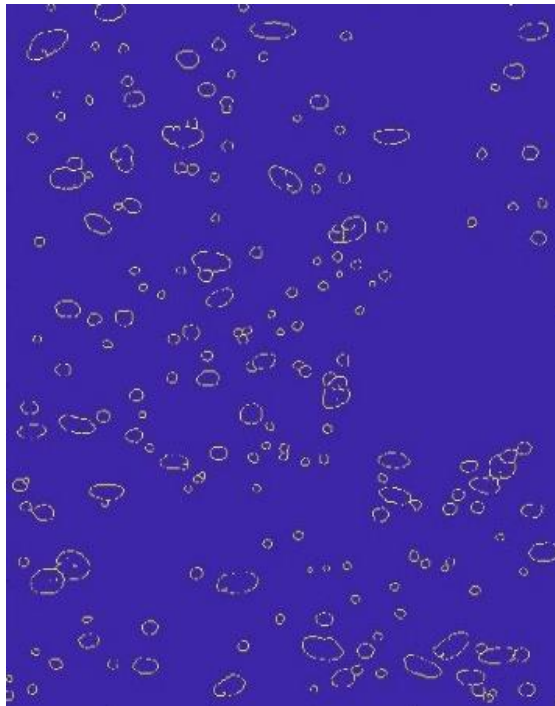
Figure 3.8: Bubble image after applying a bwmorph function and another medfilt2 function
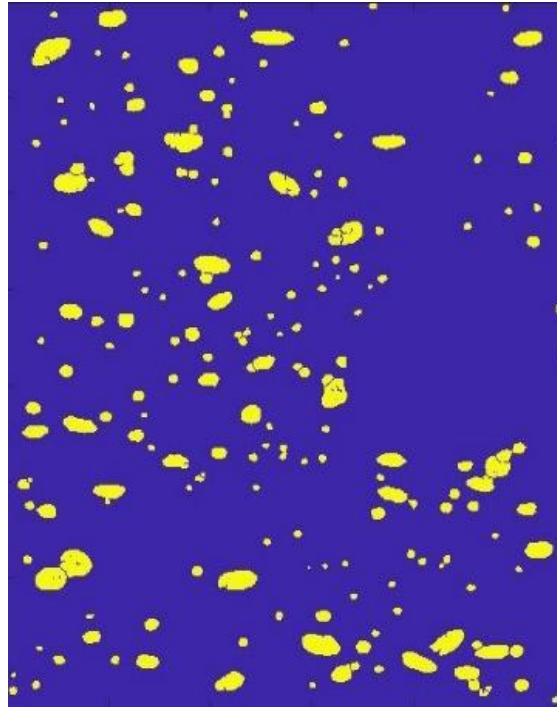
Figure 3.9: Bubble image after the bubble outlines were filled in
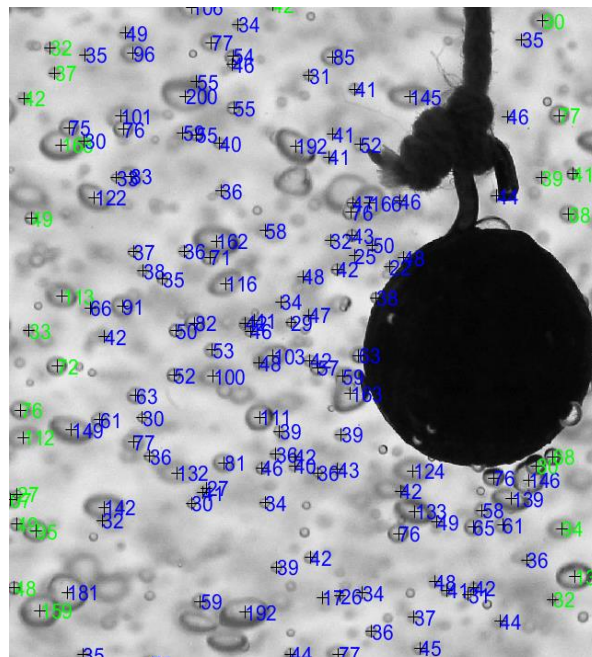
Figure 3.10: Output bubble image with the bubbles identified and their projected areas calculated

3.2.6. Measuring the interfacial area and the mass transfer coefficient

Following the determination of the areas of the bubbles within the images, the interfacial area was calculated. First the Sauter mean diameter was calculated. To do this the Feredt diameter (D_F) of each bubble was calculated, using the projected area (A_P) obtained from the MATLAB code, as shown by equation 21.

$$D_F = 2 * \sqrt{\frac{A_P}{\pi}} \tag{21}$$

From this the Sauter mean diameter (D_{32}) was determined as the sum of the cube of each bubble's Feredt Diameter divided by the square of each bubble's Feredt Diameter, as shown by equation 22.

$$D_{32} = \frac{\sum_{i=1}^{N} n_i D_F^3}{\sum_{i=1}^{N} n_i D_F^2} \tag{22}$$

Subsequently the interfacial area (a) was calculated using the gas holdup (ε_G) and D_{32} as shown by equation 23.

$$a = \frac{6\varepsilon_G}{D_{32}} \tag{23}$$

The mass transfer coefficient (k_L) was then determined by dividing the $k_L a$ by the interfacial area, as shown by equation 24.

$$k_L = \frac{k_L a}{a} \tag{24}$$

3.3. Experimental procedure for bentonite addition

An experiment was performed in order to examine whether desorption would occur at different rates for a wine that underwent different processing steps prior to nitrogen sparging. Bentonite addition is commonly done in winemaking to reduce the 'haze' in wine. However, some winemakers choose not to perform this step for certain wines.

A batch of unfiltered protein unstable white wine from Kaapzicht was split into two batches of 20 litres. The wine was then racked to remove a portion of the lees at the bottom of the wine. This was done by slowly transferring each batch through a sterilised pipe into another 20-litre container, leaving the lees in the bottom of the previous container. Both batches were then filtered to remove any remaining solids and yeast cells. After this, one of the batches was treated with bentonite. The bentonite treatment consisted of adding an 8 % bentonite solution to the wine at a final concentration of 60 g/hL. Both batches were sealed and stored at 15 °C for three days to allow the bentonite and precipitated proteins to settle. The subsequent wines used for the bubble column tests were taken from the tops of these batches.

3.4. Procedure for measurement of viscosity of ethanol glycerol solutions

A rotational rheometer was used to measure the viscosity of the various ethanol glycerol solutions used in the Central Composite Design (CCD). A sample of the solutions was loaded between two plates of the rheometer, following which a torque was applied to the top plate. This exerted shear stress on the material from which the strain rate was to be measured. For Newtonian fluids, shear stress (τ) is proportional to strain rate ($\frac{d\gamma}{dt}$) and the dynamic viscosity (μ) as shown in equation 25.

$$\tau = \mu \frac{d\gamma}{dt} \qquad (25)$$

3.5. Experimental and statistical design

Four sets of experiments were performed within this study, and they are presented in the following order as shown in Figure 3.11
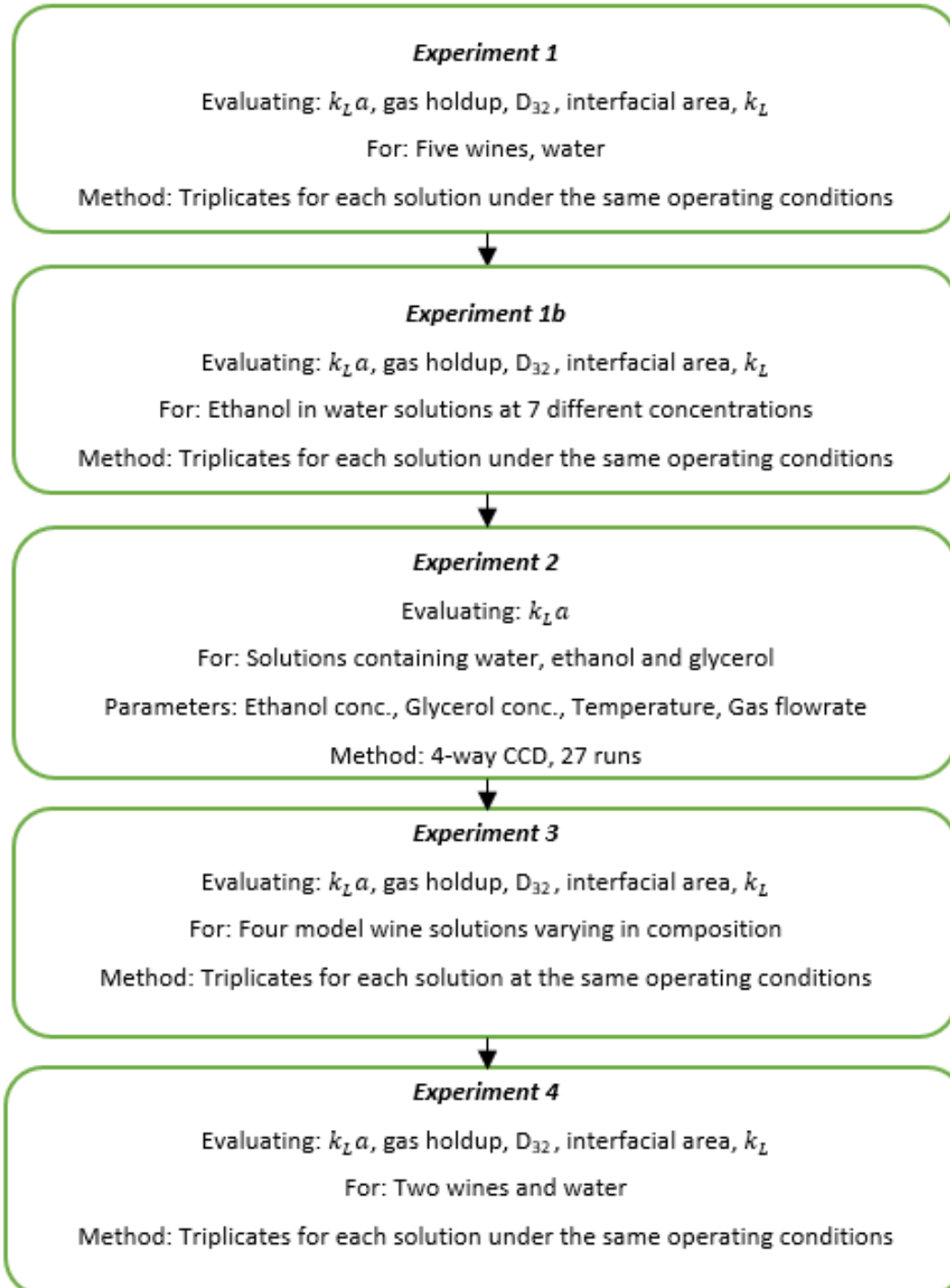
Figure 3.11: Summary of the experimental sets performed in this study

Within experimental sets 1, 3, and 4, each experimental run was performed in triplicate, with probe constants evaluated in triplicate for each experimental condition. An ANOVA analysis and the standard deviation was evaluated on the results through Excel. To determine whether there was any significant variance between the means between each experimental run, a t-test was performed using Statistica with a confidence interval of 95 %. P-values of less than 0.05 indicated a significant variance between the means.

3.5.1. Experimental set 1

Table 3.4 below shows the conditions for which each experimental run was performed for the 1st experimental set.

Table 3.4: Experimental runs for evaluating oxygen desorption in various wines

Run no.	Solution	Repeats	Temperature (°C)	Gas Flowrate (L/min)
1	Water	2	25	1.7
2	White-A	2	25	1.7
3	White-B	2	25	1.7
4	White-C	2	25	1.7
5	Rosé	2	25	1.7
6	Red	2	25	1.7

Additional experiments were done to evaluate all the parameters for different ethanol water solutions, the conditions of which are shown in Table 3.5. These experiments were an extension of the 1st experimental set.

Table 3.5: Experimental runs for evaluating oxygen desorption in aqueous ethanol solutions

Run no.	Ethanol concentrations (% v/v)	Repeats	Temperature (°C)	Gas flowrate (L/min)
1	0	2	25	2.3
2	0.01	2	25	2.3
3	0.05	2	25	2.3
4	0.1	2	25	2.3
5	0.5	2	25	2.3
6	1	2	25	2.3
7	5	2	25	2.3
8	10	2	25	2.3

3.5.2. Experimental set 2

For the second experimental set a 4-way CCD was used to assess the effect of four parameters and their interactions on the oxygen desorption $k_L a$. The CCD contains five levels for each parameter - a summary of which are shown in Table 3.6 below. The high and low points for the ethanol and glycerol concentrations used were chosen as they represent the typical range for these compounds in wine (Kunkee & Eschnauer, 2016). The temperature range was chosen as this is the typical range of temperatures that wine will be at when oxygen desorption takes place (Zoecklein *et al.*, 1999). The gas flowrates were chosen as they are all beneath the threshold at which higher flow regimes may take place and are also beneath the rate at which significant foaming begins to take place. Table 3.7 shows the values of each parameter for each individual experimental run performed.

Table 3.6: The points used for testing the effect of four parameters on the $k_L a$

Factor level	Low point	Low star point	Centre point	High star point	High point
Parameters	-2	-1	0	1	2
Temperature (°C)	10	12.5	15	17.5	20
Gas Flowrate (cm/s)	0.09	0.16	0.23	0.30	0.37
Ethanol concentration (% v/v)	9	10.5	12	13.5	15
Glycerol concentration (g/L)	5	10	15	20	25

Table 3.7: The details for each experimental run performed through the 4-way CCD, in which the centre point is repeated twice

	Ethanol (% v/v)	Glycerol (g/L)	Temperature (°C)	Superficial gas velocity(cm/s)
1	10.5	10	12.5	0.16
2	10.5	10	12.5	0.30
3	10.5	10	17.5	0.16
4	10.5	20	12.5	0.16
5	13.5	10	12.5	0.16
6	13.5	20	17.5	0.30
7	13.5	20	17.5	0.16
8	13.5	20	12.5	0.30
9	13.5	10	17.5	0.30
10	10.5	20	17.5	0.30
11	13.5	20	12.5	0.16
12	13.5	10	17.5	0.16
13	10.5	20	17.5	0.16
14	13.5	10	12.5	0.30
15	10.5	20	12.5	0.30
16	10.5	10	17.5	0.30
17	12	15	15	0.37
18	12	15	15	0.09
19	12	15	20	0.23
20	12	15	10	0.23
21	12	25	15	0.23
22	12	5	15	0.23
23	15	15	15	0.23
24	9	15	15	0.23
25	12	15	15	0.23
26	12	15	15	0.23
27	12	15	15	0.23

3.5.3. Experimental set 3

Table 3.8 shows the conditions for which each experimental run was performed within the third set of experiments. It should be noted that for the third set of experiments, a different sparger (with the same properties as the sparger used for the other experimental sets) was used, however it was slightly older, and produced slightly larger bubbles.

Table 3.8: Experimental runs for evaluating oxygen desorption in model wine solutions

Run no.	Solution used	Repeats	Temperature (°C)	Gas Flowrate (L/min)
1	Water	2	25	2.3
2	10 % Ethanol solution	2	25	2.3
3	MWS-Glycerol	2	25	2.3
4	MWS-Acids	2	25	2.3
5	MWS-BSA	2	25	2.3
6	MWS-Yeast	2	25	2.3

3.5.4. Experimental set 4

Table 3.9 shows the conditions for which each experimental run was performed for the fourth set of experiments.

Table 3.9: Experimental runs for evaluating oxygen desorption in a protein unstable (PU) and a bentonite treated wine (BT)

Run no.	Solution used	Repeats	Temperature (°C)	Gas Flowrate (L/min)
1	Water	2	25	1.7
2	PU-Wine	2	25	1.7
3	BT-Wine	2	25	1.7

Chapter 4: Results and Discussion

4.1. Introduction

Four sets of experiments were performed within this study. The experiments evaluated the oxygen desorption volumetric mass transfer coefficient ($k_L a$), Sauter mean bubble diameter (D_{32}), gas holdup (ε), interfacial area (a), and the oxygen mass transfer coefficient (k_L), during desorption of oxygen from wine, model wine solutions and water, using nitrogen sparged through a bubble column.

The first experiments evaluated oxygen desorption in five wines. The results from these demonstrated the extent of the variation of oxygen desorption in different wines. It was also shown whether these variations were due to differences in the interfacial area or oxygen mass transfer coefficient. Subsequent sets of experiments were performed to identify which compound(s) in wine were responsible for the variations.

The second set of experiments evaluated how changing the concentrations of ethanol and glycerol in a model wine solution affected the oxygen desorption $k_L a$. Additionally, in order to gauge how changing operating conditions affected desorption within the bubble column, the effect that varying temperature and gas flowrate had on the oxygen desorption $k_L a$ was also examined. The results from these experiments indicated a need to evaluate whether other compounds in wine may significantly affect desorption rates.

A third set of experiments evaluated the desorption rate in model wine solutions containing varying amounts of ethanol, glycerol, organic acids and proteins. The results of these showed which compounds were significant in affecting a change on the $k_L a$ and the k_L, and gave an indication as to which compound in wine could significantly affect oxygen desorption.

Following this, a fourth set of experiments was performed to examine how bentonite fining of wine could impact the oxygen desorption rate within the wine. A summary of all the findings is then presented. The results are split into four sections - one for each set of experiments.

4.2. Evaluating the oxygen desorption $k_L a$, Sauter mean bubble diameter, gas holdup, interfacial area and the k_L for different wines

In order to get an understanding of the sort of variation in the desorption rates that occur in different wines, the oxygen desorption $k_L a$ was evaluated during the desorption of five different wines. The wines were chosen so as to get a wide representation of wines: A sweet rosé, a

dry red, and three dry white wines – a blend (White-A), a Chenin Blanc (White-B), and a Sauvignon Blanc (White-C).

4.2.1. *Evaluating the oxygen desorption $k_L a$ for five different wines*

Figure 4.1 shows oxygen desorption $k_L a$ values, obtained during the desorption of oxygen from five different wines and water. There was a statistically significant variance (p-values < 0.05) in the $k_L a$ values. The $k_L a$ value was significantly greater during the desorption of red wine than during the desorption of the white wines and the rosé. The $k_L a$ values during the desorption of the rosé and the Chenin Blanc (White-B) were found to be significantly greater than the value obtained during desorption in Sauvignon Blanc (White-C).

It took approximately 90 s of nitrogen sparging to reduce the dissolved oxygen content in the red wine from a saturation concentration of 7.8 mg/L to 1 mg/L, whereas it took approximately 190 s to do the same for the Sauvignon Blanc. These results confirm the untested hypothesis by winemakers that under the same conditions, desorption rates can vary within different wines. Consequently, significantly more nitrogen gas might be required to remove the same amount of dissolved oxygen from one wine relative to another. As differences in desorption rates were found within the same experimental setup, under the same operating conditions, which indicates that it is variation in wine composition that affects the desorption rate.

In the past, simple graphs have been used in industry to estimate the amount of gas required to remove a certain amount of oxygen from wine, such as the one presented by (Zoecklein *et al.*, 1999) in Figure 2.2. The results presented here show that generalised graphs can be inaccurate when it comes to estimating the amount of gas required for a desorption operation. Such graphs don't account for potential variation in desorption rates due to different operating conditions and vessel design. As shown by these results, they also do not account for the significant variation in the desorption rates that can occur depending on the composition of the wine.

Figure 4.1 also shows that the $k_L a$ values obtained during the desorption of oxygen from the white blend and water, were not statistically different. It has been observed that solutions containing an alcohol typically have much greater gas-liquid mass transfer rates than pure water (Chiciuc *et al.*, 2010; Gurol & Nekouinaini, 1985; Ramezani, Legg, Haghighat, *et al.*, 2017). Chiciuc et al. (2010) found that for aqueous solutions containing ethanol at concentrations between 2 and 20 % v/v, there was an increase in the oxygen absorption $k_L a$ by a factor of between 1.75 and 2.5 relative to pure water. Gurol & Nekouinaini (1985) found

a 200 % improvement in the oxygen absorption $k_L a$ when tertiary butyl alcohol was added to water to form a 4 mM alcoholic solution.

However, these studies, in addition to being absorption studies, were performed on mono-component solutions and elucidating the effect that a compound has on mass transfer based on studies done on mono-component solutions may not be representative of that happening in a complex solution such as wine. While these studies provide some indication of an effect, they can be limiting.

The data these studies provide may not always correlate with measured results from operations that involve complex solutions such as wine, biomass cultures or wastewater. It is likely then, that the complexity of wine means that there are compounds, or interactions between compounds within wine, that hinder oxygen transfer. This may explain why the $k_L a$ found during oxygen desorption within some of the wines was not significantly greater than found during oxygen desorption within water, despite the presence of ethanol.
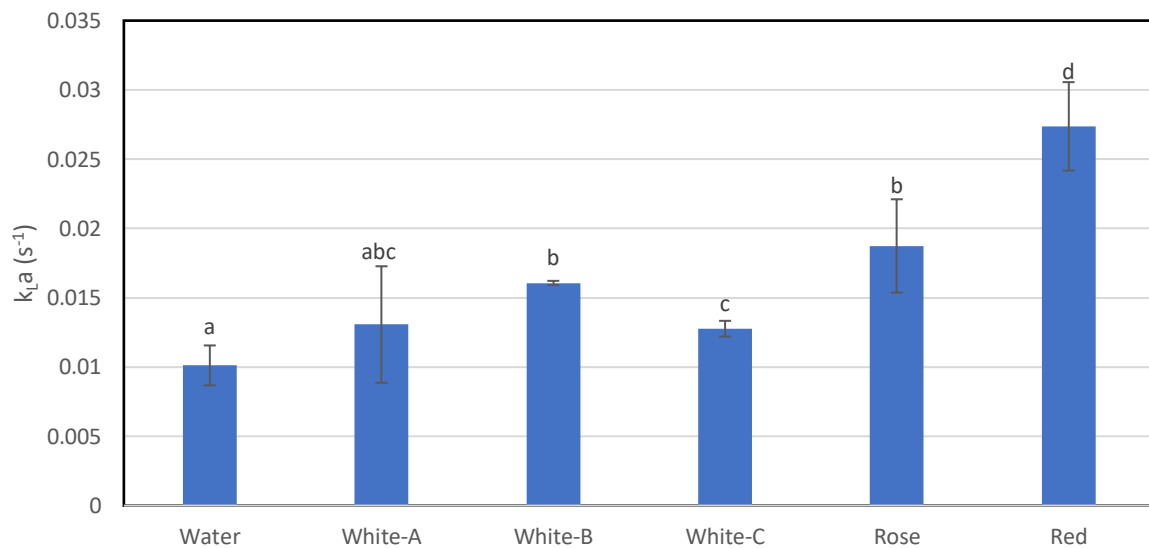

Figure 4.1: The $k_L a$ values obtained during the desorption of oxygen from five different wines and water, at 25 °C and at a nitrogen gas flowrate of 1.7 L/min (0.17 cm/s). The error bars represent the standard deviation of three experimental runs. The letters indicate whether the variation of the mean was significant (p-value<0.05). White-A is a dry white blend, White-B is a dry Chenin Blanc, White-C is a dry Sauvignon Blanc.

It is clear from these results that $k_L a$ values can vary significantly for desorption operations conducted in different wines. Numerous compounds in wine could be responsible for the variations. To get a greater understanding as to how $k_L a$ was affected within these systems, its individual parameters were also investigated.

4.2.2. Evaluating the Sauter mean bubble diameter (D_{32}), gas holdup, and interfacial area for five different wines

The specific interfacial area during the desorption of oxygen from the wines was evaluated by measuring the D_{32} and the gas holdup. Figure 4.2 shows the Sauter mean bubble diameter measured during the desorption of oxygen from five different wines and water. No significant difference between the D_{32} was found within the wines. This indicates that the varying compositions of these wines had no impact on mean bubble size. During nitrogen sparging, the D_{32} was found to be approximately 2.5 times lower in the wines compared to in water. This significant drop in the mean bubble size is likely due to other compounds found within all the wines.

In order to understand how the presence and concentration of a compound affects bubble size, it is important to understand the factors that contribute to bubble size and formation. Besides design and operating factors, there are two predominant physical phenomena that affect bubble size within a system. The first is the surface tension of the solution. Higher surface tensions result in bubbles that gain in size for a longer time before detaching from the base of the sparger, resulting in larger bubble sizes (Kazakis, Mouza & Paras, 2008).

Any variations in surface tension between the different wines did not affect bubble size. However any variation in the surface tension between wines is relatively small compared to the difference between the surface tension of wines and water (Glampedaki *et al.*, 2010). The surface tension of water in air at 25 °C is approximately 72 mN/m (Belda, Herraez & Diez, 2005), whereas the surface tension of wines under the same conditions has been found to be between 43 and 47 mN/m (Glampedaki *et al.*, 2010). This indicates that differences in the surface tension of the wines and water are likely to have contributed to the significant difference in the D_{32} found during oxygen desorption in wine versus water.

In addition to the change in surface tension, the other phenomenon that affects bubble size is the frequency of bubble coalescence (Kazakis *et al.*, 2008). Typically, bubbles coalesce at the base of the sparger as they form and are released from the sparger pores. This is the case with bubbles in water, however, it is known that the addition of ethanol can suppress coalescence, resulting in smaller bubbles in the column (Wang, Guo, Liu, *et al.*, 2020; Zahradník *et al.*, 1999). Zahradník et al. (1999) found significant reduction in the coalescence of two bubbles in a chamber when the concentration of ethanol in an aqueous solution was raised to 1% v/v.

It is likely then, that the difference in D_{32} between the systems containing wine and water is affected by the presence of ethanol in the wines. Variations in ethanol concentrations in the wines (7 - 12.5 % from the sweet rosé to the dry red) did not result in different D_{32} values or interfacial areas. This may be because, once the ethanol concentration crosses a threshold value - in the region of 1 % v/v (Zahradník *et al.*, 1999), it no longer affects a rate of change on bubble size.

To confirm this for desorption cases, the bubble sizes during the desorption of oxygen from different aqueous solutions with varying ethanol concentrations were also evaluated in this study. The results from this are shown in Figure 4.3. This data was obtained at a slightly higher gas flowrate with an alternate stone sparger and is not directly comparable to results from Figure 4.2.

This data shows that there was a significant drop in the D_{32} when the ethanol concentration was raised to 0.10 % v/v. There was no significant drop in the D_{32} within the system when the ethanol concentration was further raised up to 10% v/v, with the D_{32} approximately 1/3rd of that observed when sparging was taking place in water. This reflects the similar drop in mean bubble size found in Figure 4.2 between the system containing water and the systems containing wine.

Therefore, it is likely that the surface-active properties of ethanol, at concentrations of 0.10 % v/v and greater, prevent bubble coalescence at the gas flowrates tested. This data supports the idea that ethanol is a significant contributor to the differences in the D_{32} found during nitrogen sparging in wines and water. The results also indicate that the variations in ethanol concentrations that are typically found in wine, may not contribute to changes in the D_{32} that may occur during nitrogen sparging within different wines. This is backed up by the lack of variation in the D_{32} observed during the nitrogen sparging of different wines.

Ethanol is clearly a big determinate of bubble size during sparging in wine. Following these results, the mean bubble size was evaluated within a 10 % v/v ethanol solution under the same conditions and using the same sparging stone as the one used for evaluating the the D_{32} in the wines. The Sauter mean bubble diameter was found to be approximately 0.249 mm. The results are shown in Table S24 and Table S25 in the supplementary material. This value fit into the range of D_{32} values found during oxygen desorption in the different wines shown in Figure 4.2, indicating that there was likely no compound in the wines tested that was suppressing the ability of ethanol to prevent bubble coalescence. This also shows that a simple ethanol solution may be an accurate indicator for estimating the bubble sizes that may

occur during the oxygen desorption within a specific wine, from a specific sparger. It is also possible that sparging in alcohol-free wines (<0.1 % v/v), may result in greater bubble sizes relative to other wines, and consequently a smaller interfacial area and lower desorption rate.

Figure 4.4 shows images taken of bubbles in three different wines and water at nitrogen gas flowrates of 1.7 L/min and 0.5 L/min. It can be qualitatively observed the significant variation of the sizes of the bubbles in the water and the three wines. It can also be observed that there was no significant variation in the bubble sizes within the different wines at different gas flowrates, while there was significant increase in the bubble sizes found in water when the gas flowrate was increased. This is further indicative of the effect of ethanol on inhibiting coalescence, as increases in bubble size are expected with increases in gas flowrate, as bubbles coalesce more frequently at higher gas flowrates. However, Kazakis, Mouza and Paras (2008) found this not to be the case for an alcoholic solution.
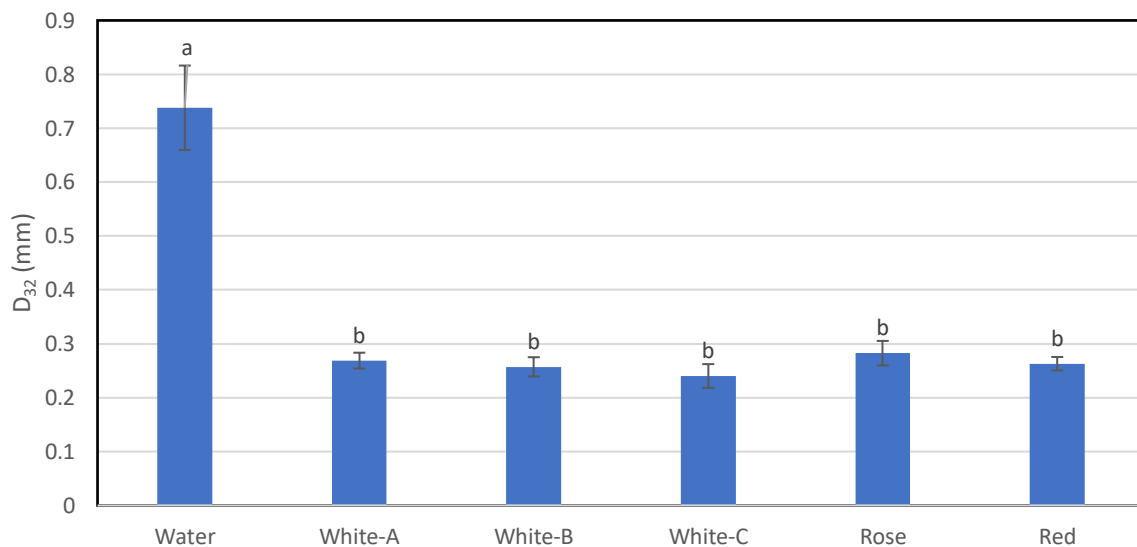
Figure 4.2: The D_{32} obtained during the desorption of oxygen from five different wines and water, at 25 °C and at a nitrogen gas flowrate of 1.7 L/min (0.17 cm/s). The error bars represent the standard deviation of the D_{32} from 5 images, with each image containing at least 200 measured bubbles. The letters indicate whether the variation of the mean was significant (p<0.05). White-A is a dry white blend, White-B is a dry Chenin Blanc, White-C is a dry Sauvignon Blanc.

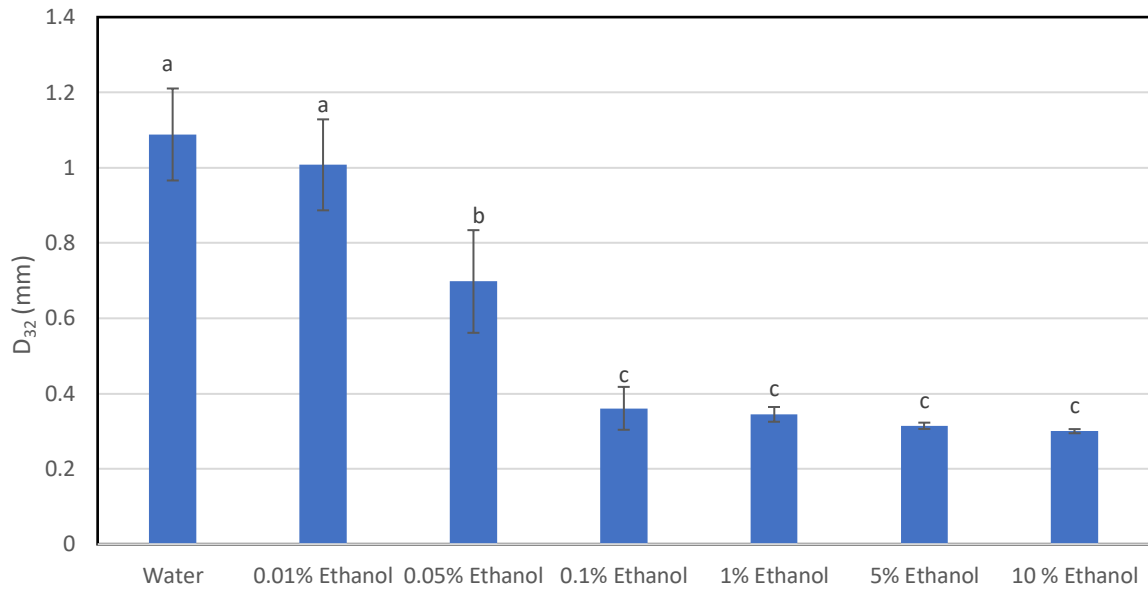*Figure 4.3: The D_{32} obtained during the desorption of oxygen from solutions containing different ethanol concentrations (% v/v), at 25 °C and at a nitrogen gas flowrate of 2.3 L/min (0.23 cm/s). The error bars represent the standard deviation of the D_{32} from 5 sets of images, each containing at least 200 measured bubbles. The letters indicate whether the variation of the mean was significant (p<0.05).*
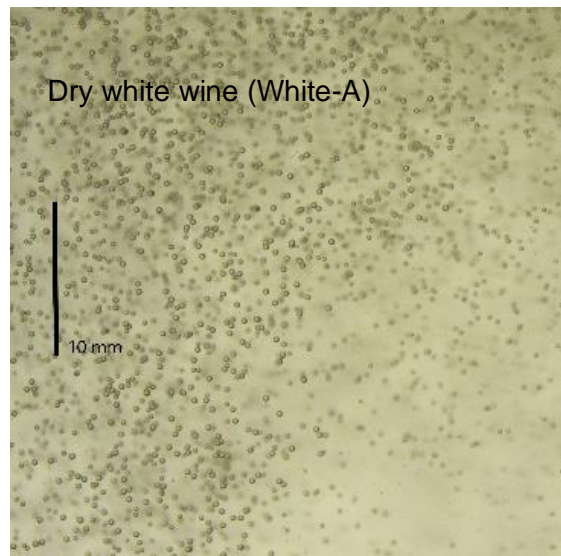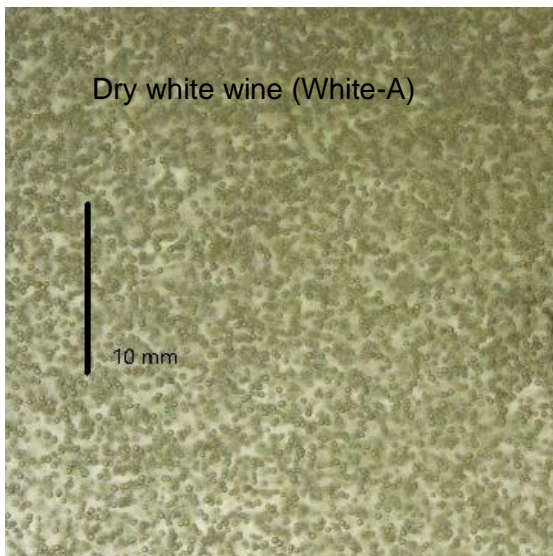
Figure 4.4: Bubbles flowing within the bubble column at 25 °C and at 1.7 L/min (0.17 cm/s, left) and at 0.5 L/min (0.05 cm/s, right). From top to bottom is: Dry white wine (White A), Sauvignon Blanc (White C), Rosé, Water. The left column are images taken at a gas flowrate of 1.7 L/min (0.17 cm/s), and the right column are images taken at a gas flowrate of 0.5 L/min (0.05 cm/s).

The measured gas holdups obtained within the bubble column during oxygen desorption are shown in Figure 4.5. It can be observed that the gas holdups were unaffected by the type of wines in the bubbl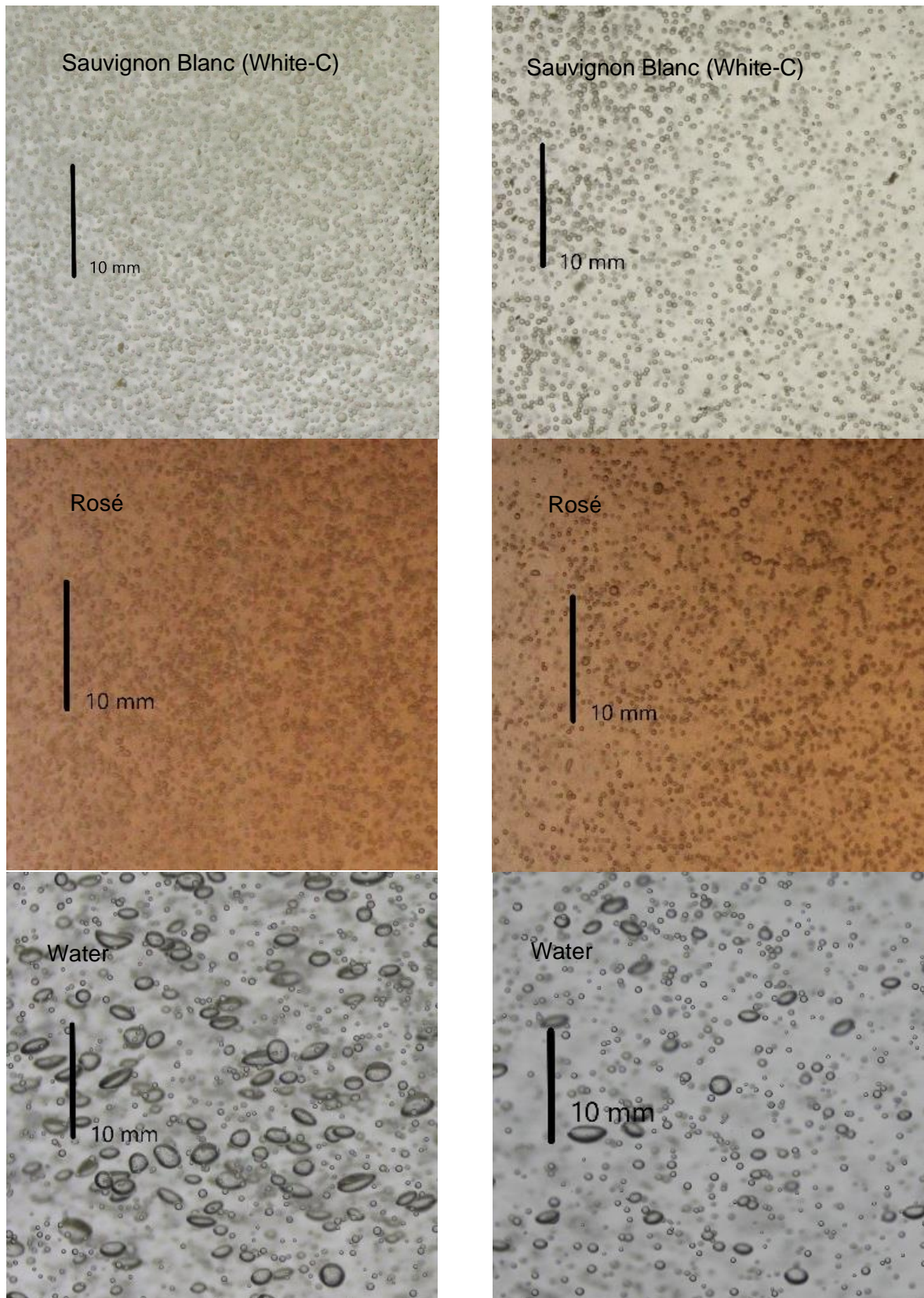e column, while the gas holdup during the desorption of oxygen from water was significantly lower, at approximately 1/3rd of that found when sparging through the wines.

The lack of variation in the gas holdup is likely due to similar mean bubble sizes found in the wines, and similar flow regimes within the bubble column during sparging. The gas holdup was significantly lower in water due to larger bubble sizes. Larger bubble rise to the surface more rapidly, resulting in lower residence times and a lower gas holdup. It should be noted that the standard deviation of the gas holdup was significantly less in the red wine relative to the other wines. The reason for this is that there was significantly less foaming in the red wine compared to the other wines, which made it easier to measure the gas holdup accurately. The head of foam for the red wine was approximately 1 cm, while the remainder of the wines had heads of foam in the region of 5 to 10 cm.

The creation and stabilisation of foam in wines would typically be due to the presence of carbon dioxide and surface-active compounds within the wine. However, in this case, as the carbon dioxide was removed from all the wines prior to oxygen desorption, the presence of foam could be attributed to surface-active compounds. Stable foams remain in place for longer and build a head more rapidly, as opposed to unstable foams which collapse more easily. Kulkarni et al. (2020) indicated that certain surface-active proteins are the prime contributors to the development and stabilisation of foam in beverages. Núñez et al. (2006) have suggested that glycoproteins in wine are the significant contributors to foam, while polysaccharides may also affect foam properties. Both these compounds have been shown to be surface-active (Moeller *et al.*, 2018). Consequently, foam heavy wines may be an indicator of significantly higher concentrations of these compounds.

Large amounts of foaming can have negative consequences during the processing of wine in industry. Foaming can result in overpressure within a vessel if the foaming blocks an exit filter, or it could result in the loss of sterility in a vessel if the foam escapes (Routledge, 2012). This may mean that the working volume within the vessel would have to be reduced in order to account for a large head of foam.

To reduce the formation of foam, antifoam is often added to solution, however, antifoam in not a legal additive in winemaking, and it can also compromise oxygen desorption, as antifoams can change the system properties and have been shown to decrease the k_L (Galpin, 2006;

Morao, Maia, Fonseca, *et al.,* 1999). To avoid excessive foaming, slow continuous sparging or rapid bursts of sparging could be performed, or a mechanical foambreaker could be employed.

Figure 4.5: Gas holdups during the desorption of oxygen from five different wines and water, at 25 °C and at a nitrogen gas flowrate of 1.7 L/min (0.17 cm/s). The error bars represent the standard deviation of measurements taken from three runs. The letters indicate whether the variation of the mean was significant (p<0.05). White-A is a dry white blend, White-B is a dry Chenin Blanc, White-C is a dry Sauvignon Blanc.

Figure 4.6 shows the measured interfacial areas during the desorption of oxygen from the five wines and the water, calculated from the D_{32} and the gas holdup. As expected, there was little significant variance between the interfacial areas occurring within the wines. The specific interfacial area of the gas bubbles in water was significantly lower, due to the reduced gas holdup and significantly larger D_{32} relative to the those values found during the desorption in wines.

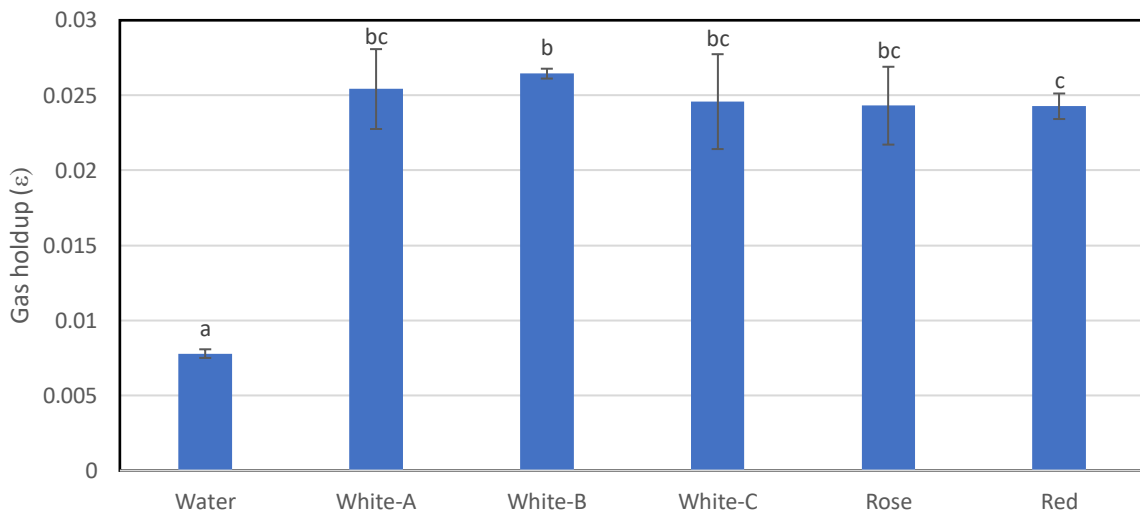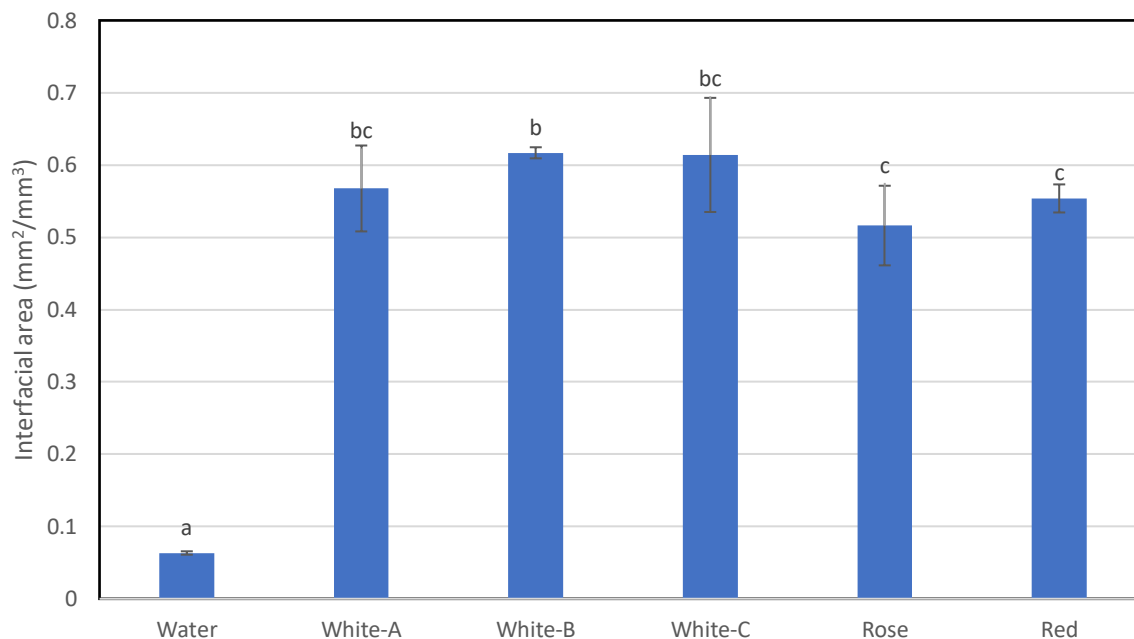*Figure 4.6: The interfacial areas during the desorption of oxygen from five different wines and water, at 25 °C and at a nitrogen gas flowrate of 1.7 L/min (0.17 cm/s). The error bars represent the standard deviation of the samples taken for each gas holdup measurement and the Sauter mean diameter. The letters indicate whether the variation of the mean was significant (<0.05). White-A is a dry white blend, White-B is a dry Chenin Blanc, White-C is a dry Sauvignon Blanc.*

4.2.3. Evaluating the oxygen mass transfer coefficient (k_L) for five wines and water

Figure 4.7 shows the oxygen mass transfer coefficients (k_L) obtained during the desorption of oxygen from five different wines and water. There was a statistically significant variation between the k_L values obtained. This was expected due to the significant variation in the measured $k_L a$ values and the minor variation in the measured interfacial areas during desorption of oxygen from the wines. The value of k_L obtained during the desorption of oxygen from water was found to be approximately 0.16 mm/s, while during the desorption of oxygen from the wine, it varied between 0.025 and 0.05 mm/s, depending on the type of wine.

It has typically been accepted that for bubble sizes less than 1.5 mm (as was the case in this study), k_L values will be in the region of 0.1 mm/s (Sardeing, Painmanakul & Hébrard, 2006). Values as low as 0.029 mm/s have been found by Bredwell and Worden (1998) for oxygen in a surfactant solution. Calderbank and Moo-Young (1961) found k_L values, for carbon dioxide in aqueous glycerol solutions, between 0.02 and 0.1 mm/s for bubbles with diameters below 1.5 mm.

The significantly higher k_L value obtained during desorption of oxygen fromwater, relative to the wines, is probably not due to the relatively larger bubbles in the water during desorption. Wang et al. (2020) found that for bubble sizes less than 1.5 mm, bubble diameter had no effect on k_L. There is typically only a correlation between increasing bubble size and increasing k_L for bubbles with diameters between 1.5 mm and 4 mm (Wang *et al.*, 2020). The probable reason for lower k_L values during the desorption of oxygen from wines, is that there are compounds in the wine creating a resistance to mass transfer at the gas-liquid interface.

Numerous compounds in wine could contribute to increasing the resistance to oxygen mass transfer. Major compounds such as ethanol, glycerol, sugar, organic acids, or differences in pH, could all potentially contribute to increases in mass transfer resistance.

As already demonstrated, ethanol is surface-active, while glycerol affects viscosity, which can consequently affect k_L as well (Clarke & Correia, 2008). Surfactants strongly affect k_L, and the presence of compounds in wine that act as surfactants, such as proteins and polysaccharides, could potentially reduce k_L.
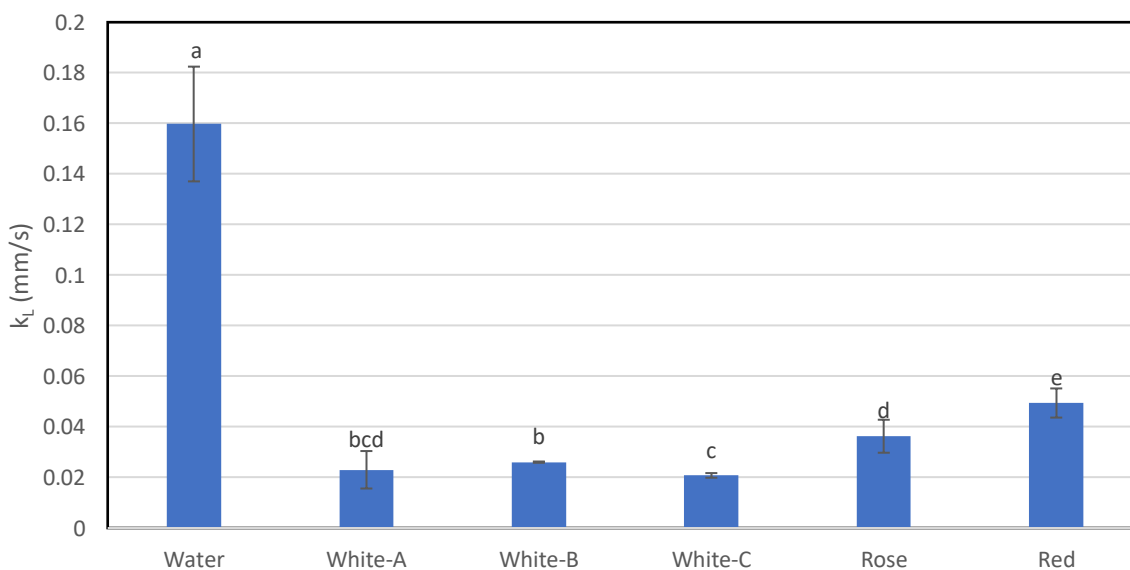
Figure 4.7: The oxygen mass transfer coefficients obtained during the desorption of oxygen from five different wines and water, at 25 °C and at a nitrogen gas flowrate of 1.7 L/min (0.17 cm/s). The error bars represent the standard deviation of three measurements obtained from the measurement of the $k_L a$ and the interfacial area. The letters indicate whether the variation of the mean was significant (p<0.05). White-A is a dry white blend, White-B is a dry Chenin Blanc, White-C is a dry Sauvignon Blanc.

In this study, the k_L values obtained were for bubbles that may be different in size than what would typically be found at industry scale. In an industrial setting, bubble sizes will differ depending on the type of sparger used or if a simple nozzle is used. The use of simple nozzles or open pipes will result in larger bubbles. The oxygen mass transfer coefficients in these

cases would not necessarily be the same as those found for the microbubbles in this study, as the general trend is that the k_L values tend to increase as the bubble diameter increases between the diameter range of 1.5 mm and 4 mm. The oxygen mass transfer coefficient in water for bubbles greater than 4 mm is typically around 0.4 mm/s (Sardeing *et al.*, 2006). However, in a surfactant solution, even for bubble diameters greater than 4 mm, the k_L continues to be affected by the liquid and surfactant properties, with differences in the k_L for surfactant solutions having been shown to remain in place or even be more accentuated relative to water (Sardeing *et al.*, 2006). Therefore, variations in the oxygen k_L during the desorption of oxygen from different wines will likely remain in place when desorption takes place in systems containing bigger bubbles.

As a winemaker, increasing the oxygen desorption rate can most easily be done by increasing the interfacial area. This can be done by increasing the gas flowrate through the system or by introducing smaller bubbles into the system. The results just presented have shown that differences in the desorption rates occurring in different wines are due to differences in the k_L. While increasing the interfacial area is a way to compensate for lower k_L values, it may also be possible to increase the k_L within the system.

It has been suggested that increasing the turbulence within the system results in increases in the k_L (Clarke & Correia, 2008; Rosso, Huo & Stenstrom, 2006). Rosso et al. (2006) indicated that increased turbulence results in higher interfacial renewal rates. This can displace the negative effect that surfactants can have on the k_L, by exposing the gas-liquid interface to turbulent upflows. This consequently brings bulk fluid closer to the interface, and increases the flux of components from the liquid to the gas.

Clarke and Correia (2008) state that increased turbulence affects k_L by reducing the width of the liquid side film (as described by the two-film theory) around the gas bubble, reducing resistance to mass transfer. Clarke and Correia (2008) present several correlations for k_L and power input over volume (P/V) for stirred tank reactors. They indicate that increasing power input increases k_L. This may be dependent on the bubble size, as it has been suggested that increased turbulence does not increase the k_L when bubbles are less than 1.5 mm in diameter (Calderbank & Moo-Young, 1961).

Increasing the turbulence in the system could most easily be done by increasing the gas flowrate such that the system transitions from a homogenous flow regime into a heterogeneous flow regime. It should be noted though that operating in the heterogeneous

regime is often cited as being less efficient in terms of gas usage (Besagni *et al.*, 2019; Ruzicka *et al.*, 2003). However, in this case, the reduction in efficiency could be overcome by the improvement in the k_L. Increasing the gas flowrate also simultaneously increases the interfacial area. The presence of an impeller could also increase the turbulence in the system, and would also likely encourage bubble breakup and a subsequent increase in interfacial area.

In this section, significant variation in the oxygen desorption rates in wines have been demonstrated. This has been attributed to differences in the oxygen mass transfer coefficient values measured during the desorption of oxygen from the different wines. At an industrial scale, these variations are likely to remain in place, and possible ways to overcome k_L limitations have been suggested. The reason for the variation in the k_L and the $k_L a$ is due to differences in the compositions of the wines. The following sections seek to determine what compounds in wine could contribute to these changes.

4.3. The effect of changing temperature, gas flowrate, ethanol concentration, glycerol concentration on the oxygen desorption $k_L a$ in aqueous ethanol glycerol solutions

In this set of experiments, two likely candidate compounds for affecting a change on the oxygen desorption $k_L a$ were investigated: Ethanol and glycerol. In addition, the effect that changing operating conditions had on $k_L a$, for the specific experimental setup used in this study, was investigated. In order to do this a 4-way Central Composite Design (CCD) was created to examine the effect of four parameters on $k_L a$: Ethanol concentration, glycerol concentration, temperature, and gas flowrate.

The temperature was varied between 10 and 20 °C. This temperature range was chosen as this is the typical range under which wine is packaged and desorption operations are conducted. The nitrogen gas flowrate varied between 0.9 and 3.7 L/min. These flowrates correlated to superficial gas velocities of 0.09 and 0.36 cm/s. These gas flowrates were chosen to reduce foaming and to ensure a homogeneous flow regime within the system. The superficial gas velocities were well below the 5 cm/s often indicated as the upper boundary for which the homogeneous regime ends and transitions to a more turbulent regime (Besagni *et al.*, 2019).

Remaining within the homogeneous regime was important for the study, as sudden differences in oxygen transfer may occur when a fluid regime switches, potentially resulting in confusing results if unaccounted for. Within a steady homogeneous regime, oxygen transfer will increase

with increasing gas flowrate. As more bubbles are drawn through the system the interfacial area is enhanced, while the simple upwards trajectory of the bubbles minimises bubble collisions, reducing coalescence.

However, increasing the superficial gas velocity beyond a certain threshold (around 5 cm/s for bubble columns) can cause the hydrodynamics in the system to rapidly change to a heterogeneous regime. Within this regime there is increased radial and downward flows of bubbles, and greater bubble coalescence, which can consequently result in reduced bubble residence times, and a less uniform improvement in mass transfer. During the transition regime, described in Figure 2.5, mass transfer may be completely stifled as the effect of the increased coalescence temporarily results in a reduced interfacial area. This can be overcome by increasing the gas flowrate, transitioning to the heterogeneous regime. Ensuring that all experiments take place under a homogeneous regime makes it easier to elucidate any correlations between the parameters and the $k_L a$.

Ethanol and glycerol concentrations were varied between 9 and 15 % v/v, and 5 and 25 g/L, respectively. The ethanol concentration ranges were chosen as they represent a good variation of ethanol concentration for wines. Additionally, the wines tested in the first set of experiments had ethanol concentrations within this range and exhibited significant differences in desorption rates. This indicated that this was a range necessary to investigate for changes in desorption rates. The concentration ranges for glycerol were chosen as they represent the typical upper and lower boundary for most common wines (Kunkee & Eschnauer, 2016).

The significant (p < 0.05) correlations between the parameters and the oxygen desorption $k_L a$ are shown through a pareto chart in Figure 4.8. The bars in Figure 4.8 decrease in order of the correlation strength between the parameter and the $k_L a$.

Significant linear correlations were found for the effect of gas flowrate and temperature on the $k_L a$. The positive linear correlation for the gas flowrate on the $k_L a$ is indicative of the system operating within the homogeneous regime (Ruzicka *et al.*, 2003). It is well known that increases in temperature results in increases in $k_L a$, and this was found in this study. Typically the viscosity of the system decreases with an increase in temperature, which results in an increase in the $k_L a$ (Sehabiague & Morsi, 2013). The oxygen diffusion coefficient in water is also strongly related to temperature, with increases in temperature increasing the diffusion coefficient which in turn increases k_L.

The positive effect that temperature has on the $k_L a$ is well described. A correlation often used is described by Bewtra et al. (1970), shown by equation 26.

$$k_L a_T = k_L a_{T=20°C}(\theta^{(T-20)}) \qquad (26)$$

The θ value regularly used for water oxygen systems in bubble columns is 1.024. For other systems, values as high as 1.048, and as low as 1.008 have been used (Stenstrom & Gilbert, 1981). This correlation is not linear, however it can be observed from Figure 4.9 that the linear correlation obtained from this experiment is a very good approximation of the correlation described by Bewtra et al. (1970). However, the θ value is dependent on the aeration system and vessel design. A θ value of 1.024 fitted well for this bubble column setup, but it might be inaccurate for other bubble column systems under other operating conditions. A surface plot for the effect of temperature and gas flowrate on the $k_L a$ can be seen in Figure 4.10.

It can be observed how sensitive this system is to changes in gas flowrate. In this case, an increase in 1 L/min gas flowrate (0.075 L/minute per L of solution) was equivalent to about an increase in 8 °C in terms of the increase in the $k_L a$. In an industrial setting it would be beneficial to perform oxygen desorption under conditions at which the wine is warmer (ie. Not directly after refrigeration). Performing sparging at a point when the wine is at a higher temperature may be beneficial. However, the gains in desorption rate obtained by actively increasing the temperature of the wine would have to be measured against the energy required to raise the temperature, which might be too excessive to make it a cost-effective option.

In terms of optimising operating conditions for the system, enhancing gas flowrate should be prioritised over increasing temperature. However as discussed, increasing the gas flowrate beyond a homogeneous regime may reduce the oxygen transfer efficiency, so although speeding up the process, it would require a greater amount of inert gas to remove the same amount of dissolved oxygen. If the desorption step is not a bottleneck process during winemaking, then it may be best to operate within the homogeneous regime, which would be the more resource friendly operating condition.
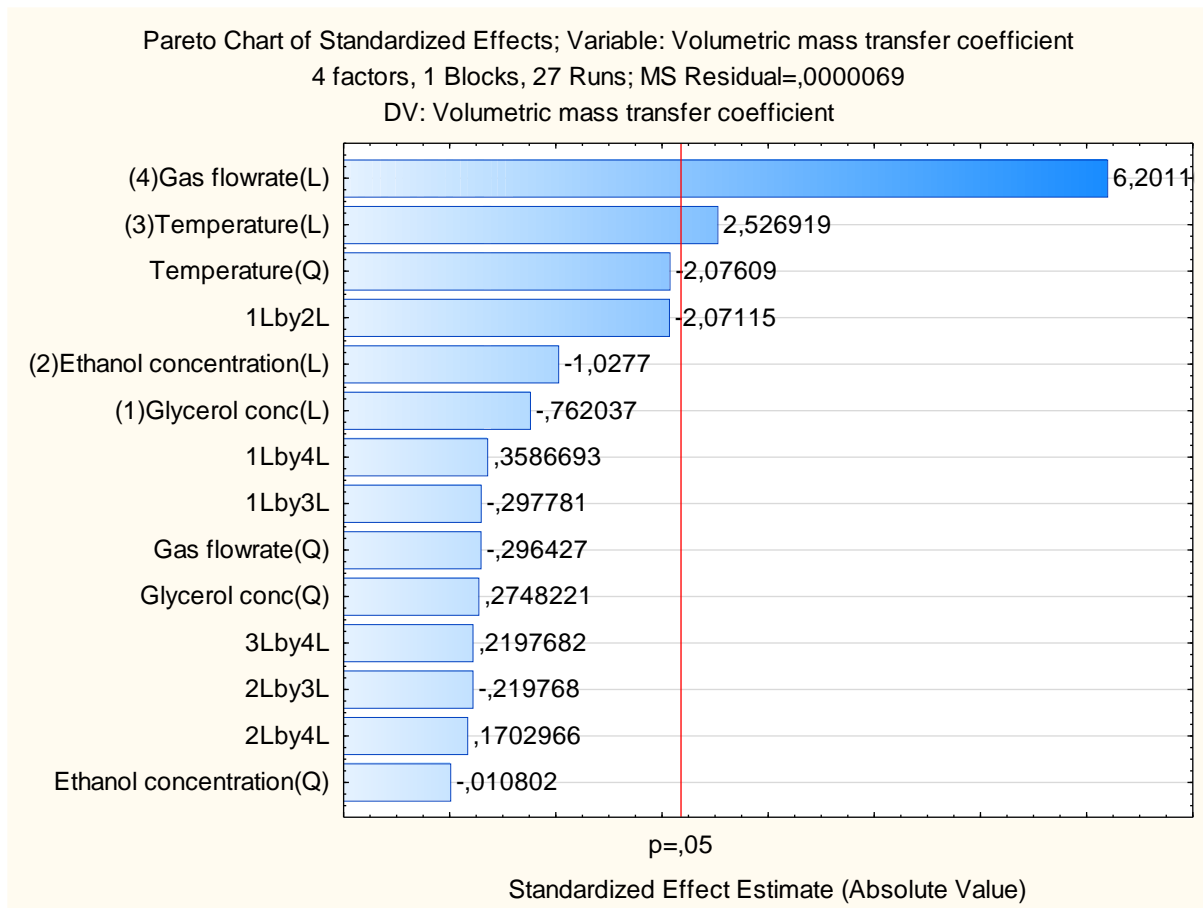
Figure 4.8: Pareto chart for the 4-way CCD experiment showing the linear, quadratic, and interaction correlations for gas flowrate, temperature, ethanol concentration, glycerol concentration on the $k_L a$. The red line represents a p-value of 0.05, with bars to the right, indicating p-values less than 0.05 and significant correlations. 'L' and 'Q' refer to linear and quadratic correlations respectively, while 'xL by yL' refers to the correlation for an interaction effect between two parameters, where x and y are the parameters in question
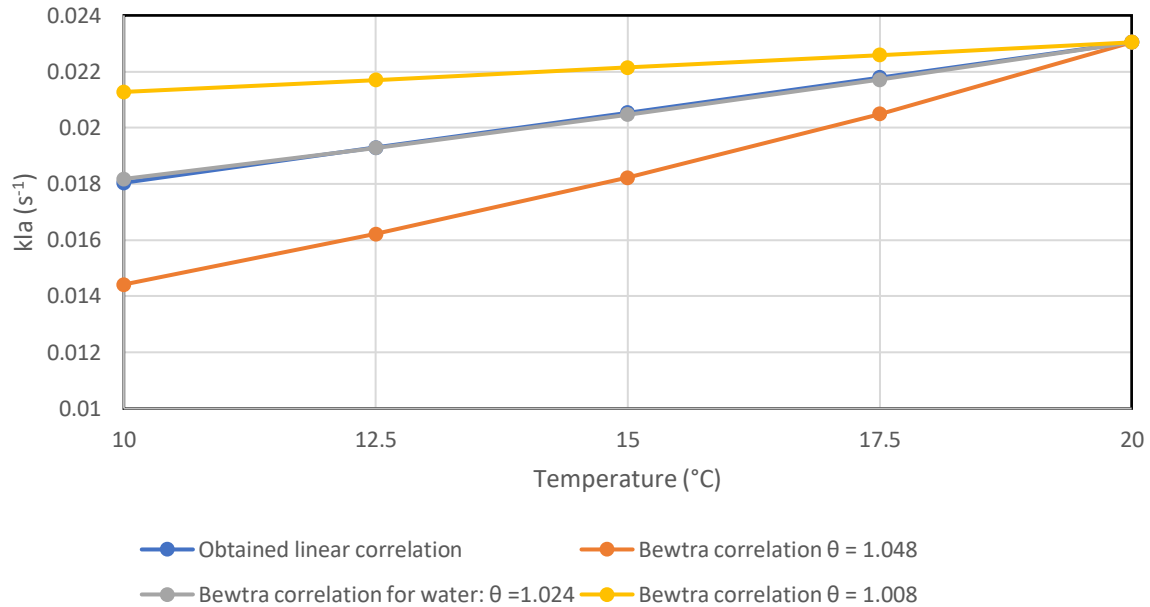
Figure 4.9: Graph showing the effect of temperature on the k_La from the obtained linear correlation in this work, and three correlations based on the equation given by Bewtra et al. (1970), with θ = 1.048 and θ = 1.008 representing the estimated upper and lower bounds found for liquid gas systems. The standard Bewtra correlation for air-water in a bubble column is θ = 1.024.
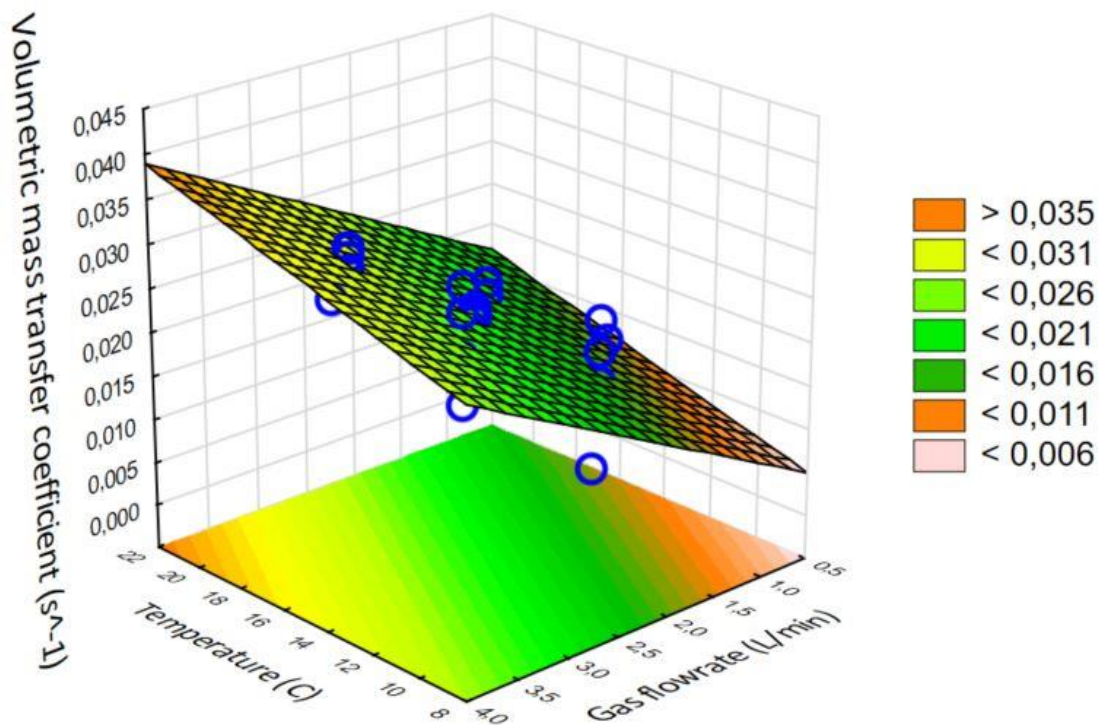
Figure 4.10: Surface plot showing the linear correlation effect of temperature and gas flowrate on the k_La

It is further observed from Figure 4.8 that there were no significant quadratic or interactive correlations found for all the parameters on the k_La. The lack of effect on the k_La somewhat

mirrors results from absorption experiments on aqueous ethanol solutions performed by Chiciuc et al. (2010), in which no significant change in the oxygen absorption k_La was observed when ethanol concentrations were increased from 2 % v/v up to 20 % v/v.

The physico-chemical properties of the system do change for different glycerol and ethanol concentrations. The viscosity for the different solutions used within this set of experiments fell within the range of 1.4 to 1.7 mPa.s when measured at 20 °C. The surface tension of aqueous ethanol solutions at 10 % v/v and 20 % v/v at 20 °C has previously been determined as 53.4 and 43.7 mN/m respectively (Khattab, Bandarkar, Fakhree, *et al.*, 2012). While there are changes in the physico-chemical properties of the various solutions tested, it is possible that these changes in viscosity and surface tension may be too minor to result in an observable change in the k_La. A surface plot showing the linear correlation effect of ethanol and glycerol concentration on the k_La is shown in Figure 4.11.
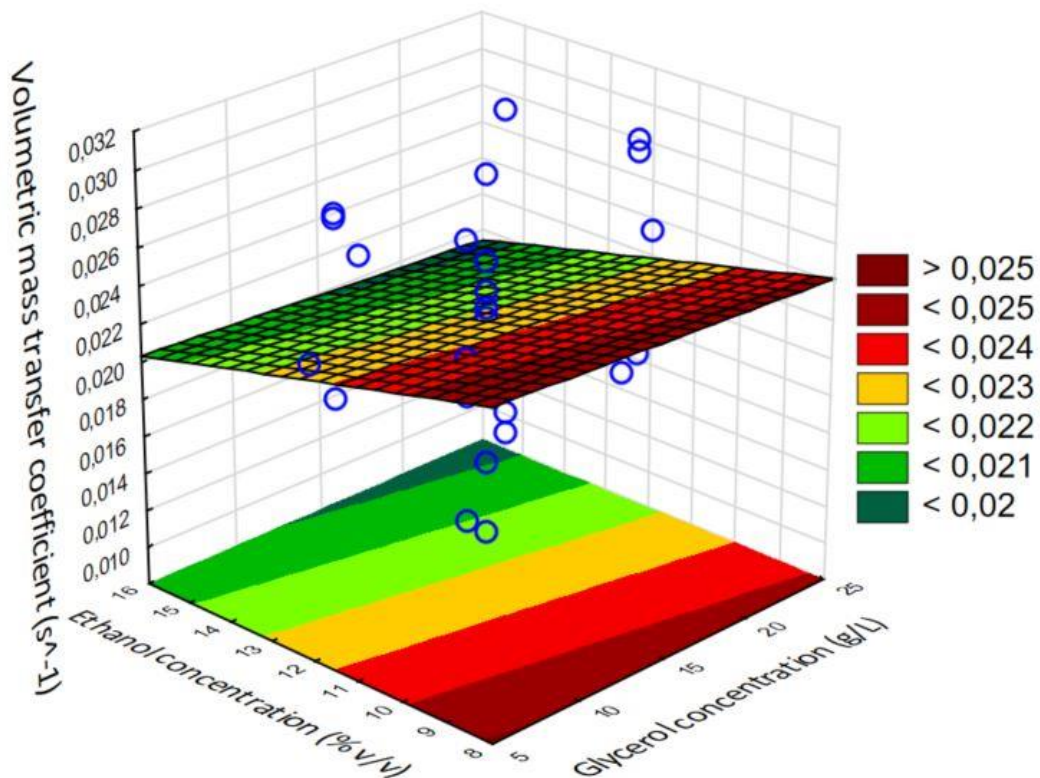
Figure 4.11: Surface plot showing the linear correlation effect of ethanol and glycerol concentration on the k_La

While there was no effect on the desorption k_La for the range of ethanol concentrations tested in the CCD, previous absorption studies have indicated that there was a significant effect of ethanol on the absorption k_La at much lower ethanol concentrations (Chiciuc *et al.*, 2010).

To confirm that there would be similar significant observable changes in the oxygen desorption k_La within the bubble column setup used in this study, a subsequent set of experiments was done to evaluate how the desorption k_La changed for a wider range of ethanol solutions. The results are shown in Figure 4.12.
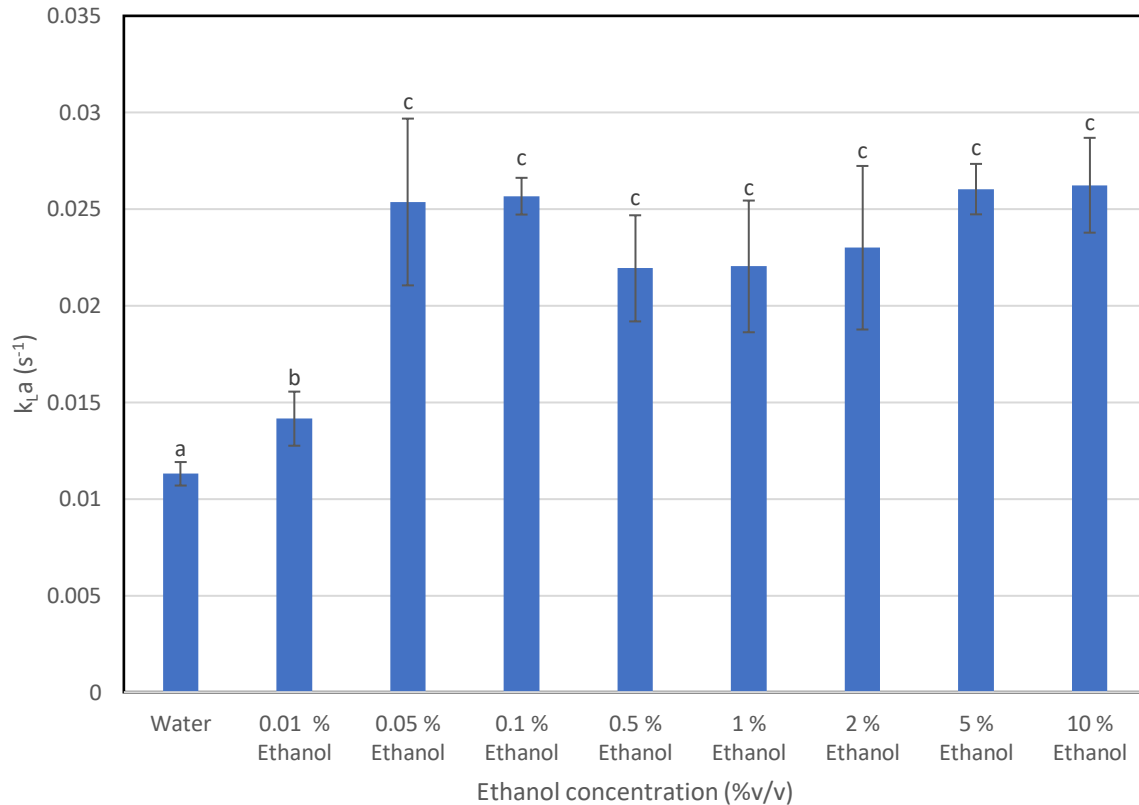
Figure 4.12: The k_La for water and various ethanol solutions (0.01, 0.05, 0.1, 1, 2, 5, 10 % v/v) at a gas flowrate of 2.3 L/min (0.23 cm/s), and at 25 °C. The error bars represent the standard deviation from three runs. The letters indicate whether the variation of the mean was significant (p<0.05).

The change in surface tension between 0.01 % and 1 % v/v ethanol is approximately 70 to 60 mN/m at 20 °C (Belda *et al.*, 2005). This is not a great enough drop to suggest that the change in surface tension was the reason for the increase in the observed desorption k_La at these two concentrations.

As has previously been observed in Section 4.4.2, small concentrations of ethanol can result in a significant reduction in bubble size, and it is likely that this reduction in bubble size causes the significant increase in the k_La by increasing the interfacial area.

It has been suggested that ethanol acts as a surface-active compound, and that even at very small concentrations, the bubble size can be significantly reduced, consequently increasing the interfacial area (Chiciuc *et al.*, 2010). The results from Figure 4.3 confirm this, as the D$_{32}$

within the bubble column dropped by approximately 40 % when as little as 0.05 % v/v ethanol was added to water.

There was no significant difference in the $k_L a$ during the desorption of oxygen from aqueous ethanol solutions containing ethanol concentration of 0.05 % v/v and greater. This is despite changes in surface tension and viscosity between a 0.05 % v/v and a 10 % v/v ethanol solution. This indicates that further increases in viscosity, and decreases in surface tension, had no effect on the $k_L a$, or had opposing effects. The lack of change in $k_L a$ between solutions containing the typical ethanol concentrations found in wine indicate that changes in ethanol concentration don't contribute to the observed changes in desorption rate of different wines. However, the significant changes in the desorption rate between solution containing 0 and 0.05 % v/v ethanol, demonstrates how the mass transfer of oxygen can be significantly enhanced with the addition of a very small amount of ethanol.

Based on the results from this experiment, with regards to optimising operating conditions for the system, enhancing gas flowrate should be prioritised rather than an energy intensive system such as increasing temperature. The results also indicate that there are other compounds within wine that affect the oxygen desorption $k_L a$, and a further set of experiments were performed on model wine solutions containing a greater complexity of compounds.

4.4. Evaluating the oxygen desorption $k_L a$, Sauter mean bubble diameter, gas holdup, interfacial area and k_L for different model wine solutions

In this section, the desorption of oxygen from four different model wine solutions, as well as a simple 10% ethanol solution was evaluated. The compositions of the five model wine solutions are shown in Table 4.1. One was a solution of ethanol and glycerol (MWS-Glycerol). Another had the addition of tartaric acid, malic acid, citric acid, and a small amount of sugar (MWS-Acids). The concentration of acids added was in the range of that typically found in wines (Kunkee & Eschnauer, 2016).

The two other model wine solutions had additions of protein in the form of bovine serum albumen (MWS-BSA), and yeast extract (MWS-Yeast). Bovine serum albumen was used as a model protein in this scenario, while a yeast extract was used to better represent the suite of proteins found in wine, given that a large number of proteins in wine come from the walls of lysed yeast, including glycoproteins (Fukui & Yokotsuka, 2003). The $k_L a$, Sauter mean bubble diameter, gas holdup, interfacial area and k_L were all evaluated,

Table 4.1: Summary of composition of different model wine solutions

Compound	10 % Ethanol	MWS-Glycerol	MWS-Acids	MWS-BSA	MWS-Yeast
Ethanol (% v/v)	10	10	10	10	10
Glycerol (g/L)	0	15	15	15	15
Tartaric acid (g/L)	0	0	5	5	5
Malic acid (g/L)	0	0	5	5	5
Citric acid (g/L)	0	0	2	2	2
Sugar (g/L)	0	0	5	5	5
Bovine Serum Albumen	0	0	0	0.1	0
Yeast extract (g/L)	0	0	0	0	0.2

4.4.1. The effect of the addition of glycerol, organic acids, and proteins on the $k_L a$ in model wine solutions

Figure 4.13 shows the $k_L a$ values obtained during the desorption of oxygen from the different model wine solutions, a 10% ethanol solution, and water. There were significant variations between some of the values. The addition of glycerol at 15 g/L to the 10 % ethanol solution reduced the $k_L a$ when compared to the 10 % ethanol alone. The addition of organic acids to the MWS-Glycerol solution did not have a significant effect on the $k_L a$.. All the $k_L a$ values obtained during the desorption of oxygen from the model wine solutions were lower than that obtained for the 10 % ethanol solution.

Results from Figure 4.8 showed no effect of glycerol on $k_L a$ within the range of 5 to 15 g/L for various aqueous ethanol and glycerol solutions. It is possible then that glycerol had an effect on the $k_L a$ of a 10% ethanol solution when at a concentration below 5 g/L, beyond which a threshold value is reached, and it no longer affects a change on $k_L a$ in an ethanol solution.

The lack of significant difference in the $k_L a$ values during desorption of oxygen from the MWS-Glycerol and MWS-Acids solutions, may suggest that the change in the pH resulting from the addition of organic acids, has no significant effect on the $k_L a$. Ferreira et al. (2013) showed reductions in $k_L a$ when the pH of water was reduced, however this effect does not seem to be present in an ethanol solution.

It can be observed that during desorption, the $k_L a$ values were lower in the MWS-BSA and MWS-Yeast solutions, relative to the other model wine solutions. This could be attributed to the presence of protein in the form of either bovine serum albumen or yeast extract. This suggests that protein might be inhibiting mass transfer. Many proteins are surface-active. These proteins are known as amphiphilic, containing both hydrophobic and hydrophilic properties (Moeller *et al.*, 2018). They appear at the gas-liquid interface and can form a film around the interface.

It is likely that BSA and the proteins in the yeast extract were surface active. They could inhibit mass transfer by increasing the film thickness, increasing resistance to mass transfer, resulting in a lower $k_L a$ value. The protein concentration used in the MWS-BSA and MWS-Yeast solutions was meant to reflect the upper limit of protein content found in wine (100 mg/L) (Kunkee & Eschnauer, 2016).

In the following sections, how the presence of protein affected the interfacial area and the k_L of the model wine solutions is discussed.

Figure 4.13: The $k_L a$ values obtained during desorption of oxygen from four model wine solutions, a 10 % ethanol solution, and water, at 25 °C, and at a nitrogen gas flowrate of 2.3 L/min (0.23 cm/s). The error bars represent the standard deviation from at least three measurements. The letters indicate whether the variation of the mean was significant (p<0.05).

4.4.2. The effect of the addition of glycerol, organic acids, and proteins on the Sauter mean bubble diameter (D_{32}), gas holdup, and the interfacial area in model wine solutions

Figure 4.14 shows the D_{32} values obtained during the desorption of oxygen from the model wine solutions, the 10% ethanol solution and water, at 25 °C and a gas flowrate of 2.3 L/min. There was no significant variation in the D_{32} found during the desorption of oxygen in the different model wine solutions and 10 % ethanol solution. The addition of organic acids and subsequent reduction in pH did not affect the bubble size, nor did the addition of BSA or yeast extract.

In a study by Chen et al. (1992) the concentration of protein in an aquaculture was found to affect the bubble sizes rising from the sparger. It was found that the mean bubble diameter decreased with increases in protein concentration. This was attributed to a reduced surface tension caused by the addition of the protein.

However, in this study, the presence of ethanol in the model wine solution already significantly reduces the surface tension relative to pure water. This may explain why there were no significant reductions in the Sauter mean bubble diameter in the bubble column when protein was added to a model wine solution.

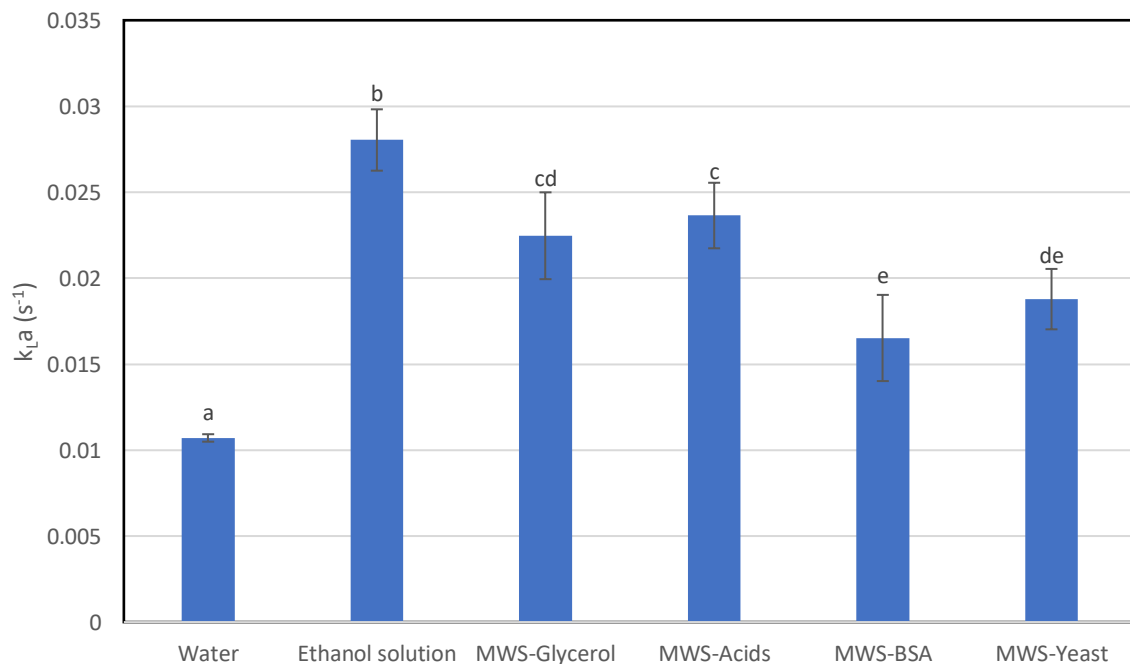Figure 4.14: The D_{32} values obtained during the desorption of oxygen from four model wine solutions, a 10 % ethanol solution, and water, at 25°C, and at a nitrogen gas flowrate of 2.3 L/min (0.23 cm/s). The error bars represent the standard deviation from at least five bubble images, each containing at least 200 measured bubbles. The letters indicate whether the variation of the mean was significant (p<0.05).

Figure 4.15 and Figure 4.16 show images of nitrogen bubbles within the bubble column. In Figure 4.15, from left to right are images of nitrogen bubbles in: water, a 0.05 % v/v ethanol solution, and a 10 % ethanol solution, taken at 25 °C and at a gas flowrate of 1.1 L/min. In Figure 4.16 from left to right are images of nitrogen bubbles in: a MWS-Glycerol Solution, a MWS-BSA solution, and a MWS-Yeast solution, taken at 25 °C and at a gas flowrate of 1.1 L/min.
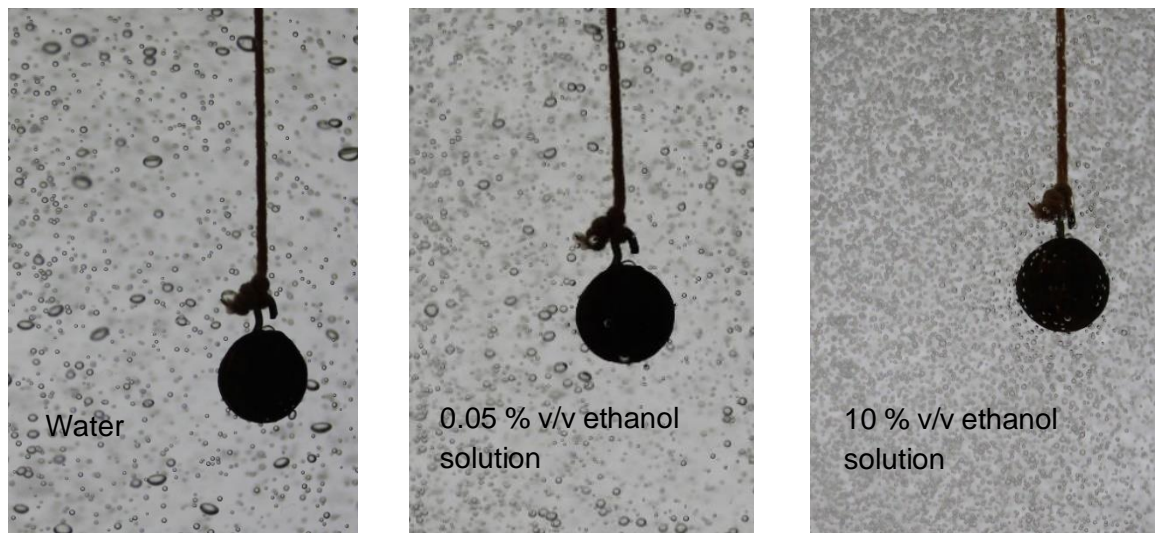
Figure 4.15: From left to right: Images of nitrogen bubbles in water, a 0.05 % v/v ethanol solution, a 10% v/v ethanol solution. Images taken at a temperature of 25 °C and a gas flowrate of 1.1 L/min.
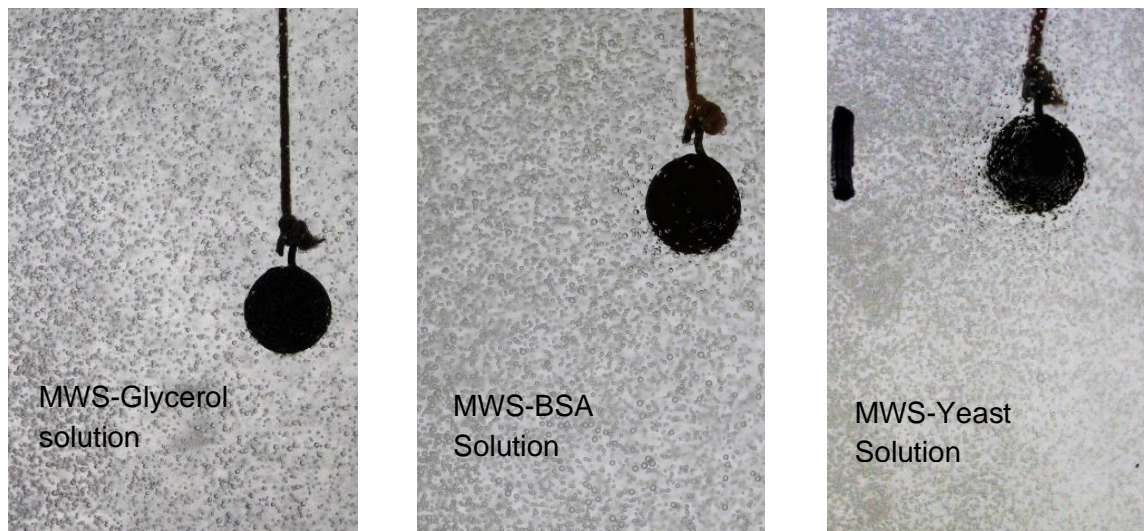
Figure 4.16: From left to right: Images of nitrogen bubbles in a MWS-Glycerol solution, a MWS-BSA solution, a MWS-Yeast solution. Images taken at a temperature of 25 °C and a gas flowrate of 1.1 L/min.

The gas holdup and interfacial area obtained during the desorption of oxygen from the four model wine solutions, the 10% ethanol solution, and water, are shown in Figure 4.17 and Figure 4.18 respectively. There was no significant difference in the gas holdup in any of the model wine solutions and the ethanol solution during nitrogen sparging. However, there was

significant foaming in the MWS-BSA and MWS-Yeast solutions, probably as a result of proteins stabilising any foam formed on top of the solution. There was no significant variation in the interfacial areas during the desorption of oxygen from any of the model wine solutions and the 10 % ethanol solution.
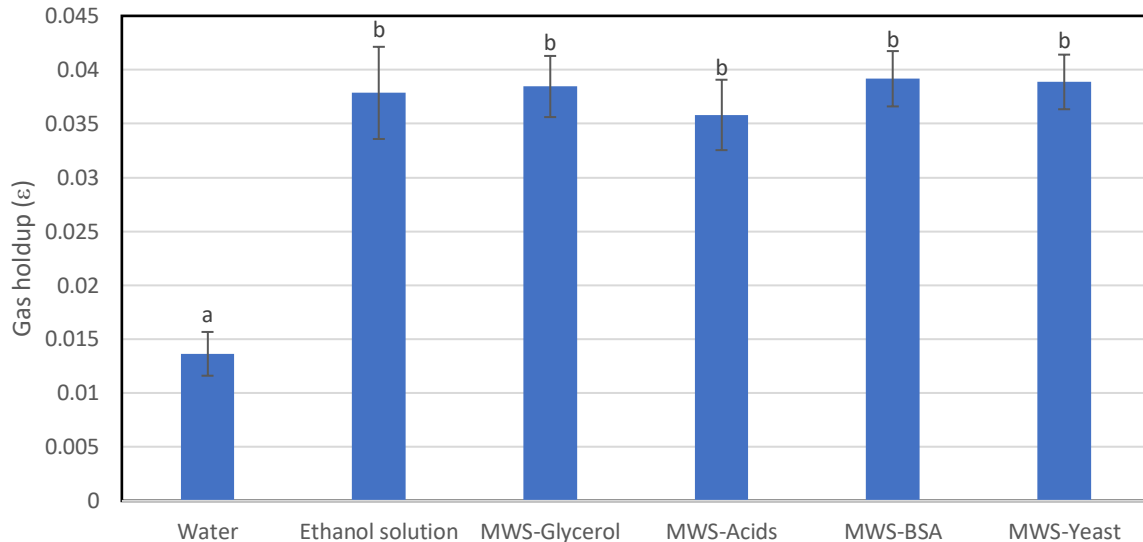
Figure 4.17: The gas holdups obtained during the desorption of oxygen from four model wine solutions, a 10 % ethanol solution, and water, at 25 °C and at a nitrogen gas flowrate of 2.3 L/min (0.23 cm/s). The error bars represent the standard deviation from at three measurements. The letters indicate whether the variation of the mean was significant (p<0.05).
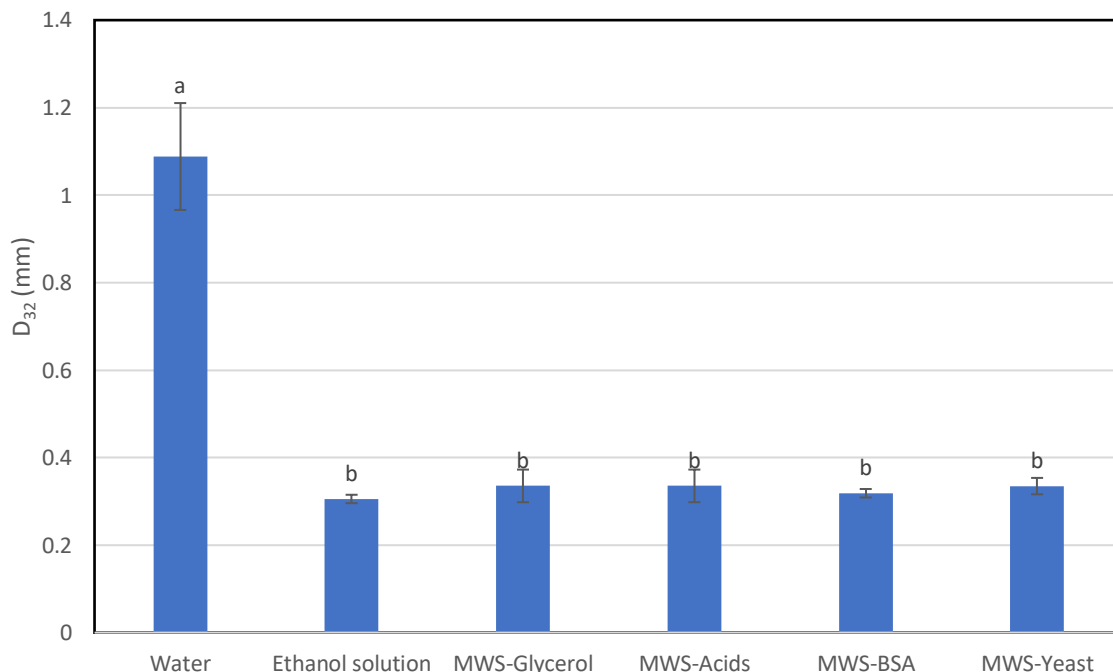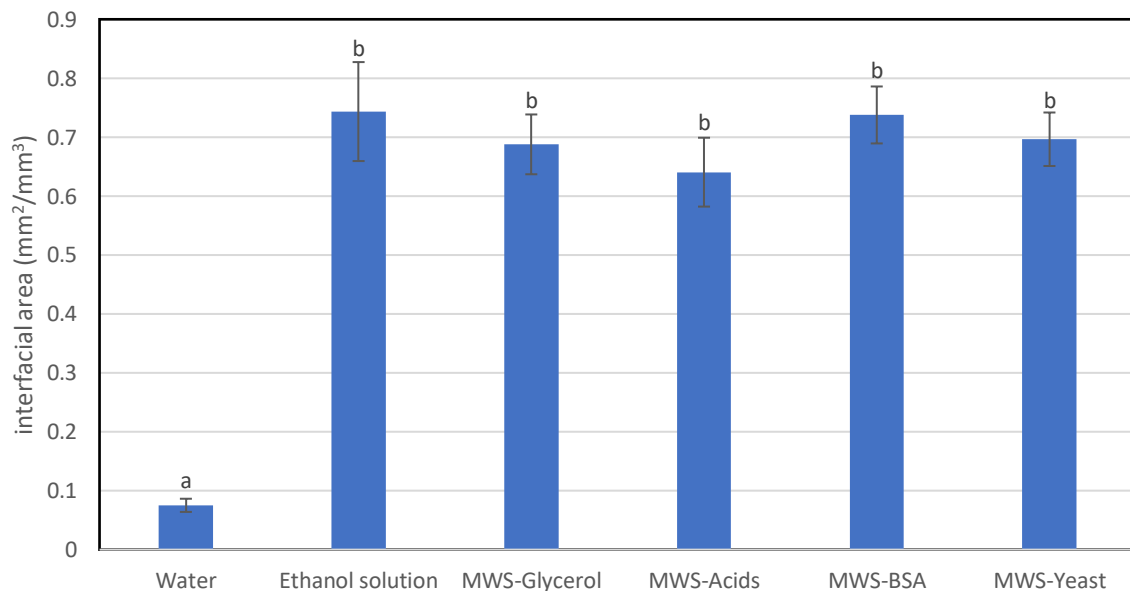

Figure 4.18: The interfacial areas obtained during the desorption of oxygen from four model wine solutions, a 10 % ethanol solution, and water, at 25 °C, and at a nitrogen gas flowrate of 2.3 L/min (0.23 cm/s). The error bars represent the standard deviation for three interfacial area measurements calculated from each gas holdup measurement and the D_{32}. The letters indicate whether the variation of the mean was significant (p<0.05).

4.4.3. The effect of the addition of glycerol, organic acids, and proteins on the oxygen mass transfer coefficient (k_L) in model wine solutions

Figure 4.19 shows the oxygen mass transfer coefficents (k_L) obtained during the desorption of oxygen from the model wine solutions, the 10% ethanol solution and water. The oxygen mass transfer coefficient in water in this set of experiments was found to be 0.14 mm/s during oxygen desorption, and was within the range of error for the oxygen mass transfer coefficient found in the first set of experiments, shown in Figure 4.7. In that case, the k_L was evaluated at the same temperature but at a slightly lower gas flowrate of 1.7 L/min. For such small bubble sizes, it is not expected that k_L values will change for varying gas flowrates, so long as a homogenous regime is maintained within the bubble column.

k_L values are typically only susceptible to change with changing gas flowrates for bubble sizes greater than 1.5 mm, or when the flow regime becomes more turbulent (Sardeing *et al.*, 2006). Therefore it is expected that the oxygen k_L values obtained during the desorption of oxygen from water, should be statistically similar between the experimental sets.

The oxygen mass transfer coefficients obtained during the desorption of oxygen from the MWS-Glycerol and MWS-Acids solutions were not significantly different. However, the addition of BSA or yeast extract to the model wine solution reduced the k_L. It is possible that the proteins in the model wine solution adsorbed to the gas bubbles rising through the bubble column, increasing the resistance to mass transfer, and consequently reducing the desorption rate.

When comparing the k_L values from the first set of experiments (Figure 4.7) to the values from this set of experiments, it was found that during desorption, the obtained mass transfer coefficients were lower in all three white wines, relative to the ethanol, MWS-Glycerol and MWS-Acids solution. The difference is likely due to compounds in the wines, not present in the MWS-Glycerol and MWS-Acids solution, adsorbing to the gas-liquid interface.

k_L values were similar during the desorption of oxygen from the rosé and model wine solutions, while the k_L value during the oxygen desorption from the red wine was found to be slightly larger than those obtained in the model wine solutions. The k_L values obtained during the desorption of oxygen from the model wine solutions containing proteins, and the white wines, have similar values. It is possible therefore that the presence of proteins in these wines inhibited k_L as well. If this were the case, then this may indicate that the protein concentration of red wine and the rosé wine were too low to significantly reduce k_L.

The protein concentrations in the model wine solutions were meant to represent the upper limits typically found in wine – 100 mg/L. Typical protein concentrations in wines would be between 5 and 100 mg/L (Fukui & Yokotsuka, 2003). The primary factors that will affect the final protein concentrations in wine will be the processing steps that the wine goes under before being packaged, the protein content of the grape, and the amount of protein released and produced from the microorganisms during wine fermentation and processing.

Different wines undergo different processing steps depending on winemaker preference. Some wines may only be filtered through coarse gravity fed filtrations, while other wines are filtered through microfiltration, undergo clarification, and are treated with bentonite to remove haze-forming proteins (Kemp, Marangon, Curioni, *et al.*, 2021). The k_L could be significantly affected by the processing stages that wine undergoes. If protein in wine is a significant factor affecting the desorption of oxygen in wine, then the type of treatment the wine undergoes could also consequently affect the desorption rate.
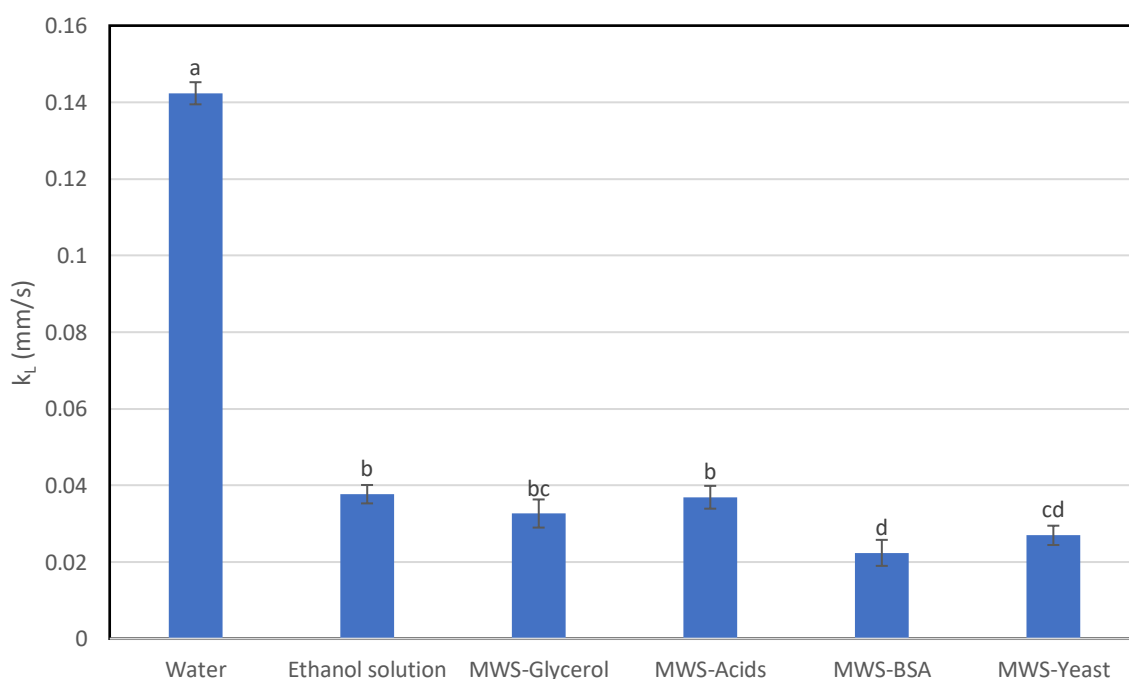
Figure 4.19: The oxygen mass transfer coefficients (k_L) obtained during the desorption of oxygen from four model wine solutions, a 10 % ethanol solution, and water, at 25 °C and at a gas flowrate of 2.3 L/min (0.23 cm/s).The error bars represent the standard deviation from the calculated k_La values and the mean interfacial area. The letters indicate whether the variation of the mean was significant (p<0.05).

Protein seems to be able to have an effect on k_L despite its relative low concentration in solution. It is important to understand why this is the case and what are the potential mechanisms through which proteins can affect the oxygen mass transfer coefficient.

Proteins can act as surfactants and accumulate at the gas-liquid interface, creating a physical barrier around the gas bubble. There are a variety of organic compounds that can act as surfactants and accumulate at the gas-liquid interface in addition to proteins, including polysaccharides, saponins, and polyelectrolytes (Moeller *et al.*, 2018). The manner in which surfactants reduce the k_L has been widely discussed, and various mechanisms presented (Jamnongwong *et al.*, 2010; Painmanakul, Loubiere, Hebrard, *et al.*, 2005; Rosso *et al.*, 2006; Sardeing *et al.*, 2006).

Rosso, Huo and Stenstrom (2006) describe the accumulation of the hydrophobic heads of the compound at the interface, with the hydrophobic tails reaching into the bubble. This results in an increase in the thickness of the liquid boundary layer described by the two-film theory, reducing the renewal rate of the bulk liquid around the interface and consequently increasing the travel path for the gas molecule, with the overall effect of reducing the k_L (Painmanakul *et al.*, 2005; Vasconcelos, Rodrigues, Orvalho, *et al.*, 2003).

The stagnant cap model has also been used to describe how surfactants reduce oxygen mass transfer as they increase their coverage around the gas-liquid interface (Nekoeian, Aghajani, Alavi, *et al.*, 2019). A stagnant cap model describes surfactants dragging and collecting around the bottom of a bubble as it rises, resulting in two liquid side coefficients (one at the clean front, and the other at the stagnant bottom). The liquid side coefficient at the stagnant bottom is significantly lower, due to surfactants acting as a barrier to mass transfer, consequently decreasing the overall k_L. The contribution of the liquid side coefficient at the stagnant bottom, to the overall coefficient, is dependent on the coverage of the surfactant around the bubble, which is affected by surfactant type and concentration (Jamnongwong *et al.*, 2010).

The results from this third set of experiments point towards protein being a significant compound in affecting the desorption rate, and another set of experiments was performed to further validate this. It was assessed how the desorption rate in a wine was affected by the removal of protein through bentonite fining.

4.5. Evaluating the $k_L a$, Sauter mean bubble diameter, gas holdup, interfacial area and the k_L for a bentonite treated and untreated wine

A protein unstable wine was split into two batches. In order to determine whether protein concentration could affect the desorption of wine, one of the batches was treated with bentonite while the other was not, and the $k_L a$, interfacial area, and k_L was determined during the desorption of oxygen from each batch of wine at 25 °C and at a nitrogen gas flowrate of

1.7 L/min. These were the same conditions for which the oxygen desorption in wines from the first set of experiments were evaluated at.

4.5.1. Evaluating the $k_L a$, Sauter mean bubble diameter (D_{32}), gas holdup, and interfacial area for a bentonite treated and untreated wine

Figure 4.20 shows the $k_L a$ values obtained during the desorption of oxygen from the bentonite treated wine (BT-Wine) and the non-bentonite treated wine (PU-wine). It can be observed that the $k_L a$ measured in the system was greater in the bentonite treated white wine compared to the untreated protein unstable wine.

The dosage of bentonite for the bentonite treated white wine was 60 g/hL. Depending on the type of wine, a dose of 60 g/hL of bentonite would typically reduce the protein content of the wine to about 10-30 % of the original concentration (Lambri, Dordoni, Giribaldi, *et al.*, 2012). It is not clear whether the addition of bentonite removes fractions of proteins selectively (Lambri *et al.*, 2012). The addition of bentonite resulted in an increase in the $k_L a$ of the system. It is likely that this was due to the removal of a large portion of the proteins.

This further validates the idea that protein content plays a big part in controlling the rate of oxygen mass transfer in complex solutions. It also demonstrates how the timing of the desorption of oxygen from wine can affect the desorption efficacy, as the $k_L a$ value of the system was approximately 50 % when the wine was treated with bentonite. Most wines undergo oxygen desorption just prior to packaging and these results confirm that this is probably the best stage to perform desorption, as it is likely that protein content will be at its lowest at this point.

It can be observed that the $k_L a$ value obtained during the desorption of oxygen from the PU-Wine was not significantly different from that obtained during the desorption of oxygen from water. This was despite a significantly reduced bubble size (Figure 4.21), and increased interfacial area (Figure 4.23), within the PU-Wine during sparging, indicating that there is a significant increase in the resistance to the mass transfer during the desorption of oxygen in the PU-Wine.

This instance also displays how a model wine solution may significantly overestimate the oxygen desorption $k_L a$ that would occur during the desorption of oxygen from a wine. Although the $k_L a$ values found during the desorption of oxygen from model wine solutions containing protein were lower relative to those in simpler model wine solutions, these $k_L a$ values were still greater than those found during the desorption of oxygen from water by a factor of

84

approximately 1.5, whereas the $k_L a$ value in the PU-Wine was not greater than the water value. It is possible that there was an even greater concentration of surface-active proteins in the PU-Wine than in the MWS-Yeast solution, or that there were additional compounds in this wine, such as polysaccharides, that were also affecting an additional resistance to oxygen desorption.

The complexity of wine means that a multitude of potentially surface-active compounds could interact significantly to enhance the resistance to gas-liquid mass transfer. As with the other wines from the first set of experiments, the D_{32}, gas holdup and interfacial area did not vary significantly during the oxygen desorption of the PU-Wine and BT-Wine, and were also not significantly different to those found during the desorption of oxygen from the wines tested in the first set of experiments. The D_{32}, gas holdup, and interfacial area are shown in Figure 4.21, Figure 4.22, and Figure 4.23 respectively.

Figure 4.20: The $k_L a$ values obtained during the desorption of oxygen from bentonite treated (BT-Wine) and untreated (PU-Wine) white wine, and water, at 25 °C, and at a nitrogen gas flowrate of 1.7 L/min (0.17 cm/s). The error bars represent the standard deviation from three measurements.

Figure 4.21: D_{32} obtained during the desorption of oxygen from the bentonite treated (BT-Wine) and untreated (PU-Wine) white wine, and water, at 25 °C. and at a nitrogen gas flowrate of 1.7 L/min (0.17 cm/s), The error bars represent the standard deviation from at least five bubble images, each containing at least 200 measured bubbles.
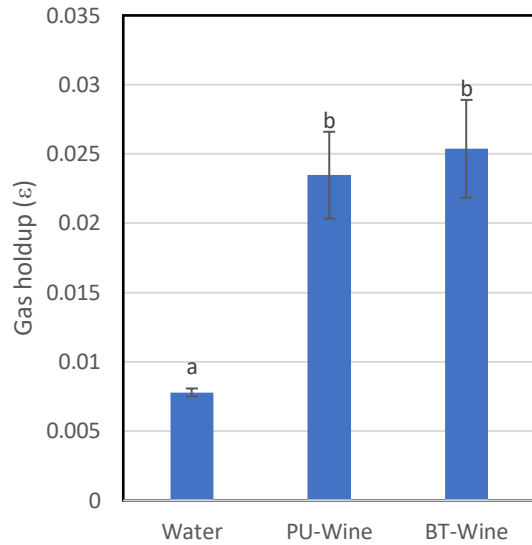
Figure 4.22: The gas holdup values obtained during the desorption of oxygen from the bentonite treated (BT-Wine) and untreated (PU-Wine) white wine, and water, at 25 °C. and at a nitrogen gas flowrate of 1.7 L/min (0.17 cm/s), The error bars represent the standard deviation from three measurements.
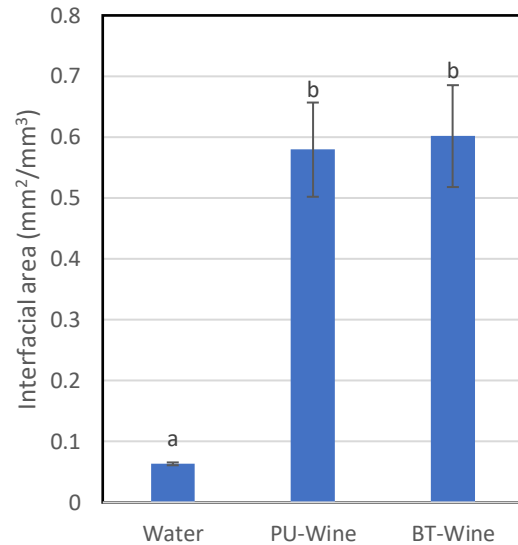
Figure 4.23: The interfacial areas obtained during the desorption of oxygen from the bentonite treated (BT-Wine) and untreated (PU-Wine) white wine, and water, at 25 °C. and at a nitrogen gas flowrate of 1.7 L/min (0.17 cm/s), The error bars represent the standard deviation for three interfacial area measurements calculated from each gas holdup measurement and the D_{32}.

4.5.2. Evaluating the k_L for a bentonite treated and untreated wine

Figure 4.24 shows the k_L values obtained during the desorption of oxygen from the bentonite treated and untreated wine relative to the values found in the other wines. The results show that treating the wine with bentonite increased the k_L, relative to the untreated protein unstable wine. This is possibly due to reduced coverage of proteins around the gas-liquid interface. Accordingly in a stagnant cap model, the greater protein content in the PU-wine would result in a greater coverage around the back of the rising bubble, increasing the weighting of the liquid side coefficient for the stagnant side of the bubble, reducing the overall k_L. A reduction in protein concentration would increase the weighting of the liquid side coefficient of the clean front of the bubble, resulting in a larger overall k_L.

The results from this, in addition to the reduced k_L values obtained from the desorption of oxygen from the model wine solutions containing yeast, provide strong evidence for the effect that certain proteins have at the gas-liquid interface, and consequently on oxygen desorption

rate. However it will not only be the concentration of proteins that would have an affect on the k_L, but the type and structure of the proteins.

Different wines will possess different surface-active properties based on the presence and amount of hydrophobic and hydrophilic domains in the protein. A likely candidate for surface-active proteins is mannoproteins. Mannoproteins, which are a type of glycoprotein, make up a large portion of the proteins found in wine. Mannoproteins in wine come from yeast cell wall polysaccharides, and the longer wine is aged on lees, the more mannoproteins tend to leach into the wine. This is the same for all yeast derived proteins in wine (Zoecklein *et al.*, 1999). Mannoproteins have been found to be adept at foam stabilisation in sparkling wine, and have both hydrophobic and hydrophilic domains, indicating that they have surface-active properties (Núñez *et al.*, 2006).

Mannoproteins seem like good candidates for contributing to increased mass transfer resistance, however, the very complex nature of wine and its wide suite of proteins means that it would be incredibly difficult to determine the exact extent that different protein fractions would have on the oxygen mass transfer coefficient. This will limit the possible accuracy that can be obtained for estimating the desorption rate in a certain wine, based simply on its composition.
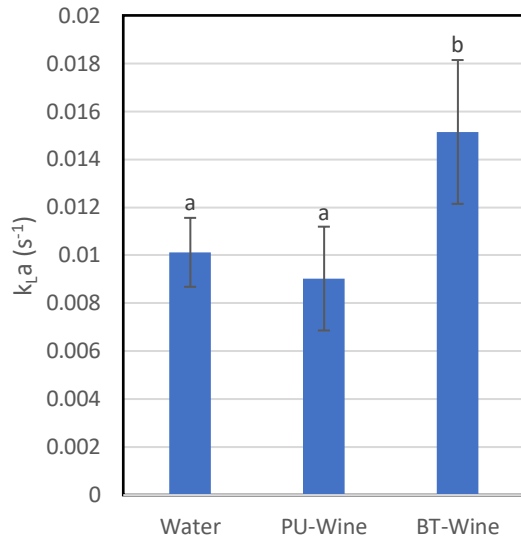

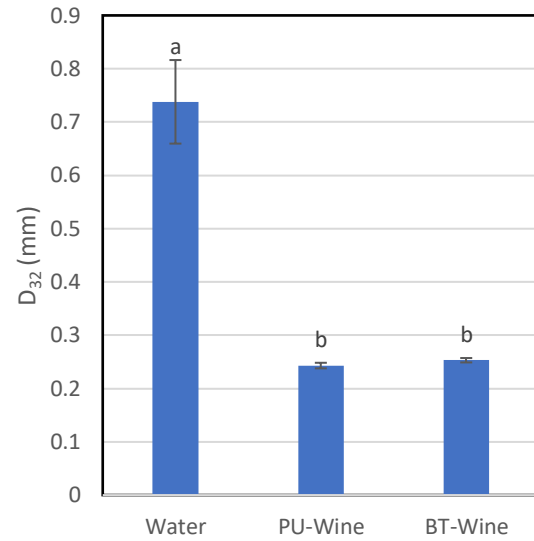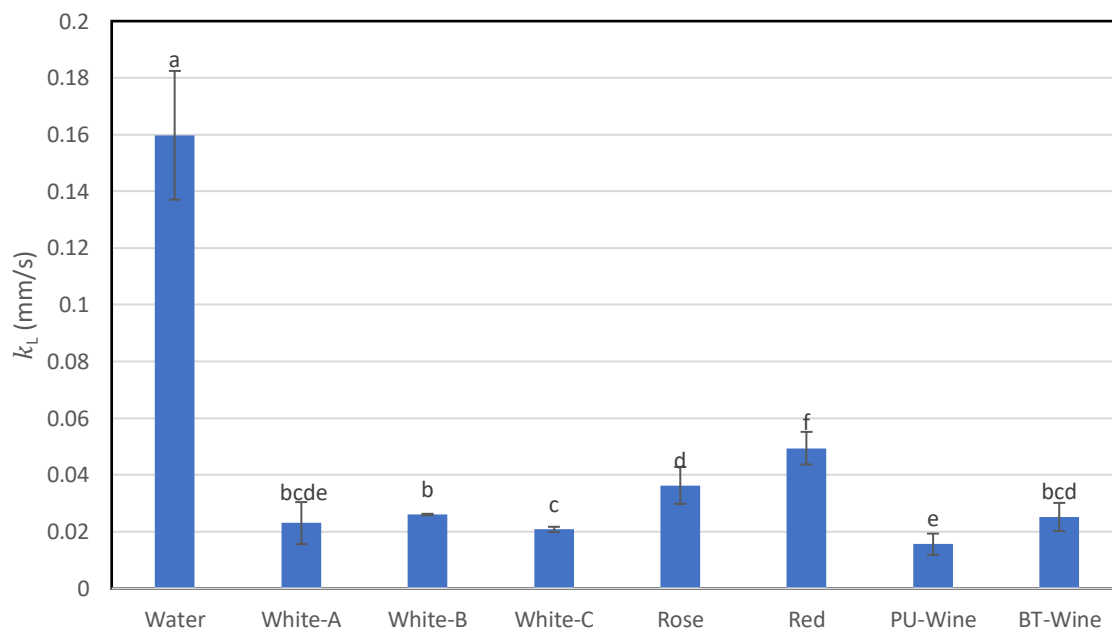*Figure 4.24: The oxygen k_L values obtained during the desorption of oxygen from the bentonite treated (BT-Wine) and untreated (PU-Wine) white wine, and water, at 25 °C, and at a gas flowrate of 1.7 L/min (0.17 cm/s), compared to the k_L values obtained during the desorption of oxygen from all the other wines tested under the same conditions. The error bars represent the standard deviation from three measurements. White-A is a dry white blend, White-B is a dry Chenin Blanc, White-C is a dry Sauvignon Blanc.*

4.6. Summary of results

The oxygen desorption rate can vary significantly in different wines, with $k_L a$ values between 0.0125 and 0.0275 s[1] obtained. during the desorption of oxygen from different wines under the same operating conditions. The $k_L a$ obtained during the desorption of oxygen from water was found to be 0.01 s[1]. The D_{32} of the nitrogen bubbles during sparging in the wines were in the region of 0.25 mm, while the D_{32} was 0.75 mm in water. The variation was probably due to the presence of ethanol, which significantly reduces surface tension and bubble coalescence.

The reason for the varying oxygen desorption rates was attributed to significantly varying oxygen mass transfer coefficients. The oxygen mass transfer coefficient obtained during the desorption of oxygen from water was found to be 0.16 mm/s, while it was found to vary between 0.02 and 0.045 mm/s during the desorption of oxygen from the different wines. These values were in the region of those found in literature for bubbles with diameters less than 1 mm. Literature values for the oxygen mass transfer coefficient are in the region of 0.1 mm/s for oxygen in water, and as low as 0.02 mm/s for oxygen in solutions containing surfactants (Bredwell & Worden, 1998; Sardeing *et al.*, 2006).

The effect that changing the temperature and gas flowrate had on the oxygen desorption rate in the bubble column was also investigated. It was found that the oxygen desorption $k_L a$ in a model aqueous glycerol ethanol solution increased linearly with an increase in temperature and gas flowrate. For the bubble column used in these experiments, it was found that an increase in the gas flowrate of nitrogen of 0.075 L/min per L of solution, had an equivalent effect on the desorption $k_L a$ as an 8 °C increase in the temperature of the solution.

In order to investigate which compounds in wine contributed to the significantly varying oxygen desorption rates in wine, a set of experiments investigating oxygen desorption in a range of model wine solutions was performed. It was found that varying the ethanol concentration between 9 and 15 % v/v had no effect on $k_L a$, while the addition of glycerol reduced the $k_L a$ slightly. However, changing the glycerol concentrations between 5 and 25 g/L had no effect on the $k_L a$. The presence of tartaric, malic, and citric acid in model wine solutions did not affect the $k_L a$, while the addition of protein in the form of BSA or yeast extract was found to reduce the $k_L a$.

The $k_L a$ values obtained during the desorption of oxygen were 0.0275 s[1] in the 10 % ethanol solution, approximately 0.0225 s[1] in the model wine solutions containing glycerol and organic

acids, and approximately 0.0175 s^1 in the model wine solutions containing BSA and yeast extract. The reason for these variations was due to changes in the oxygen mass transfer coefficient. The k_L values obtained during the desorption of oxygen from the model wine solutions were between 0.03 and 0.04 mm/s for the model wine solutions containing no protein, and between 0.02 and 0.03 mm/s for the model wine solutions containing protein. In this particular set of experiments the k_L value obtained during the desorption of oxygen from water was found to be 0.14 mm/s.

It is likely that the BSA and the proteins in the yeast extract, acted as surfactants in the solution, adsorbing to the gas-liquid interface. This increased the resistance to oxygen mass transfer by reducing the mass transfer coefficient. This suggested that it may be the protein content in wine that is a factor affecting the oxygen mass transfer coefficients during desorption. The protein content in wine can vary significantly and is particularly affected by the processing steps that wine undergoes.

In order to investigate whether treating a wine to remove protein would affect the rate of oxygen desorption from the wine, a protein unstable wine was obtained and split into two batches, with one batch treated with bentonite to remove protein. It was found that during the desorption of oxygen, the $k_L a$ in the bentonite treated wine was significantly higher than that in the protein unstable wine, at 0.015 s^1 compared to 0.009 s^1. The D$_{32}$ during sparging was found to be approximately 0.025 mm for both the wines – no different from the rest of the wines. The difference in the $k_L a$ values was attributed to differences in the oxygen mass transfer coefficients between the differently treated wines during nitrogen sparging. The k_L value during the desorption of oxygen from the protein unstable wine was 0.017 mm/s, while it was 0.0225 mm/s in the bentonite treated wine.

Chapter 5: Conclusion

This study confirmed the untested hypotheses that oxygen desorption in different wines can occur at different rates under the same operating conditions. The reason for this is due to varying oxygen mass transfer coefficients in different wines during nitrogen sparging.

Based on this study, it was found that the protein content in wine could play a significant role in the desorption rate of oxygen from the wine. It was found that typical variations of ethanol, glycerol, and organic acids are unlikely to significantly affect the desorption rate of wines, although for wines containing very low ethanol or glycerol concentrations this may not be the case. It is likely that proteins reduce the oxygen mass transfer coefficient, probably in a similar manner that common surfactants do, by adsorbing to the gas-liquid interface, which increases the resistance to mass transfer.

Consequently, the types of filtration, fining and processing that wine undergoes before packaging probably affect the oxygen desorption rate in the wine. It was found that treating a wine with bentonite to remove proteins significantly improved the desorption rate, which also further suggests that protein content can play a significant role in the desorption rate.

The complexity of wines makes it very difficult to accurately predict what the desorption rate of a certain wine will be without prior testing on that specific wine. Winemakers should account for this variation when considering the timeframe of the desorption step, and assume a worst-case scenario, as it may take up to twice as long to remove the same amount of dissolved oxygen in one wine compared to another. It is recommended that the desorption of wine is performed at the end of wine processing, or at a stage at which the protein content in the wine is at its lowest.

It is also recommended that desorption be performed when wine is at a higher temperature. However, actively increasing the temperature is energy intensive and desorption improvements are likely to be more easily obtained by increasing the gas flowrate, or by using a sparger that produces smaller bubbles, both of which will increase the interfacial area within the system.

It is clear that the limiting step for oxygen desorption in wine is the k_L, and although it may be easier to increase the interfacial area than the k_L, there are still ways in which the k_L can be increased. The best way to do this would be by increasing the turbulence within the vessel during desorption. This can be done via introducing an impeller into the system or increasing

the gas flowrate. Using in-line sparging in pipes through which wine is flowing in a turbulent regime, may result in improved mass transfer efficiency, rather than via sparging into a bubble column, where it may be more difficult to create a turbulent regime.

This study also demonstrates how model solutions can overestimate the mass transfer that may occur in more complex solutions. It shows how effects that are observed in mono-component solutions may not necessarily occur in multicomponent solutions. Oxygen transfer in complex media such as wine can vary significantly, and it can be difficult to ascribe this to a single compound.

All in all, winemakers can improve desorption by:
- Performing it as the last processing step or after protein fining
- Performing it when wine temperatures are higher
- Increasing the interfacial area in the system by reducing the mean bubble size within the system
- Increasing the turbulence during mass transfer through increasing the gas flowrate or using a mechanical component such as an impeller

It is recommended that in order to further elucidate which compounds in wine significantly affect oxygen mass transfer, tests should be done on a much wider range of wines, in which the wine composition is analysed in more detail, from which a regression analysis could be done to determine which compounds may be significant indicators of mass transfer rate.

It is also recommended that the desorption of wine be performed in pilot scale bubble columns, so as to determine whether the k_L in the system can be increased by increasing the turbulence within the bubble column, and whether this occurs for different bubble sizes.

Reference List

Abufalgha, A. 2018. Behaviour of oxygen transfer in a simulated multiphase hydrocarbon-based bioprocess in a bubble column reactor. Stellenbosch University.

Akita, K. & Yoshida, F. 1973. Gas Holdup and Volumetric Mass Transfer Coefficient in Bubble Columns Effects of Liquid Properties. *Industrial and Engineering Chemistry Process Design and Development*. 12(1):76–80.

Al-hindi, M. & Azizi, F. 2018. Absorption and Desorption of Carbon Dioxide in Several Water Types. *The Canadian Journal of Chemical Engineering*. 96:274–284.

Al-Hindi, M. & Azizi, F. 2020. The effect of water type on the absorption and desorption of carbon dioxide in bubble columns. *Chemical Engineering Communications*. 207(3):339–349.

Azzopardi, B. 2011. Sauter Mean Diameter. in *Thermopedia*. [Online], Available: https://www.thermopedia.com/content/1108/.

Belda, R., Herraez, J. V. & Diez, O. 2005. A study of the refractive index and surface tension synergy of the binary water/ethanol: influence of concentration. *Physics and Chemistry of Liquids*. 43(1):91–101.

Besagni, G., Inzoli, F. & Ziegenhein, T. 2018. Two-Phase Bubble Columns: A Comprehensive Review. *ChemEngineering*. 2(2):13.

Besagni, G., Gallazzini, L. & Inzoli, F. 2019. On the scale-up criteria for bubble columns. *Petroleum*. 5:114–122.

Bewtra, J., Nicholas, W. & Polkowski, L. 1970. Effect of Temperature on Oxygen Transfer in Water. *Water Research*. 4:115–123.

Boudin, L., Grec, B., Salvarani, F., Boudin, L., Grec, B. & A, F.S. 2012. A mathematical and numerical analysis of the Maxwell-Stefan diffusion equations. *Discrete and Continuous Dynamical Systems - Series B, American Institute of Mathematical Sciences*. 17(5):1427–1440.

Bredwell, M.D. & Worden, R.M. 1998. Mass-transfer properties of microbubbles. 1. Experimental studies. *Biotechnology Progress*. 14(1):31–38.

Butler, I.B., Schoonen, M.A.A. & Rickard, D.T. 1994. Removal of dissolved oxygen from water: A comparison of four common techniques. *Talanta*. 41(2):211–215.

Calderbank, P.H. & Moo-Young, M.B. 1961. The continuous phase heat and mass-transfer properties of dispersions. *Chemical Engineering Science*. 16:39–54.

Cant, R.R. 1960. The Effect of Nitrogen and Carbon Dioxide Treatment of Wines on Dissolved Oxygen Levels. *American Journal of Enology and Viticulture*. 11(4):164–169.

Castellari, M., Simonato, B., Tornielli, G.B., Spinelli, P. & Ferrarini, R. 2004. Effects of different enological treatments on dissolved oxygen in wines. *Italian Journal of Food Science*. 16(3):387–396.

Chen, S., Timmons, M.B., Aneshansley, D.J. & Bisogni, J.J. 1992. Bubble size distribution in a bubble column applied to aquaculture systems. *Aquacultural Engineering*. 11(4):267–280.

Chiciuc, I., Farines, V., Mietton-Peuchot, M. & Devatine, A. 2010. Effect of wine properties and operating mode upon mass transfer in micro-oxygenation. *International Journal of Food Engineering*. 6(6):1–38.

Clarke, K.G. & Correia, L.D.C. 2008. Oxygen transfer in hydrocarbon-aqueous dispersions and its applicability to alkane bioprocesses: A review. *Biochemical Engineering Journal*. 39(3):405–429.

Clarke, K.G. & Manyuchi, M.M. 2012. Methodology for advanced measurement accuracy of the overall volumetric oxygen transfer coefficient with application to hydrocarbon-aqueous dispersions. *Journal of Chemical Technology and Biotechnology*. 87(11):1615–1618.

Coetzee, C. & Du Toit, W.J. 2015. Sauvignon Blanc Wine: Contribution of Ageing and Oxygen on Aromatic and Non-aromatic Compounds and Sensory Composition : A Review. *South African Journal of Enology and Viticulture*. 36(3):347–365.

Cussler, E.L. 2009. *Diffusion: Mass Transfer in Fluid Systems*. Third ed. Cambridge, UK: Cambridge University Press.

Deckwer, W.. & Schumpe, A. 1993. Improved Tools for Bubble Column Reactor Design and Scale-Up. *Chemical Engineering Science*. 48(5):889–911.

Devatine, A., Chiciuc, I., Poupot, C. & Mietton-Peuchot, M. 2007. Micro-oxygenation of wine in presence of dissolved carbon dioxide. *Chemical Engineering Science*. 62(17):4579–4588.

Devatine, A., Chiciuc, I. & Mietton-Peuchot, M. 2011. The protective role of dissolved carbon dioxide against wine oxidation: A simple and rational approach. *Journal International des Sciences de la Vigne et du Vin*. 45(3):189–197.

Elhajj, J., Al-Hindi, M. & Azizi, F. 2014. A review of the absorption and desorption processes of carbon dioxide in water systems. *Industrial and Engineering Chemistry Research*. 53:2–22.

Federico Cassasa, L. 2017. Flavonoid Phenolics in Red winemaking. in *Phenolic Compounds - Natural Sources, Importance and Applications* M. Soto-Hernández (ed.). San Luis Obispo, USA: Intech Open M. Soto-Hernández (ed.). 153–196.

Ferreira, A., Cardoso, P., Teixeira, J.A. & Rocha, F. 2013. pH influence on oxygen mass transfer coefficient in a bubble column . Individual characterization of k L and a. *Chemical Engineering Science*. 100:145–152.

Fukui, M. & Yokotsuka, K. 2003. Content and origin of protein in white and red wines: Changes during fermentation and maturation. *American Journal of Enology and Viticulture*. 54(3):178–188.

Fukuma, M., Muroyama, K. & Yasunishi, A. 1987. Properties of Bubble Swarm in a Slurry Bubble Column. *Journal of Chemical Engineering of Japan*. 20(1):28–33.

Galpin, V.C. 2006. *A comparison of legislation about wine-making additives and processes*.

Garcia-Ochoa, F. & Gomez, E. 2009. Bioreactor scale-up and oxygen transfer rate in microbial processes: An overview. *Biotechnology Advances*. 27(2):153–176.

Gawel, R., Schulkin, A., Smith, P.A., Espinase, D. & McRae, J.M. 2020. Effect of dissolved carbon dioxide on the sensory properties of still white and red wines. *Australian Journal of Grape and Wine Research*. 26(2):172–179.

Glampedaki, P., Hatzidimitriou, E., Paraskevopoulou, A. & Pegiadou-Koemtzopoulou, S. 2010. Surface tension of still wines in relation to some of their constituents: A simple determination of ethanol content. *Journal of Food Composition and Analysis*. 23(4):373–381.

Gliński, J., Chavepeyer, G., Platten, J.K. & Smet, P. 1998. Surface properties of diluted

aqueous solutions of normal short-chained alcohols. *Journal of Chemical Physics*. 109(12):5050–5053.

Gurol, M. & Nekouinaini, S. 1985. Effect of organic substances on mass transfer in bubble aeration. *Journal of Chemical Information and Modeling*. 53(3):235–240.

Gutiérrez-Escobar, R., Aliaño-González, M.J. & Cantos-Villar, E. 2021. Wine polyphenol content and its influence on wine quality and properties: A review. *Molecules*. 26(3).

Hamborg, E.S., Kersten, S.R.A. & Versteeg, G.F. 2010. Absorption and desorption mass transfer rates in non-reactive systems. *Chemical Engineering Journal*. 161(1–2):191–195.

Jamnongwong, M., Loubiere, K., Dietrich, N. & Hébrard, G. 2010. Experimental study of oxygen diffusion coefficients in clean water containing salt, glucose or surfactant: Consequences on the liquid-side mass transfer coefficients. *Chemical Engineering Journal*. 165(3):758–768.

Jordan, U. & Schumpe, A. 2001. The gas density effect on mass transfer in bubble columns with organic liquids. *Chemical Engineering Science*. 56:6267–6272.

Kantarci, N., Borak, F. & Ulgen, K.O. 2005. Bubble column reactors. *Process Biochemistry*. 40(7):2263–2283.

Kazakis, N.A., Mouza, A.A. & Paras, S. V. 2008. Experimental study of bubble formation at metal porous spargers: Effect of liquid properties and sparger characteristics on the initial bubble size distribution. *Chemical Engineering Journal*. 137(2):265–281.

Kemp, B., Marangon, M., Curioni, A., Waters, E. & Marchal, R. 2021. New directions in stabilization, clarification, and fining. in *Managing wine quality: Oenology and wine quality, Vol. 2* 2nd editio ed. A. Reynolds (ed.). Cambridge, UK: Woodhead Publishing Limited A. Reynolds (ed.). 245–286.

Khattab, I.S., Bandarkar, F., Fakhree, M.A.A. & Jouyban, A. 2012. Density, viscosity, and surface tension of water+ethanol mixtures from 293 to 323K. *Korean Journal of Chemical Engineering*. 29(6):812–817.

Krishna, R. & Wesselingh, J.A. 1997. The Maxwell-Stefan approach to mass transfer. *Chemical Engineering Science*. 52(6):861–911.

Kulkarni, S.S., Nene, S.N. & Joshi, K.S. 2020. Exploring malted barley waste for fungi producing surface active proteins like hydrophobins. *SN Applied Sciences*. 2(11):1–14.

Kunkee, R.E. & Eschnauer, H.R. 2016. Wine, 2. Chemical and Physical Composition. *Ullmann's Encyclopedia of Industrial Chemistry*. 1–17.

Lambri, M., Dordoni, R., Giribaldi, M., Violetta, M.R. & Giuffrida, M.G. 2012. Heat-unstable protein removal by different bentonite labels in white wines. *LWT - Food Science and Technology*. 46(2):460–467.

Lee, J. 2017. Development of a model to determine mass transfer coefficient and oxygen solubility in bioreactors. *Heliyon*. 3:1–35.

Lopes, P., Silva, M.A., Pons, A., Tominaga, T., Lavigne, V., Saucier, C., Darriet, P., Teissedre, P.-L., et al. 2009. Impact of Oxygen Dissolved at Bottling and Transmitted through Closures on the Composition and Sensory Properties of a Sauvignon Blanc Wine during Bottle Storage. *Journal of Agricultural and Food Chemistry*. 57:10261–10270.

Manjrekar, O. 2016. Hydrodynamics and Mass Transfer in Bubble Columns. Washington University.

Matsunaga, N., Kano, K., Maki, Y. & Dobashi, T. 2009. Estimation of dissolved carbon dioxide stripping in a large bioreactor using model medium. *Journal of Bioscience and Bioengineering*. 107(4):419–424.

Moeller, L., Zehnsdorf, A., Pokorná, D. & Zábranská, J. 2018. Foam Formation in Anaerobic Digesters. in *Advances in Bioenergy* 1st Editio ed. Vol. 3. L. Yebo & G. Xumeng (eds.). Academic Press L. Yebo & G. Xumeng (eds.).

Moenne, I.M. 2013. Oxygen Management During Alcoholic Fermentation. Pontificia Universidad Catolica De Chile.

Moenne, M.I., Saa, P., Laurie, V.F., Pérez-Correa, J.R. & Agosin, E. 2014. Oxygen Incorporation and Dissolution During Industrial-Scale Red Wine Fermentations. *Food and Bioprocess Technology*. 7(9):2627–2636.

Morao, A., Maia, C.I., Fonseca, M.M.R., Vasconcelos, J.M.T. & Alves, S.S. 1999. Effect of antifoam addition on gas-liquid mass transfer in stirred fermenters. *Bioprocess Engineering*. 20:165–172.

Nekoeian, S., Aghajani, M., Alavi, S.M. & Sotoudeh, F. 2019. Effect of surfactants on mass transfer coefficients in bubble column contactors : an interpretative critical review study. *Reviews in Chemical Engineering*. 1–33.

Neto, F.S.P.P., de Castilhos, M.B.M., Telis, V.R.N. & Telis-Romero, J. 2014. Effect of ethanol, dry extract and reducing sugars on density and viscosity of Brazilian red wines. *Journal of the Science of Food and Agriculture*. 95(7):1421–1427.

Nordestgaard, S. 2018. Gains in speed , labour and gas consumption for winemakers. *The Australian and New Zealand Grapegrower and Winemaker*. (648):61–67.

Núñez, Y.P., Carrascosa, A. V., González, R., Polo, M.C. & Martínez-Rodríguez, A. 2006. Isolation and characterization of a thermally extracted yeast cell wall fraction potentially useful for improving the foaming properties of sparkling wines. *Journal of Agricultural and Food Chemistry*. 54(20):7898–7903.

Ough, C.S. 2018. *Winemaking Basics*. 1st Editio ed. R. Gough (ed.). New York, USA: Food Products Press.

Painmanakul, P., Loubiere, K., Hebrard, G., Mietton-Peuchot, M. & Roustain, M. 2005. Effect of Surfactants on Liquid Side Mass Transfer Coefficients. *Chemical Engineering Science*. 60(22):6480–6491.

Pittoors, E., Guo, Y. & Van Hulle, S.W.H. 2014. Modeling Dissolved Oxygen Concentration for Optimizing Aeration Systems and Reducing Oxygen Consumption in Activated Sludge Processes: A Review. *Chemical Engineering Communications*. 201(8):983–1002.

Ramezani, M., Legg, M.J., Haghighat, A., Li, Z., Vigil, R.D. & Olsen, M.G. 2017. Experimental investigation of the effect of ethyl alcohol surfactant on oxygen mass transfer and bubble size distribution in an air-water multiphase Taylor- Couette vortex bioreactor. *Chemical Engineering Journal*. 319:288–296.

Rawle, A. 2003. [Online], Available: http://cat.inist.fr/?aModele=afficheN&cpsidt=14620810.

Rosso, D., Huo, D.L. & Stenstrom, M.K. 2006. Effects of interfacial surfactant contamination on bubble gas transfer. *Chemical Engineering Science*. 61:5500–5514.

Routledge, S.J. 2012. Beyond de-foaming: The effects of antifoams on bioprocess productivity. *Computational and Structural Biotechnology Journal*. 3(4).

Ruzicka, M.C., Drahoš, J., Mena, P.C. & Teixeira, J.A. 2003. Effect of viscosity on

homogeneous – heterogeneous flow regime transition in bubble columns. *Chemical Engineering Journal*. 96:15–22.

Saa, P.A., Pérez-Correa, J.R., Celentano, D. & Agosin, E. 2013. Impact of carbon dioxide injection on oxygen dissolution rate during oxygen additions in a bubble column. *Chemical Engineering Journal*. 232:157–166.

Sardeing, R., Painmanakul, P. & Hébrard, G. 2006. Effect of surfactants on liquid-side mass transfer coefficients in gas – liquid systems : A first step to modeling. *Chemical Engineering Science*. 61:6249–6260.

Sehabiague, L. & Morsi, B.I. 2013. Hydrodynamic and mass transfer characteristics in a large-scale slurry bubble column reactor for gas mixtures in actual Fischer-Tropsch cuts. *International Journal of Chemical Reactor Engineering*. 11(1):83–102.

Shehadeh, A., Kechagia, D., Evangelou, A. & Tataridis, P. 2019. Effect of ethanol , glycerol , glucose and tartaric acid on the viscosity of model aqueous solutions and wine samples. *Food Chemistry*. 300:1–8.

Singleton, V.L., Trousdale, E. & Zaya, J. 1979. Oxidation of Wines. I. Young White Wines Periodically Exposed to Air. *American Journal of Enology and Viticulture*. 30(1):49–54.

Song, D., Seibert, A.F. & Rochelle, G.T. 2014. Effect of liquid viscosity on the liquid phase mass transfer coefficient of packing. *Energy Procedia*. 63:1268–1286.

Steiner, T. 2013. *Wines & Vines - Strategies to Manage Dissolved Oxygen*. [Online], Available: https://winesvinesanalytics.com/features/article/119752/Strategies-to-Manage-Dissolved-Oxygen [2020, July 21].

Stenstrom, M.K. & Gilbert, R.G. 1981. Effects of alpha, beta and theta factor upon the design, specification and operation of aeration systems. *Water Research*. 15(6):643–654.

Tribe, L.A., Briens, C.L. & Margaritis, A. 1995. Determination of the Volumetric Mass. *Biotechnology and Bioengineering*. 46:388–392.

Ugliano, M. 2013. Oxygen contribution to wine aroma evolution during bottle aging. *Journal of Agricultural and Food Chemistry*. 61(26):6125–6136.

Van't Riet, K. 1979. Review of Measuring Methods. *Industrial & Engineering Chemistry Process Design and Development*. 18(3):357–364.

Vasconcelos, J.M.T., Rodrigues, J.M.L., Orvalho, S.C.P., Alves, S.S., Mendes, R.L. & Reis, A. 2003. Effect of contaminants on mass transfer coefficients in bubble column and airlift contactors. *Chemical Engineering Science*. 58:1431–1440.

Vidal, J.-C. & Moutounet, M. 2008. Control of the Oxygen Supply During the Conditioning Part 1: Principles And Wine Preparation? *Revue Française d'Œnologie n°229*. (May).

Walls, J.R. 2019. Role of oxygen management on white wine composition. Stellenbosch University.

Wang, Z., Guo, K., Liu, H., Liu, C., Geng, Y., Lu, Z., Jiao, B. & Chen, D. 2020. Effects of bubble size on the gas–liquid mass transfer of bubble swarms with Sauter mean diameters of 0.38–4.88 mm in a co-current upflow bubble column. *Journal of Chemical Technology and Biotechnology*. 95(11):2853–2867.

Wiesmann, U., Choi, I.S. & Dombrowski, E.-M. 2006. Gas/Liquid Oxygen Transfer and Stripping. in *Fundamentals of Biological Wastewater Treatment* Weinheim: Wiley-VCH. 83–117.

Yanniotis, S., Kotseridis, G., Orfanidou, A. & Petraki, A. 2007. Effect of ethanol, dry extract

and glycerol on the viscosity of wine. *Journal of Food Engineering*. 81(2):399–403.

Zahradník, J., Fialová, M., Růžička, M., Drahŏs, J., Kaštánek, F. & Thomas, N.H. 1997. Duality of the gas-liquid flow regimes in bubble column reactors. *Chemical Engineering Science*. 52(21–22):3811–3826.

Zahradník, J., Fialová, M. & Linek, V. 1999. The effect of surface-active additives on bubble coalescence in aqueous media. *Chemical Engineering Science*. 54(21):4757–4766.

Zedníková, M., Orvalho, S., Fialová, M. & Ruzicka, M.C. 2018. Measurement of Volumetric Mass Transfer Coefficient in Bubble Columns. *ChemEngineering*. 2(19):1–14.

Zoecklein, B., Fugelsang, K., Gump, B. & Nury, F. 1999. *Wine Analysis and Production*. New York, USA: Aspen Publishers, Inc.

Supplementary Material

S1: Experimental data

Table S10: Kla data for the different wines (s⁻¹)

Wine	Wine Code	Temperature (°C)	Gas flowrate (L/min)	Kla Run 1	Kla Run 2	Kla Run 3	Kla Average (s⁻¹)
Water	Water	25	1.7	0.01064	0.01122	0.01107	0.01098
Dry white blend	White-A	25	1.7	0.01134	0.01001	0.01786	0.01307
Chenin Blanc	White-B	25	1.7	0.01590	0.01610	0.01620	0.01607
Sauvignon Blanc	White-C	25	1.7	0.01238	0.01252	0.01342	0.01277
Semi-sweet Rose	Rose	25	1.7	0.02190	0.01912	0.01519	0.01874
Dry red blend	Red	25	1.7	0.02819	0.02385	0.03007	0.02737
Protein heavy white	PU-Wine	25	1.7	0.01138	0.00711	0.00859	0.00903
Bentonite treated white	BT-Wine	25	1.7	0.01320	0.01859	0.01363	0.01514

Table S11: Kp data for the different wines (s⁻¹)

Wine	Wine Code	Temperature (°C)	Gas flowrate (L/min)	Kp Run 1	Kp Run 2	Kp Run 3	Kp Average (s⁻¹)
Water	Water	25	1.7	0.0337	0.0380	0.0355	0.0357
Dry white blend	White-A	25	1.7	0.0370	0.0352	0.0399	0.0374
Chenin Blanc	White-B	25	1.7	0.0300	0.0320	0.0347	0.0322
Sauvignon Blanc	White-C	25	1.7	0.0361	0.0337	0.0379	0.0359
Semi-sweet Rose	Rose	25	1.7	0.0409	0.0380	0.0356	0.0382
Dry red blend	Red	25	1.7	0.0361	0.0337	0.0340	0.0346
Protein heavy white	PU-Wine	25	1.7	0.0349	0.0378	0.0382	0.0370
Bentonite treated white	BT-Wine	25	1.7	0.0349	0.0401	0.0369	0.0373

Table S12: Gas holdup data for the different wines

Wine	Wine Code	Temperature (°C)	Gas flowrate (L/min)	Take 1	Take 2	Take 3	Gas holdup average
Water	Water	25	1.7	0.0076	0.0081	0.0077	0.0078
Dry white blend	White-A	25	1.7	0.0243	0.0235	0.0285	0.0254
Chenin Blanc	White-B	25	1.7	0.0264	0.0262	0.0268	0.0264
Sauvignon Blanc	White-C	25	1.7	0.0209	0.0264	0.0264	0.0246
Semi-sweet Rose	Rose	25	1.7	0.0227	0.0273	0.0230	0.0243
Dry red blend	Red	25	1.7	0.0253	0.0238	0.0238	0.0243
Protein heavy white	PU-Wine	25	1.7	0.0203	0.0265	0.0236	0.0235
Bentonite treated white	BT-Wine	25	1.7	0.0214	0.0280	0.0268	0.0254

Table S13: Sauter mean bubble diameter (mm) for the different wines

Wine	Wine Code	Temperature (°C)	Gas flowrate (L/min)	Take 1	Take 2	Take 3	Take 4	Take 5	D32 average (mm)
Water	Water	25	1.7	0.6803	0.7683	0.8590	0.6657	0.7161	0.7379
Dry white blend	White-A	25	1.7	0.2864	0.2729	0.2885	0.2764	0.2572	0.2763
Chenin Blanc	White-B	25	1.7	0.2844	0.2607	0.2684	0.2605	0.2477	0.2643
Sauvignon Blanc	White-C	25	1.7	0.2516	0.2927	0.2561	0.2217	0.2229	0.2490
Semi-sweet Rose	Rose	25	1.7	0.2963	0.2949	0.2791	0.2571	0.2648	0.2784
Dry red blend	Red	25	1.7	0.2683	0.2730	0.2523	0.2743	0.2470	0.2630
Protein heavy white	PU-Wine	25	1.7	0.2516	0.2436	0.2411	0.2379	0.2408	0.2430
Bentonite treated white	BT-Wine	25	1.7	0.2489	0.2563	0.2579	0.2489	0.2531	0.2530

Table S14: Interfacial area data for the different wines (mm^2/mm^3)

Wine	Wine Code	Temperature (°C)	Gas flowrate (L/min)	Measurement 1	Measurement 2	Measurement 3
Water	Water	25	1.7	0.0615	0.0660	0.0626
Dry white blend	White-A	25	1.7	0.5428	0.5245	0.6353
Chenin Blanc	White-B	25	1.7	0.6154	0.6101	0.6252
Sauvignon Blanc	White-C	25	1.7	0.5228	0.6591	0.6599
Semi-sweet Rose	Rose	25	1.7	0.4815	0.5798	0.4876
Dry red blend	Red	25	1.7	0.5762	0.5419	0.5433
Protein heavy white	PU-Wine	25	1.7	0.5001	0.6547	0.5837
Bentonite treated white	BT-Wine	25	1.7	0.5065	0.6634	0.6353

Table S15: Kl data for the different wines (mm/s)

Wine	Wine Code	Temperature (°C)	Gas flowrate (L/min)	Measurement 1	Measurement 2	Measurement 3	Kl average (mm/s)
Water	Water	25	1.7	0.1680	0.1771	0.1747	0.1733
Dry white blend	White-A	25	1.7	0.0200	0.0176	0.0315	0.0230
Chenin Blanc	White-B	25	1.7	0.0258	0.0261	0.0263	0.0260
Sauvignon Blanc	White-C	25	1.7	0.0202	0.0204	0.0219	0.0208
Semi-sweet Rose	Rose	25	1.7	0.0424	0.0370	0.0294	0.0363
Dry red blend	Red	25	1.7	0.0509	0.0431	0.0543	0.0494
Protein heavy white	PU-Wine	25	1.7	0.0196	0.0123	0.0148	0.0156
Bentonite treated white	BT-Wine	25	1.7	0.0219	0.0309	0.0226	0.0252

Table S16: Kla and Kp data for the experiments performed in the CCD

Run no.	Ethanol (% v/v)	Glycerol (g/L)	Temperature (°C)	Superficial gas velocity (cm/s)	Kla 2nd order (s⁻¹)	Kp (s⁻¹)
1	10.5	10	12.5	0.16	0.0139	0.0195
2	10.5	10	12.5	0.30	0.0208	0.0198
3	10.5	10	17.5	0.16	0.0186	0.0189
4	10.5	20	12.5	0.16	0.01876	0.0199
5	13.5	10	12.5	0.16	0.01677	0.0202
6	13.5	20	17.5	0.30	0.02342	0.019
7	13.5	20	17.5	0.16	0.0116	0.0203
8	13.5	20	12.5	0.30	0.0157	0.01985
9	13.5	10	17.5	0.30	0.02366	0.0204
10	10.5	20	17.5	0.30	0.0241	0.0211
11	13.5	20	12.5	0.16	0.0127	0.0188
12	13.5	10	17.5	0.16	0.0175	0.0201
13	10.5	20	17.5	0.16	0.017	0.02
14	13.5	10	12.5	0.30	0.02468	0.0189
15	10.5	20	12.5	0.30	0.0249	0.018
16	10.5	10	17.5	0.30	0.02447	0.0199
17	12	15	15	0.37	0.0252	0.0223
18	12	15	15	0.09	0.0129	0.0189
19	12	15	20	0.23	0.0211	0.0232
20	12	15	10	0.23	0.0089	0.0178
21	12	25	15	0.23	0.0202	0.0182
22	12	5	15	0.23	0.0205	0.0198
23	15	15	15	0.23	0.02007	0.0198
24	9	15	15	0.23	0.0193	**0.022**
25	12	15	15	0.23	0.0197	0.0202
26	12	15	15	0.23	0.01945	0.0187
27	12	15	15	0.23	0.02065	0.0194

Table S17: Kla (s⁻¹) values for different model wine solutions part 1 (s⁻¹)

Solution	Temperature (°C)	Gas flowrate (L/min)	Runs	Kla Run 1	Kla Run 2	Kla Run 3	Kla Run 4	Kla Run 5
Water	25	2.3	5	0.0105	0.0105	0.0107	0.0109	0.0110
Ethanol solution	25	2.3	10	0.0274	0.0278	0.0300	0.0295	0.0292
MWS-Glycerol	25	2.3	9	0.0211	0.0214	0.0194	0.0282	0.0237
MWS-Acids	25	2.3	10	0.0222	0.0218	0.0220	0.0209	0.0245
MWS-BSA	25	2.3	4	0.0142	0.0139	0.0184	0.0196	
MWS-Yeast	25	2.3	6	0.0186	0.0185	0.0214	0.0188	0.0199

Table S18: Kla (s⁻¹) values for different model wine solutions part 2 (s⁻¹)

Solution	Temperature (°C)	Gas flowrate (L/min)	Runs	Kla Run 6	Kla Run 7	Kla Run 8	Kla Run 9	Kla Run 10	Kla Average (s⁻¹)
Water	25	2.3	5						0.01071
Ethanol solution	25	2.3	10	0.0295	0.0282	0.0276	0.0234	0.0277	0.02804
MWS-Glycerol	25	2.3	9	0.0248	0.0216	0.0205	0.0215		0.02247
MWS-Acids	25	2.3	10	0.0257	0.0235	0.0270	0.0232	0.0257	0.02364
MWS-BSA	25	2.3	4						0.01652
MWS-Yeast	25	2.3	6	0.0155					0.01878

Table S19: Kp (s⁻¹) values for the different model wine solutions

Solution	Temperature (°C)	Gas flowrate (L/min)	Runs	Kp take 1	Kp take 2	Kp take 3	Kp average
Water	25	2.3	3	0.0279	0.0257	0.0231	0.025567
Ethanol solution	25	2.3	3	0.027555	0.026459	0.024327	0.026113
MWS-Glycerol	25	2.3	3	0.0279	0.0257	0.0231	0.025567
MWS-Acids	25	2.3	3	0.0252	0.0268	0.0237	0.025233
MWS-BSA	25	2.3	3	0.024	0.0225	0.0259	0.024133
MWS-Yeast	25	2.3	3	0.0251	0.0232	0.0245	0.024267

Table S20: Gas holdup data for the different model wine solutions part 1

Solution	Temperature (°C)	Gas flowrate (L/min)	Takes	Take 1	Take 2	Take 3	Take 4	Take 5
Water	25	2.3	9	0.0127	0.0164	0.0148	0.0161	0.0144
Ethanol solution	25	2.3	9	0.0351	0.0339	0.0364	0.0376	0.0375
MWS-Glycerol	25	2.3	8	0.0368	0.0388	0.0431	0.0360	0.0368
MWS-Acids	25	2.3	8	0.0366	0.0412	0.0388	0.0351	0.0358
MWS-BSA	25	2.3	3	0.0385	0.0370	0.0420		
MWS-Yeast	25	2.3	4	0.0363	0.0404	0.0372	0.0416	

Table S21: Gas holdup data for the different model wine solutions part 2

Solution	Tempera ture (°C)	Gas flowrate (L/min)	Takes	Take 6	Take 7	Take 8	Take 9	Gas holdup average
Water	25	2.3	9	0.0144	0.0115	0.0115	0.0110	0.0136
Ethanol solution	25	2.3	9	0.0335	0.0372	0.0430	0.0465	0.0379
MWS-Glycerol	25	2.3	8	0.0372	0.0426	0.0363		0.0384
MWS-Acids	25	2.3	8	0.0352	0.0304	0.0334		0.0358
MWS-BSA	25	2.3	3					0.0392
MWS-Yeast	25	2.3	4					0.0389

Table S22: Sauter mean bubble diameter (mm) data for the model wine solutions part 1 (Sparger 1)

Solution	Tempera ture (°C)	Gas flowrate (L/min)	Takes	Take 1	Take 2	Take 3	Take 4	Take 5
Water	25	2.3	5	1.041	1.203	0.898	1.169	1.129
Ethanol solution	25	2.3	8	0.300	0.303	0.299	0.292	0.307
MWS-Glycerol	25	2.3	5	0.382	0.350	**0.310**	**0.368**	0.272
MWS-Acids	25	2.3	5	0.285	0.337	0.320	0.390	0.340
MWS-BSA	25	2.3	4	0.310	0.332	0.314	0.319	
MWS-Yeast	25	2.3	10	**0.336**	**0.361**	**0.345**	**0.360**	**0.350**

Table S23: Sauter mean bubble diameter (mm) data for the model wine solutions part 2 (Sparger 1)

Solutio n	Temper ature (°C)	Gas flowrat e (L/min)	Takes	Take 6	Take 7	Take 8	Take 9	Take 10	D32 Averag e (mm)
Water	25	2.3	5						1.088
Ethanol solution	25	2.3	8	**0.312**	**0.307**	**0.324**			0.306
MWS-Glycerol	25	2.3	5						0.337
MWS-Acids	25	2.3	5						0.334
MWS-BSA	25	2.3	4						0.319
MWS-Yeast	25	2.3	10	0.321	0.314	0.327	0.325	0.308	0.335

Table S24: Sauter mean bubble diameter (mm) data for the model wine solutions part 1 (Sparger 2)

Solution	Temperature (°C)	Gas flowrate (L/min)	Takes	Take 1	Take 2	Take 3	Take 4	Take 5
Water	25	2.3	5	0.680	0.768	0.859	0.666	0.716
MWS-Glycerol	25	2.3	5	**0.296**	**0.287**	**0.269**	**0.262**	**0.281**
MWS-Acids	25	2.3	7	0.268	0.273	0.245	0.249	0.299
Ethanol solution	25	2.3	10	0.251	0.242	0.237	0.265	0.271
MWS-Yeast	25	2.3	10	0.247	0.254	0.262	0.254	0.243

Table S25: Sauter mean bubble diameter (mm) data for the model wine solutions part 2 (Sparger 2)

Solution	Temperature (°C)	Gas flowrate (L/min)	Takes	Take 6	Take 7	Take 8	Take 9	Take 10	D32 Average
Water	25	2.3	5						0.738
MWS-Glycerol	25	2.3	5						0.279
MWS-Acids	25	2.3	7	0.311	0.274				0.274
Ethanol solution	25	2.3	10	0.253	0.243	0.243	0.240	0.251	0.250
MWS-Yeast	25	2.3	10	0.275	0.272	0.266	0.266	0.251	0.259

Table S26: Interfacial area data for the model wine solutions part 1 (mm^2/mm^3)

Solution	Temperature (°C)	Gas flowrate (L/min)	Takes	Take 1	Take 2	Take 3	Take 4	Take 5
Water	25	2.3	9	0.070	0.091	0.081	0.089	0.080
Ethanol solution	25	2.3	9	0.689	0.665	0.715	0.738	0.737
MWS-Glycerol	25	2.3	8	0.658	0.694	0.771	0.644	0.659
MWS-Acids	25	2.3	8	0.655	0.737	0.694	0.627	0.640
MWS-BSA	25	2.3	3	0.725	0.697	0.791		
MWS-Yeast	25	2.3	4	0.650	0.723	0.667	0.746	

Table S27: Interfacial data for the model wine solutions part 2 (mm²/mm³)

Solution	Temperature (°C)	Gas flowrate (L/min)	Takes	Take 6	Take 7	Take 8	Take 9	Interfacial area average (mm²/mm³)
Water	25	2.3	9	0.080	0.063	0.063	0.061	0.075
Ethanol solution	25	2.3	9	0.659	0.730	0.844	0.913	0.743
MWS-Glycerol	25	2.3	8	0.666	0.762	0.649		0.688
MWS-Acids	25	2.3	8	0.629	0.544	0.598		0.641
MWS-BSA	25	2.3	3					0.738
MWS-Yeast	25	2.3	4					0.696

Table S28: KI data for the model wine solutions part 1 (mm/s)

Solution	Temperature (°C)	Gas flowrate (L/min)	Takes	Take 1	Take 2	Take 3	Take 4	Take 5
Water	25	2.3	5	0.139	0.139	0.142	0.145	0.146
Ethanol solution	25	2.3	10	0.037	0.037	0.040	0.040	0.039
MWS-Glycerol	25	2.3	9	0.031	0.031	0.028	0.041	0.035
MWS-Acids	25	2.3	10	0.035	0.034	0.034	0.033	0.038
MWS-BSA	25	2.3	4	0.019	0.019	0.025	0.027	
MWS-Yeast	25	2.3	6	0.027	0.027	0.031	0.027	0.029

Table S29: KI data for the model wine solutions part 2 (mm/s)

Solution	Temperature (°C)	Gas flowrate (L/min)	Takes	Take 6	Take 7	Take 8	Take 9	Take 10	KI average (mm/s)
Water	25	2.3	5						0.142
Ethanol solution	25	2.3	10	0.040	0.038	0.037	0.031	0.037	0.038
MWS-Glycerol	25	2.3	9	0.036	0.031	0.030	0.031		0.033
MWS-Acids	25	2.3	10	0.040	0.037	0.042	0.036	0.040	0.037
MWS-BSA	25	2.3	4						0.022
MWS-Yeast	25	2.3	6	0.022					0.027

Table S30: Kla data for different ethanol solutions (s⁻¹)

Ethanol concentration	Gas flowrate (L/min)	Temperature (°C)	Kla take 1	Kla take 2	Kla take 3	Kla Average
0	2.3	25	0.0120	0.0109	0.0110	0.0113
0.01	2.3	25	0.0132	0.0135	0.0158	0.0142
0.05	2.3	25	0.0275	0.0282	0.0204	0.0254
0.1	2.3	25	0.0266	0.0257	0.0247	0.0257
0.5	2.3	25	0.0250	0.0197	0.0211	0.0219
1	2.3	25	0.0239	0.0241	0.0181	0.0220
2	2.3	25	0.0269	0.0185	0.0236	0.0230
5	2.3	25	0.0250	0.0256	0.0275	0.0260
10	2.3	25	0.0276	0.0234	0.0277	0.0262

Table S31: Sauter mean bubble diameter (mm) for different ethanol solutions

Ethanol concentration	Gas flowrate (L/min)	Temp (°C)	Take 1	Take 2	Take 3	Take 4	Take 5	D32 Average (mm)
0	2.3	25	1.041	1.203	0.898	1.169	1.129	1.088
0.01	2.3	25	0.868	1.068	1.086			1.008
0.05	2.3	25	**0.543**	**0.799**	**0.751**			0.698
0.1	2.3	25	**0.330**	**0.326**	**0.427**			0.361
1	2.3	25	0.318	0.347	0.349	0.365		0.345
5	2.3	25	**0.312**	**0.307**	**0.324**			0.314
10	2.3	25	0.300	0.303	0.299	0.292	0.307	0.300

Table S32: Interfacial area (mm²/mm³) and gas holdup data for different ethanol solutions

Ethanol concentration	Gas flowrate (L/min)	Temp (°C)	Gas holdup average	Take 1	Take 2	Take 3	Take 4	Take 5	Interfacial area average (mm²/mm³)
0	2.3	25	0.011	0.066	0.057	0.076	0.059	0.061	0.064
0.01	2.3	25	0.012	0.083	0.068	0.067			0.073
0.05	2.3	25	0.014	0.154	0.105	0.111			0.123
0.1	2.3	25	0.022	0.404	0.409	0.312			0.375
1	2.3	25	0.035	0.655	0.601	0.598	0.570		0.606
5	2.3	25	0.037	0.713	0.724	0.687			0.708
10	2.3	25	0.033	0.671	0.664	0.671	0.688	0.655	0.670

Table S33: KI data for different ethanol solutions (mm/s)

Ethanol concentration	Gas flowrate (L/min)	Temp (°C)	Take 1	Take 2	Take 3	KI average (mm/s)
0	2.3	25	0.188	0.171	0.173	0.177
0.01	2.3	25	0.182	0.186	0.217	0.195
0.05	2.3	25	0.223	0.229	0.165	0.206
0.1	2.3	25	0.071	0.069	0.066	0.068
1	2.3	25	0.039	0.040	0.030	0.036
5	2.3	25	0.035	0.036	0.039	0.037
10	2.3	25	0.041	0.035	0.041	0.039

S2: MATLAB code for bubble image analysis

The following is an exact copy of the MALTAB code used for the bubble image analysis. This code is mostly presented in the same format by Abufalgha (2018).

```matlab
A=imread('INSERT_FILENAME.jpg')
bubsize_range=[2,numel(A)/10];
fit_ellipses=true;
plotstages=true;

if size(A,3)==3
    A=rgb2gray(A);
end
calibrate=true
if islogical(calibrate)&&calibrate
    figure('Units','normalized','Position',[0 0 1 1])
if ndims(A)==3
if size(A,3)==3
    imshow(rgb2gray(A));
end
else
    imshow(A);
end
    title('click and drag calibration line')
    refH = imline(gca);
    position = wait(refH);
    close(gcf)
    dposition=abs(position(1,:)-position(2,:));
%  pixLength = max(position(3),position(4));
    pixLength = max(dposition);

    answer = inputdlg({'Reference length(mm)'},'Reference measurements',1,{'10'});
    mmLength = str2double(answer{1});

    scale=mmLength/pixLength;
    disp(['Calibration factor is: ',num2str(scale),'[mm/pixel]'])
else
    scale = calibrate;
end


A=double(A);
Aref=A;
A=medfilt3(A,[3,3]);

%get background
C=A;
[bb,aa]=size(C);
inc_background=5;
medf_background=3;

linxs=round(linspace(1,aa,round(aa/inc_background)));
```

```matlab
linys=round(linspace(1,bb,round(bb/inc_background)));
[xxs,yys]=meshgrid(linxs,linys);
Bs=C(linys,linxs);
Bsmed=medfilt3(Bs,[medf_background,medf_background]); %Based of medf_background
which is actually 5 in Ayman's code

linx=1:aa;
liny=1:bb;
[xx,yy]=meshgrid(linx,liny);
underlying_shape=interp2(xxs,yys,double(Bsmed),xx,yy,'linear');
C=underlying_shape-C; %image here looks good
C(C<0)=0;
cvec=C(:);
cvec=cvec(~isnan(cvec));
C=(C-mean(cvec))/(std(cvec)); %image here sitll alright, but perhaps not quite as tasty
thresh=0.7;
imi=1;
imi=imi+1;lkim_fif(Aref,plotstages,'original');
imi=imi+1;lkim_fif(C,plotstages,'backgnd sub');

bw=C>thresh; %I have a decent looking black and white photo
imi=imi+1;lkim_fif(bw,plotstages,['# ',num2str(imi),':thresh']);

bw=medfilt2(bw);
imi=imi+1;lkim_fif(bw,plotstages,['# ',num2str(imi),':medf']);

joinpixels=3;
bw=imdilate(bw,strel('disk',joinpixels));
bw=imerode(bw,strel('disk',joinpixels));
imi=imi+1;lkim_fif(bw,plotstages,['# ',num2str(imi),':joinpixels']);

bw=imdilate(bwmorph(bw,'skel',inf),strel('square',2));
bwh= imfill(bw,'holes');
bw=bwh-bw;
bwborder=imdilate(bw,strel('disk',2))-bw;
imi=imi+1;lkim_fif(bwborder,plotstages,['# ',num2str(imi),':final edges']);

bwholes=medfilt2(bw); % looks fine;
imi=imi+1;lkim_fif(bw,plotstages,['# ',num2str(imi),':final']);

[GL,L]=bwboundaries(bwholes,'noholes');
numbubs=max(L(:));
[X,Y]=meshgrid(1:size(L,2),1:size(L,1));

pcent_border=0.2;
pcent_border=pcent_border/2;
ignore_edge=round(pcent_border*mean(size(L)));
minx=ignore_edge;
maxx=max(X(:))-ignore_edge;
miny=ignore_edge;
maxy=max(Y(:))-ignore_edge;

figure
subplot(1,2,1),imagesc(1:size(L,2),1:size(L,1),Aref);
hold on
```

```matlab
subplot(1,2,2),imagesc(1:size(L,2),1:size(L,1),logical(bw));
colormap gray
hold on


bubbles=1:numbubs;
dl=scale;
da=scale^2;
count=0
disp(['measuring ',num2str(numbubs),' bubbles'])
data='no data was saved';
headers={'scale','bubble number (ii)','perimeter length', 'projected area','ellipse
perimeter','ellipse
area','ellipse_centre_position_x','ellipse_centre_position_y','ellipse_avg_diameter','ellipse_a',
'ellipse_b'};
circularity=0.2;

for ii=bubbles
    Lid=(L==ii);
if any(Lid(:))

    elx=X(Lid);
    ely=Y(Lid);
    midbubx=mean(elx);
    midbuby=mean(ely);
    perimx=GL{ii}(:,2);
    perimy=GL{ii}(:,1);
    perim_i=integrate_border_fif(perimx,perimy)*dl;
    area_i=sum(Lid(:))*da;
    circularity_i=4*pi()*area_i/(perim_i^2);

    dothisbubble=true

if (area_i<(bubsize_range(1)*da))
    dothisbubble=false;
    disp(['bubble ',num2str(ii),' was outside size range: too small'])
elseif (area_i>(bubsize_range(2)*da))
    dothisbubble=false;
    disp(['bubble ',num2str(ii),' was outside size range: too big'])
end

if   ~((midbubx>minx)&&(midbubx<maxx)&&(midbuby>miny)&&(midbuby<maxy))
    dothisbubble=false;
    disp(['bubble ',num2str(ii),' outside position range'])
end

if circularity_i<circularity
    dothisbubble=false;
    disp(['bubble ',num2str(ii),' circularity',num2str(circularity_i),' was smaller then set
circularity', num2str(circularity)])
end

if dothisbubble
    count=count+1
```

```
    data_i=[scale,ii,perim_i,area_i];

subplot(1,2,1),text(midbubx,midbuby,num2str(ii),'Color','b');
    subplot(1,2,1),plot(midbubx,midbuby,'k+');

subplot(1,2,2),fill(perimx,perimy,[0,0,1]*0.5,'facealpha',0.5);

subplot(1,2,2),text(midbubx,midbuby,num2str(ii),'Color','b');

        data_ellipse_i=[];
if fit_ellipses
try
    [ellipse_t,ellipse_plot]=fit_ellipse_fif(perimx,perimy);
    ai=ellipse_t.a;
    bi=ellipse_t.b;
    ellipse_area_i=pi()*ai*bi*scale^2;
    hh=(ai-bi)^2/(ai+bi)^2;

ellipse_perim_i=pi()*(ai+bi)*(1+(3*hh)/(10+sqrt(4-3*hh)))*scale;
ellipse_centre_position_xy=mean([ellipse_plot.xr(:),ellipse_plot.yr(:)]);
    ellipse_a=ai;
    ellipse_b=bi;
    ellipse_average_diameter=(ai+bi)/2*scale;

data_ellipse_i=[ellipse_perim_i,ellipse_area_i,ellipse_centre_position_xy,ellipse_average_di
ameter,ellipse_a,ellipse_b];

subplot(1,2,2),plot(ellipse_plot.xr,ellipse_plot.yr,'r-');
subplot(1,2,2),plot(ellipse_plot.new_ver_line(1,:),ellipse_plot.new_ver_line(2,:),'r-');

subplot(1,2,2),plot(ellipse_plot.new_horz_line(1,:),ellipse_plot.new_horz_line(2,:),'r-');

catch

    warning on;
    warning('ellipse was not fitted')
end
end
    rowdata=[data_i,data_ellipse_i];
if count==1
    data=nan(numbubs,length(rowdata));
end
    data(ii,1:length(rowdata))=rowdata;
else

subplot(1,2,2),text(midbubx,midbuby,num2str(ii),'EdgeColor','g','Color','g');
subplot(1,2,1),text(midbubx,midbuby,num2str(ii),'Color','g');
    subplot(1,2,1),plot(midbubx,midbuby,'k+');
end

end
end
function L=integrate_border_fif(perimx,perimy)
nn=length(perimx);
perimx=[perimx(:)',perimx(1)];
```

```matlab
perimy=[perimy(:)',perimy(1)];
L=0;
for ii=1:nn
    dx=(perimx(ii+1)-perimx(ii));
    dy=(perimy(ii+1)-perimy(ii));
    dL=sqrt(dx^2+dy^2);
    L=L+dL;
end
end
function lkim_fif(A,plotiftrue,titletext)
if plotiftrue
    figure;
    imagesc(A);
    axis square;
    title(titletext);

end

end
function [ellipse_t,ellipse_plot] = fit_ellipse_fif(x,y,axis_handle)

orientation_tolerance = 1e-3;

warning('');

x = x(:);
y = y(:);

mean_x = mean(x);
mean_y = mean(y);
x = x-mean_x;
y = y-mean_y;

X = [x.^2, x.*y, y.^2, x, y ];
a = sum(X)/(X'*X);

if ~isempty( lastwarn )
    disp( 'stopped because of a warning regarding matrixinversion' );
ellipse_t = [];
return
end

[a,b,c,d,e] = deal( a(1),a(2),a(3),a(4),a(5) );

if ( min(abs(b/a),abs(b/c)) > orientation_tolerance );
    orientation_rad = 1/2 * atan( b/(c-a) );
    cos_phi = cos( orientation_rad );
    sin_phi = sin( orientation_rad );
    [a,b,c,d,e] = deal(a*cos_phi^2 - b*cos_phi*sin_phi + c*sin_phi^2,0,a*sin_phi^2 +
b*cos_phi*sin_phi + c*cos_phi^2,d*cos_phi - e*sin_phi,d*sin_phi + e*cos_phi ); % may need
to but ellipses in front of every call
    [mean_x,mean_y] = deal(cos_phi*mean_x - sin_phi*mean_y,sin_phi*mean_x +
cos_phi*mean_y );
else
orientation_rad = 0;
```

```matlab
cos_phi = cos( orientation_rad );
sin_phi = sin( orientation_rad );
end

test = a*c;
switch (1)
    case (test>0), status = '';
    case (test==0), status = 'Parabola found'; warning( 'fit_ellipse: Did not locate an ellipse' );
    case (test<0), status = 'Hyperbola found'; warning( 'fit_ellipse: Did not locate an ellipse' );
end

if (test>0)

if a<0, [a,c,d,e] = deal( -a,-c,-d,-e );
end

X0 = mean_x - d/2/a;
Y0 = mean_y - e/2/c;
F = 1 + (d^2)/(4*a) + (e^2)/(4*c);
[a,b] = deal( sqrt( F/a ),sqrt( F/c ) );
long_axis = 2*max(a,b);
short_axis = 2*min(a,b);

R = [ cos_phi sin_phi; -sin_phi cos_phi ];
P_in = R * [X0;Y0];
X0_in = P_in(1);
Y0_in = P_in(2);


ellipse_t=struct('a',a,'b',b,'phi',orientation_rad,'X0',X0,'Y0',Y0,'X0_in',X0_in,'Y0_in',Y0_in,'long_axis',long_axis,'short_axis',short_axis,'status','' );
else
    ellipse_t =
struct('a',[],'b',[],'phi',[],'X0',[],'Y0',[],'X0_in',[],'Y0_in',[],'long_axis',[],'short_axis',[],'status',status );
end


R = [ cos_phi sin_phi; -sin_phi cos_phi ];
% the axes

ver_line = [ [X0 X0]; Y0+b*[-1 1] ];

horz_line = [ X0+a*[-1 1]; [Y0 Y0] ];
new_ver_line = R*ver_line;
new_horz_line = R*horz_line;

% the ellipse
theta_r = linspace(0,2*pi);

ellipse_x_r = X0 + a*cos( theta_r );
ellipse_y_r = Y0 + b*sin( theta_r );
rotated_ellipse = R * [ellipse_x_r;ellipse_y_r];
```

```matlab
ellipse_plot =
struct('xr',rotated_ellipse(1,:),'yr',rotated_ellipse(2,:),'rotated_ellipse',rotated_ellipse,'new_ver
_line',new_ver_line,'new_horz_line',new_horz_line);

if (nargin>2) & ~isempty( axis_handle ) & (test>0)
   hold_state = get( axis_handle,'NextPlot' );
   set( axis_handle,'NextPlot','add' );
   plot( new_ver_line(1,:),new_ver_line(2,:),'r' );
   plot( new_horz_line(1,:),new_horz_line(2,:),'r' );
   plot( rotated_ellipse(1,:),rotated_ellipse(2,:),'r' );
   set( axis_handle,'NextPlot',hold_state );
end

end

function B = medfilt3(A,siz,padopt,CHUNKFACTOR)
%MEDFILT3

if nargin~=4
CHUNKFACTOR = 1;
end

if CHUNKFACTOR<1, CHUNKFACTOR = 1;
end
%% Checking input arguments
if isscalar(A), B = A; return, end
if ndims(A)>3
   error('A must be a 1-D, 2-D or 3-D array.')
end
if all(isnan(A(:))), B = A; return, end
sizA = size(A);
if nargin==1
% default kernel size is 3 or 3x3 or 3x3x3
if isvector(A)
   siz = 3;
else
   siz = 3*ones(1,numel(sizA));
end
padopt = 'replicate';
elseif nargin==2
   padopt = 'replicate';
end

if numel(siz)==2
   siz = [siz 1];
elseif isscalar(siz)
   if sizA(1)==1
      siz = [1 siz 1];
else siz = [siz 1 1];
end
end

N = numel(A);
siz = ceil((siz-1)/2);
n = prod(siz*2+1);
```

```matlab
if n==1, B = A; return, end
nchunk = (1:ceil(N/n/CHUNKFACTOR):N);
if nchunk(end)~=N, nchunk = [nchunk N];
end
%% Change to double if needed
class0 = class(A);
if ~isa(A,'float')
   A = double(A);
end

B = A;
sizB = sizA;
try
   A = padarray(A,siz,padopt);
catch
if ~isscalar(padopt)
   padopt = 0;

   warning('MATLAB:medfilt3:InexistentPadarrayFunction',['PADARRAY function does not
exist: "only scalar padding option is available.\n"If not specified, the scalar 0 is used as
default.']);
end

   A = ones(sizB+siz(1:ndims(B))*2)*padopt;
   A(siz(1)+1:end-siz(1),siz(2)+1:end-siz(2),siz(3)+1:end-siz(3)) = B;
end
sizA = size(A);

if numel(sizB)==2
   sizA = [sizA 1];
   sizB = [sizB 1];
end

inc = zeros([3 2*siz+1],'int32');
siz = int32(siz);
[inc(1,:,:,:) inc(2,:,:,:) inc(3,:,:,:)] = ndgrid([0:-1:-siz(1) 1:siz(1)],[0:-1:-siz(2) 1:siz(2)],[0:-1:-
siz(3) 1:siz(3)]);
   inc = reshape(inc,[1 3 prod(2*single(siz)+1)]);

I = zeros([sizB 3],'int32');
sizB = int32(sizB);
[I(:,:,:,1) I(:,:,:,2) I(:,:,:,3)] = ndgrid((1:sizB(1))+siz(1),(1:sizB(2))+siz(2),(1:sizB(3))+siz(3));

I = reshape(I,[prod(single(sizB)) 3]);

existNaNmedian = exist('nanmedian','file');

for i = 1:length(nchunk)-1
   ii=i;
   Im = repmat(I(nchunk(ii):nchunk(ii+1),:),[1 1 n]);
   Im = Im + repmat(inc,[nchunk(ii+1)-nchunk(ii)+1,1,1]);

   I0 = Im(:,1,:) +(Im(:,2,:)-1)*sizA(1) + (Im(:,3,:)-1)*sizA(1)*sizA(2);
   I0 = squeeze(I0);
```

```matlab
if existNaNmedian
    B(nchunk(ii):nchunk(ii+1)) = nanmedian(A(I0),2);
else
    B(nchunk(ii):nchunk(ii+1)) = median(A(I0),2);
end
end
B = cast(B,class0);
end
```